



International Atomic Energy Agency

INDC(NDS)-431
Distr. G+NM

INDC

INTERNATIONAL NUCLEAR DATA COMMITTEE

**NUCLEAR MODEL PARAMETER TESTING
FOR NUCLEAR DATA EVALUATION
(Reference Input Parameter Library: Phase II)**

Summary Report of the Third Research Co-ordination Meeting

Vienna, Austria

3 - 7 December 2001

Prepared by

M. Herman

IAEA Vienna, Austria

April 2002

IAEA NUCLEAR DATA SECTION, WAGRAMERSTRASSE 5, A-1400 VIENNA

Reproduced by the IAEA in Austria

April 2002

**NUCLEAR MODEL PARAMETER TESTING
FOR NUCLEAR DATA EVALUATION
(Reference Input Parameter Library: Phase II)**

Summary Report of the Third Research Co-ordination Meeting

Vienna, Austria

3 - 7 December 2001

Prepared by

M. Herman

IAEA Vienna, Austria

ABSTRACT

This report summarises the results and recommendations of the third Research Co-ordination Meeting on improving and testing the Reference Input Parameter Library: Phase II. A primary aim of the meeting was to review the achievements of the CRP, to assess the testing of the library and to approve the final contents. Actions were approved that will result in completion of the file and a draft report by the end of February 2002. Full release of the library is scheduled for July 2002.

April 2002

CONTENTS

Summary of the Meeting	7
Segment 1: Masses	7
Segment 2: Levels	8
Segment 3: Resonances	9
Segment 4: Optical	10
Segment 5: Level Densities	12
Segment 6: Gamma	15
Segment: Angular	16
Segment 7: Fission	16
Retrieval Tools (WWW).....	17
Testing	19
Code Interfaces	20
TECDOC	20
Actions	20
Conclusions	23
APPENDIX 1: Meeting agenda	25
APPENDIX 2: List of participants	27
APPENDIX 3: Technical input	29

SUMMARY OF THE MEETING

The Reference Input Parameter Library (RIPL) is a collection of input parameters for theoretical calculations of nuclear reaction cross sections. RIPL is targeted at users of nuclear reaction codes and, in particular, at nuclear data evaluators. The first phase of the project was completed in 1999, and produced a Starter File and related documentation (TECDOC-1034). In 1999 the second phase of the project was initiated in order to test the RIPL-1 database and produce interfaces between RIPL and commonly used nuclear reaction codes. Substantial improvements and extensions of the original database have been made. Therefore, the resulting RIPL-2 database is considerably different and improved from the original version.

The third Research Co-ordination Meeting of the RIPL-2 CRP was held in Vienna, Austria, 3 - 7 December 2001, attended by ten CRP members and two observers. The IAEA was represented by the Head of Nuclear Data Section A.L. Nichols and M. Herman who served as a scientific secretary. Phil Young (Los Alamos, USA) served as chairman of the meeting.

Participants reviewed the status of work within the CRP. Library contents, testing, interfaces to the reaction model codes and retrieval tools were discussed. All files selected for RIPL-2 have been reformatted into the unified RIPL-2 format, agreed during the second RIPL-2 meeting held at Varenna, Italy, in June 2000 (see INDC(NDS)-416). After thorough discussions, most of the files required minor changes before final release. The participants also agreed on the uniform naming of the files in the RIPL-2 database. The actions and relative time-schedule were defined, with completion of the RIPL-2 library by the end of February 2002 and release in July 2002.

The following sections define the status of the work and recommendations with regard to RIPL-2 contents and testing.

SEGMENT 1: MASSES

(Co-ordinator S. Goriely)

The mass segment has been extended by inclusion of the file with abundances and Duflo-Zuker systematics and is considered to be almost complete. However, it was decided to replace current masses based on the ETFSI model with the more accurate data calculated in terms of the HF-BCS model. The latter ones are also consistent with the microscopic level densities accepted for the segment 5. In addition, it was decided to include HFB matter densities which are necessary for calculation of optical model parameters within semi-microscopic approach (code MOM) in segment 4. The draft of the related TECDOC chapter has been submitted but needs to be updated to account for the above changes.

Actions:

1. Goriely: replace the ETFSI table with the latest HFB masses and the associated readme file (15 January 2002).
2. Goriely: include table of HFB densities (1 file per element) (15 January 2002).
3. Goriely: finalise draft of the TECDOC chapter by including a subsection on HFB densities (15 January 2002).

Files:

- abundance.readme
- abundance.dat
- duflo-zuker.readme
- duflo-zuker.f
- mass-hfb.readme
- mass-hfb.dat
- mass-frdm.readme
- mass-frdm.dat
- gs-deformations-exp.readme
- gs-deformations-exp.dat
- matter-density-hfb.readme
- matter-density-hfb/Zxxx.dat

SEGMENT 2: LEVELS

(Co-ordinator: T. Belgya)

New versions of the level files were submitted before the meeting, and following changes as recommended at the Varenna meeting have been introduced:

- The worst fits ($\chi^2 > 0.05$) of the cumulative plots have been flagged.
- N_{\max} has been given for all nuclei with at least 20 levels. N_c has also been given for all nuclei, because this parameter does not depend on level density or completeness. The participants have agreed that for nuclei with less than 20 levels, or for which the number of uncertain levels is greater than 2, no value of N_{\max} is given, because no reliable procedure can be recommended for their determination. In such cases $U_0=0$, $dU_0=0$, $N_{\max}=1$, $N_{\min}=1$, $U_{\max}=0$ and $\chi^2=0$ will be set. The temperature T is also given for all nuclei since it is determined independently.
- Total transition probabilities, γ -emission probabilities and internal conversion coefficients (ICC) have been included for all nuclei and transitions up to U_{\max} .
- F5.1 format for spin, F10.6 for level energy [MeV], and I3 for parity have been applied.

Several RIPL participants tested the preliminary version of the database by using it in calculations and reported their observations and suggestions. A certain number of mistakes were found and most of the problems have already been corrected in the present files. In particular, the total number of uncertain (+X, +Y ...) levels, the sequential number of the first uncertain level and its energy were added to parall.dat file. Data with +SP or +SN mark have been fixed by adding proton or neutron separation energy to the level energy. Bad decoding of spins, resulting from the missing comma in the ENSDF file have been fixed and estimation of spins from γ -transitions have been improved. The errors originated from the ENSDF source files were reported to J.K. Tuli (BNL) and some of them have been corrected in the ENSDF source.

A new simple test was worked out for checking nuclear temperature (T) derived from the analysis of cumulative plots of discrete levels. It yielded temperature values which are remarkably similar to the T(A) function obtained in the global fitting procedure. The performance of the T(A) function was tested by Ignatyuk by comparing it with the temperature obtained by Gilbert and Cameron. He has found reasonable agreement and recommended to use T(A) in cases for which no direct estimation is possible.

Goriely pointed out that his microscopic calculations provide a factor of 2-3 lower N_{max} values than those obtained in the present analysis. On the other hand, Capote stressed that in the case of ^{27}Al he obtained larger N_{max} values. Herman has reported on extensive testing of N_{max} values for nearly 500 nuclei using Gilbert-Cameron procedure and level densities specific to the EMPIRE code. Perfect fit was obtained for about 50% of analysed cases, fair agreement was found for about 25% and poor for the remaining 25%. It was noted that quality of the fit depends on the model used for level densities. No formatting errors were detected while reading files with discrete levels.

Actions:

1. Belgys: include spin cut-off values obtained from discrete levels in parall.dat file and update the corresponding readme file (15 January 2002)
2. Belgys: fix problems in notation of certain spins and update levels files in the RIPL II directory (15 January 2002)
3. Belgys: provide to NDS a copy of FORTRAN codes used to prepare levels segment (for archival) (15 January 2002)
4. Belgys: send updated html description of the levels segment to Fukahori (15 January 2002)
5. Belgys: finalise TECDOC chapter for levels segment (28 February 2002)

Files:

- level-param.readme
- level-param.dat
- levels.readme
- levels/Zxxx.dat

SEGMENT 3: RESONANCES

(Co-ordinator: A. Ignatyuk)

The average resonance parameters of RIPL-1 were tested by the Brussels and Obninsk groups. Good agreement was found for Γ_γ among the tree RIPL-1 files (Obninsk, Mughabghab and Beijing). The comparison is less favourable for the neutron strength functions, especially for cases with large number of resonances. The misprint errors were noted by the Brussels group for ^{32}S , ^{33}S and ^{208}Pb and corrected. Some additional remarks concerning ^{30}Si and ^{42}K should be clarified before the end of 2001.

It was concluded that additional data for neutron resonance spacings (D_{obs}), present in the Beijing file, are of uncertain origin (based on empirical systematics rather than experimental data) and should not be included in the RIPL-2 library. On the other hand, the revised average resonance parameters were obtained for 20 additional nuclei for which the data on resolved resonance parameters are available in the Sukhoruchkin compilation. This brings total number of D_{obs} in RIPL-2 to 301. Generally, the accuracy of these additional data is rather poor due to the low number of resonances available for the analysis.

New evaluations of the average parameters for p-wave neutron resonances, prepared by the Obninsk group, have been included in the updated version of the RIPL-2 file as an additional column. These resonances provide a good check of consistency since they are known to be about factor of 3 smaller than the s-wave spacings, which is particularly relevant for magic nuclei.

The updated version of the recommended parameters were prepared and reformatted by Capote to the RIPL-2 format. Also, the draft version of the TECDOC Chapter 3 has been prepared and discussed.

Actions:

1. Ignatyuk: clarify remarks concerning ^{30}Si and ^{42}K (31 December 2001)
2. Ignatyuk: provide checked version of the resonance file (1 February 2002)
3. Ignatyuk: prepare and provide final version of the TECDOC Chapter 3 (1 February 2002)

Files:

- resonances.readme
- resonances.dat

SEGMENT 4: OPTICAL

(Co-ordinator: O. Bersillon)

The format of the optical model parameter (OMP) library was revised into final form. The existing library was reformatted, and several corrections were made to the older potentials. The OMP library is provided in two forms: the full library (archival form) and a shorter library with all single-energy potentials removed (user file).

Additions to the OMP library were made including new potentials from JENDL and from the Chinese Nuclear Data Center, as well as several new potentials from Bruyeres and Los Alamos. The new global potential for neutrons and protons from Koning and Delaroche was incorporated, as were new dispersive potentials from Capote.

Kailas agreed to provide new optical potentials for α -particles, both as a limited selection of potentials for the OMP, and a subroutine for more general use.

A file with deformation parameters for collective levels was provided by Fukahori.

Because of the relatively small number of Coupled-Channels potentials now in the OMP library, Ignatyuk will provide some additional new potentials and Young will attempt to compile new ones from the literature.

It was also decided to include general comments on OMP for deformed nuclei in the TECDOC.

An interface code (OM-RETRIEVE) was provided that will generate input files for SCAT2000 and ECIS96 from the OMP library. Utility codes for editing (OM-RIPLMOD) and summarising (OM-SUMRY, OM-TABLE) the OMP library were also provided. The OM-RETRIEVE code is to be revised to produce a concise table of parameters. Additionally, the OM-TABLE code will be changed to produce output tables ordered on Z and A of materials from the OMP library.

Where there are not enough experimental data to define phenomenological OM parameters one has to resort either to global parameterisations or to new microscopic approaches. The semi-microscopic model developed at Bruyeres was presented and the (near-)spherical version is now part of the OM segment. This contribution consists of the MOM code which relies on the Jeukenne, Lejeune, and Mahaux nuclear matter approach, carefully revisited at Bruyeres.

Actions:

1. Bersillon: provide readme for the MOM code (15 December 2001)
2. Bersillon: send corrected version of the MOM manual (15 December 2001)
3. Bersillon: provide final version of the TECDOC Chapter 4 (28 February 2002)
 - a. Young: send TECDOC subchapter to Bersillon (15 February 2002)
4. Young: compile more potentials from the literature including Mann 78 potential for α -particles (15 February 2002)
 - a. Ignatyuk: provide CC potentials to Young (end of 2001)
 - b. Kailas: send TECDOC subchapter and α -potentials to Young and Bersillon (1 February 2002)
 - c. Koning: send particular OMP to Young (15 December 2001)
5. Young: revise OMP input code (OM-RETRIEVE) to produce table of OMP in function of energy (15 January 2002)
6. Young: reorder OMP table according to Z (15 January 2002)
7. Goriely: send subchapter on alpha OMP to Bersillon (15 January 2002)

Files:

- om.readme
- om-data/
 - om-parameter.readme
 - om-parameter-a.dat
 - om-parameter-u.dat
 - om-deformations.readme
 - om-deformations.dat
- om-get/
 - om-retrieve.readme
 - om-retrieve.tgz (FORTRAN code including: om-retrieve.f, om-retrieve.cmb, and gs-mass-sp.dat)
 - alpha-input.readme
 - alpha-input.f
- om-utilities/
 - om-utility.readme
 - om-utility.tgz (FORTRAN codes including: om-summary.f, om-table.f, om-modify.f, omp.cmb, and kd-global.f)
 - om-microscopic/
 - mom.readme
 - mom.tgz
 - mom-manual.ps

SEGMENT 5: LEVEL DENSITIES

(Co-ordinator: A. Ignatyuk)

Total level density

The updated versions of the recommended level-density files for the RIPL-2 were prepared and discussed. They include the following additions and modifications:

- The revised version of the Back Shifted Fermi Gas (BSFG) model parameters consistent with both the recommended RIPL-2 neutron resonance parameters and the evaluated parameters of the recommended low-lying levels were prepared by the Obninsk group.
- The new BSFG systematics developed by the Brussels group, consistent with the recommended RIPL-2 neutron resonance parameters, were discussed and adopted for the RIPL-2 TECDOC.
- The Gilbert-Cameron (GC) and Generalised Superfluid Model (GSM) parameters were revised by Obninsk group in accordance with changes in the RIPL-2 resonance segment.

- The revised files for RIPL-2 were reformatted by R. Capote and included in the present version of the RIPL-2 library.
- The microscopic HF-BCS calculations of the nuclear level densities supplied by Goriely were accepted for the RIPL-2 library. It is recommended to include in the files flags for densities that were normalised to the available experimental data on resonance spacings.
- The single-particle schemes used in the HF-BCS calculations will be supplied by the Brussels group.
- The FRDM single-particle schemes were reformatted by Capote and recommended as corresponding to the accepted FRDM mass table.
- It was decided to move fission level densities into the new segment (FISSION) containing more detailed consideration the fission barriers and corresponding level densities required for astrophysics and ADS applications.

Actions:

1. Ignatyuk: Revise completeness and consistency of the BSFG, GC and GSM files and provide the tested versions (1 February 2002)
2. Ignatyuk: provide file with Myers-Swiatecki shell corrections (1 February 2002)
3. Ignatyuk: finalize and provide TECDOC Chapter 5 (28 February 2002)
4. Goriely: provide TECDOC sections on systematics for the BSFG model and global microscopic model (15 January 2002)
5. Goriely: provide corrected NLD tables with a flag explaining whether the level densities were renormalized to D_{obs} and/or to low-lying states (15 January 2002)
6. Goriely: provide a corrected $N_{\text{max}}_{\text{Umax}}$ file with constant-T predictions of N_{max} and U_{max} (15 January 2002)
7. Goriely: provide new HF-BCS single-particle states with readme file (15 January 2002)

Files:

- single-particle-levels.readme
- single-particle-levels/
 - sp-retrieve.readme
 - sp-retrieve.tgz (FORTRAN code)
 - sp-frdm.readme
 - sp-frdm/Zxxx.dat
 - sp-hfbc.readme
 - sp-hfbc/Zxxx.dat

- total/
 - level-densities-hfbc.readme
 - nmax-umax-hfbc.dat
 - level-densities-hfbc/Zxxx.dat
 - level-densities-bsfg.readme
 - level-densities-bsfg.dat
 - level-densities-gc.readme
 - level-densities-gc.dat
 - level-densities-gsm.readme
 - level-densities-gsm.dat
 - shell-corrections-ms.readme
 - shell-corrections-ms.dat
 - level-densities-micro.readme
 - level-densities-micro.tgz (FORTRAN code)

Partial level densities

Methods for calculating partial level densities for use in preequilibrium model calculations were critically reviewed. A microscopical formulation for the combinatorial calculation of particle-hole state densities based on a convolution of shell-model single particle-states with BCS pairing is recommended for inclusion in RIPL-2. Corresponding retrieval tools to obtain single-particle levels from Segment I tables were developed for RIPL2.

Still, one of the most useful approaches is to determine partial level densities within an equidistant single-particle model using closed-form formulae, as proposed by Williams and further modified and improved by Kalbach, Fu, Baguer *et al*, Farget-Rejmund *et al* and Mao. An AVRIGEANU code will be revised and Baguer *et al* formulation will be included. Finite hole-depth and binding energy restrictions will also be taken into account.

Actions:

1. Capote: to provide an updated version of the AVRIGEANU code (28 February 2002)
2. Capote: to revise partial level density chapter for the TECDOC, including theoretical background and references (15 January 2002)
3. Ignatyuk and Capote: provide revised version of the section of the TECDOC Chapter 5 on partial level densities, taking into account comments provided by the CRP members (February 28 2002)

Files:

- partial-level-densities.readme
- partial/
 - pld-microscopic.readme
 - pld-microscopic.tgz (FORTRAN code)
 - pld-analytical.readme
 - pld-analytical.tgz (FORTRAN code)

SEGMENT 6: GAMMA

(Co-ordinator: M. Herman/V. Plujko)

The existing files in the Gamma segment were reformatted according to the RIPL-2 standard. In particular kopecky.dat file has been brought into a computer readable form. The segment was enlarged by including the compilation of calculated GDR widths and energies provided by Goriely.

Theory-supported practical approach, based on microcanonical description of initial states (modified Lorentzian (MLO)), for calculation of the dipole radiative strength function (RSF) was compared with experimental data as well as with the SLO and EGLO models.

After discussion the CRP participants suggested that only a subroutine, which calculates γ -strength function for given A, Z, γ -ray and excitation energy, will be retained in the RIPL-2 library.

Participants agreed that strength functions for other multipolarities will be carried over from RIPL-1. Overall description of the Segment 6 in TECDOC will be provided by Herman and Plujko.

Actions:

1. Plujko: provide description and comparison between MLO approach and the Mughabghab-Dunford model for the TECDOC (28 February 2002)
2. Plujko: provide subroutine which calculates dipole radiative strength function for given A, Z, γ -ray and excitation energy (15 January 2002)
3. Goriely: provide files with dipole RSF calculations within QRPA approach (15 January 2002).

Files:

- gamma-strength-exp.readme
- gamma-strength-exp.dat
- gamma-strength-analytic.readme
- gamma-strength-analytic.tgz (FORTRAN code)
- gamma-strength-micro.readme
- gamma-strength-micro/Zxxx.dat

- gdr-parameters-exp.readme
- gdr-parameters-exp.dat
- gdr-parameters-theor.readme
- gdr-parameters-theor.dat

SEGMENT: ANGULAR

Participants decided that Angular segment will not be included in RIPL-2 library thus users interested in angular distributions in preequilibrium reactions will be referred to RIPL-1.

SEGMENT 7: FISSION

(Co-ordinator S. Goriely)

Fission is a new RIPL-2 segment introduced during the present CRP meeting. This segment will keep the RIPL-1 Maslov recommendation, but will include, in addition, global prescription for barriers and nuclear level densities at saddle points. In addition, a liquid drop estimate of the high-energy barriers will be provided.

Actions:

1. Goriely: provide experimental fission barriers into the ETFSI barriers file (15 January 2002)
2. Goriely: provide NLD tables at the inner and outer saddle points (15 January 2002)
3. Goriely and Ignatyuk: write introduction of the TECDOC stressing astrophysics and ADS appl. (15 January 2002)
4. Ignatyuk: provide prescription (subroutine) section for high energy barriers (15 January 2002)
5. Ignatyuk: provide subroutine for high energy barriers (30 December 2001)
6. Ignatyuk: extend Maslov RIPL-1 files including preactinide Smirenkin barriers (30 December 2001)
7. Goriely: simplify Maslov section of TECDOC; Ignatyuk: TECDOC section on nuclear level densities at saddle points; Goriely: TECDOC section on ETFSI fission barriers (15 January 2002).

Files:

- fis-barrier-exp.readme
- fis-barrier-exp.dat (previous maslov.dat file)
- fis-barrier-etfsi.readme
- fis-barrier-etfsi.dat
- lev-den-hfbc.s.readme
- fis-levden-hfbc-inner/Zxxx.dat
- fis-levden-hfbc-outer/Zxxx.dat
- fis-barrier-liquiddrop.readme
- fis-barrier-liquiddrop.f

RETRIEVAL TOOLS (WWW)

(Co-ordinator: T. Fukahori)

The preliminary version of the RIPL-2 Home Page (<http://wwwndc.tokai.jaeri.go.jp/~fukahori/RIPL-2/>) and Top Pages for all segments have been prepared. The available retrievals include:

Masses

- retrieval of mass excesses calculated by FRDM and HFB as well as experimental ones compiled by Audi et al.
- retrieval of abundances from BNL Wallet Card provided by Koning

Gamma

- retrieval of Giant Dipole Resonance (GDR) parameters from ETFSI and Beijing files, and γ -ray strength functions from *gamma-strength-exp.dat*

Following WWW retrieval tools will be provided:

General

- link to all README files from the WWW page

Masses

- ftp link to the individual files
- description of each parameter in the retrieved table will be merged and moved to the end of page
- Q-value calculation tool using all RIPL-2 sources

Levels

- retrieval of numerical data for discrete levels, decay data, completeness of level scheme (N_{\max}), completeness of spin assignment (N_c), etc.
- plotting of cumulative levels including N_{\max} and N_c

Resonances

- retrieval of numerical data for average resonance parameters for s- and p-wave resonances
- plot of average resonance parameters as a function of A (whole and local ($Z=\text{const.}$))

Optical

- retrieval of numerical data for optical potential parameters (index and data (raw and energy tabulated potential parameters))
- calculation of cross sections (total, elastic and non-elastic) as a function of energy, and elastic scattering angular distribution at single energy for selected parameter sets (max. 3) using SCAT2000 as well as TOTELA systematics (table and plot)
- calculation of scattering radius and reduced strength functions at 10 keV neutrons
- calculation of transmission coefficients
- calculation of potential shape (comparison plot)
- calculation of volume integral (comparison plot)
- retrieval of deformation parameters for collective levels

Densities

Total level density parameters

- retrieval of level density parameters for Gilbert-Cameron, BSFG, SFM formulas and microscopic (HF-BCS) level density
- plot of cumulative number of discrete levels compared with formulae predictions and average level spacing (D_0)
- plot of a -parameters for each formula for fixed Z , A , N
- link to the codes from RIPL-1 (including retrieval code)
- link to single-particle level files (HF-BCS and FRDM)

Partial level density

- link to the codes supplied by Capote (including retrieval code)
- link to single-particle level files (HF-BCS and FRDM)

Gamma

- plot of Giant Dipole Resonance (strength function) shape for the combinations of individual formulae and parameters (Fixed temp. $T=0$, $E_\gamma < 20$ MeV)
- link to the γ -strength function code supplied by Plujko
- calculation of the dipole radiative strength function with the code supplied by Plujko

Fission

- retrieval of numerical data for microscopic (HF-BCS) level density,
- retrieval of numerical data for microscopic and experimental fission barriers (Maslov and Smirenkin)
- link to liquid drop code

TESTING

Tests have been performed on the optical, resonance and levels segments. A number of misprints and erroneous coding has been detected and corrected. Final testing will be performed once the entire database is available from the IAEA-NDS server. Segment co-ordinators will download the segment(s) they are responsible for in order to check the integrity of the data. Herman will check all FORTRAN codes.

The global testing of RIPL-2 database has been performed in three separate exercises. Large numbers of nuclear reaction cross sections were calculated by means of the nuclear model codes EMPIRE-II, UNF and TALYS.

Herman reported on the results for the most important neutron-induced reactions on 22 targets from ^{40}Ca up to ^{208}Pb in the energy range from 1 keV up to 20 MeV. The 2-17 beta version of the statistical model code EMPIRE-II has been used with all default parameters except those differentiating the 3 series of runs. In all cases TUL MSD and Heidelberg MSC models were used for preequilibrium emission of neutrons, and exciton model (DEGAS) for preequilibrium emission of protons and γ s. These were complemented with Hauser-Feshbach calculations including widths fluctuations (HRTW model) at incident energies below 5 MeV. The results were converted into the ENDF-6 format and compared with experimental data available from the EXFOR library. Three sets of calculations were performed in order to test new levels segment (including N_{max}), Koning's global optical potential and HF-BCS level densities. No problems were encountered while processing the new RIPL-2 files, which indicates that the files are formally correct. Comparison with experimental data shows reasonable overall agreement for most of the calculations. There is a clear indication that calculations using new RIPL-2 files fit experimental data better than those with default EMPIRE-II parameters, which demonstrates improvement brought about by RIPL-2. The HF-BCS microscopic level densities were found to perform comparable to the phenomenological level densities and in some cases even better. However, significant discrepancies among the results of the three sets of calculations were observed in a number of cases. This illustrates the importance of the model parameters and proves the practical usefulness of the RIPL-2 library for applications and basic research.

The second exercise has been carried out by the Beijing group. The calculations were performed for 103 nuclei from the mass region 69-160, in the incident energy range from 0.1 to 20 MeV, using the recently developed code UNF. All input parameters were taken from the RIPL database. Agreement with the experimental data was found to be very good for total and elastic cross sections (within 3%). For other main reaction channels, calculations reproduced the shape, but some parameter adjustments were necessary in order to fit the absolute cross sections.

TALYS calculations were performed for various neutron-induced reactions on 5 isotopes from ^{52}Cr to ^{208}Pb . Default input parameters originated from RIPL-2. This exercise concentrated on the comparison of Ignatyuk-type and microscopic level densities and provided reasonable agreement with experimental data for both formulations.

CODE INTERFACES

The work on interfaces between selected nuclear model codes and RIPL-2 segments has been continued facilitated by the standard RIPL-2 format. The two optical model codes (ECIS and SCAT2) and two statistical model codes (EMPIRE-II and UNF) use RIPL-2 library to a large extent. Interface code preparing inputs for ECIS and SCAT2 have been prepared by Young and is available in the optical segment. The UNF code makes use of RIPL optical potentials, masses, levels, level densities and GDR parameters. EMPIRE-II accesses RIPL-2 database directly and retrieves optical model parameters, discrete levels and microscopic level densities (HF-BCS). Built in systematics for GDR parameters and prescriptions for γ -strength functions follow RIPL-2 recommendations. EMPIRE-II library of masses and ground state deformations is numerically identical to the *mass-frdm.dat* in the mass segment of RIPL-2.

TECDOC

As agreed in Varenna, the RIPL-2 TECDOC will closely follow the structure of its predecessor. However, two modifications to the TECDOC structure were decided during the present meeting: (i) ANGULAR segment will be removed from RIPL-2 since there were no changes introduced by the present CRP and (ii) a chapter on global testing of RIPL-2 in reaction calculations will be added. The theoretical descriptions in TECDOC-1034 will be updated to reflect changes in the library. The chapter on optical models will contain comments on the use of optical potentials for deformed nuclei. Co-ordinators of the segments are responsible for the preparation of the respective TECDOC chapters. Each chapter will contain descriptions of the testing of the corresponding RIPL-2 database. The co-ordinators will arrange for independent reviewers to cross check the contents of their segments.

ACTIONS

Actions mentioned previously in the sections regarding each segment are summarised below for convenience.

Belgys:

1. include spin cut-off values obtained from discrete levels in *parall.dat* file and update the corresponding *readme* file (15 January 2002)
2. fix problems in notation of certain spins and update levels files in the RIPL II directory (15 January 2002)
3. provide to NDS a copy of FORTRAN codes used to prepare levels segment (for archival) (15 January 2002)
4. send updated *html* description of the levels segment to Fukahori (15 January 2002)
5. finalise TECDOC chapter for levels segment (28 February 2002)

Bersillon:

1. send corrected version of the MOM manual (15 December 2001)
2. provide readme for the MOM code (15 December 2001)
3. provide final version of the TECDOC Chapter 4 (28 February 2002)

Capote:

1. revise partial level density chapter for the TECDOC, including theoretical background and references (15 January 2002)
2. with Ignatyuk: provide revised version of the section of the TECDOC Chapter 5 on partial level densities, taking into account comments provided by the CRP members (28 February 2002)
3. provide an updated version of the AVRIGEANU code (28 February 2002)

Goriely:

1. replace the ETFSI table with the latest HFB masses and the associated readme file (15 January 2002)
2. include table of HFB densities (1 file per element) (15 January 2002)
3. finalise draft of the TECDOC chapter by including a subsection on HFB densities (15 January 2002)
4. provide TECDOC sections on systematics for the BSFG model and global microscopic model (15 January 2002)
5. provide corrected NLD tables with a flag explaining whether the level densities were renormalized to D_{obs} and/or to low-lying states (15 January 2002)
6. provide a corrected $N_{\text{max}}_{\text{Umax}}$ file with constant-T predictions of N_{max} and U_{max} (15 January 2002)
7. provide new HF-BCS single-particle states with readme file (15 January 2002)
8. provide files with dipole RSF calculations within QRPA approach (15 January 2002)
9. provide experimental fission barriers into the ETFSI barriers file (15 January 2002)
10. provide NLD tables at the inner and outer saddle points (15 January 2002)
11. with A. Ignatyuk: write introduction of the TECDOC stressing astrophysics and ADS appl. (15 January 2002)
12. simplify Maslov section of TECDOC (15 January 2002)
13. provide TECDOC section on ETFSI fission barriers (15 January 2002)
14. send subchapter on alpha OMP to Bersillon (15 January 2002)

Ignatyuk:

1. provide subroutine for high energy fission barriers (30 December 2001)
2. extend Maslov RIPL-1 files including preactinide Smirenkin barriers (30 December 2001)
6. clarify remarks concerning ^{30}Si and ^{42}K (30 December 2001)
3. provide CC potentials to Young (30 December 2001)
4. revise completeness and consistency of the BSFG, GC and GSM files and provide tested versions (1 February 2002)
5. provide prescription (subroutine) section for high energy barriers (15 January 2002)
6. provide checked version of the resonance file (1 February 2002)
7. prepare and provide final version of the TECDOC Chapter 3 (1 February 2002)
8. provide file with Myers-Swiatecki shell corrections (1 February 2002)
9. finalize and provide TECDOC Chapter 5 (28 February 2002)
10. provide TECDOC section on nuclear level densities at saddle points (28 February 2002)

Young:

1. revise OMP input code (OM-RETRIEVE) to produce table of OMP in function of energy (15 January 2002)
2. reorder OMP table according to Z (15 January 2002)
3. send TECDOC subchapter to Bersillon (15 February 2002)
4. compile more potentials from the literature including Mann78 potential for α -particles (15 February 2002)

Kailas:

1. send TECDOC subchapter and alpha-potentials to Young and Bersillon (1 February 2002)

Koning:

1. send particular OMP to Young (15 December 2001)

Plujko:

1. provide subroutine which calculates dipole radiative strength function for given A, Z, γ -ray and excitation energy (15 January 2002)
2. provide description and comparison between MLO approach and the Mughabghab-Dunford model for the TECDOC (28 February 2002)

CONCLUSIONS

Presentations and discussions during the Meeting showed that the CRP is close to completion. The initial scope of the CRP has been extended during the course of the work to include large amounts of additional data and to replace certain files with updates. Most of these files were available during the Meeting. However, due to necessary minor corrections practically all of them will have to be resubmitted. All participants must keep to the agreed deadlines for their respective actions in order to release the library in a timely manner.

At the end of the Meeting participants discussed possible improvements of the current project and formulated recommendations for further activities. These findings are summarised below:

- RIPL-2 library should be complemented with a set of routines for the calculation of certain input parameters (such as level densities, binding energies, gamma strength functions, etc.) in order to facilitate user access to the database and to avoid misuse of the parameters.
- More attention should be dedicated to the use of microscopic models for producing parameters.
- Parameters related to the fission channel contained in RIPL-2 need more accurate analysis and improvements.
- RIPL-2 provides good sets of parameters for spherical and near-spherical nuclei. On the other hand, data for the deformed nuclei are scarcer and less accurate. In particular there is a need for Coupled Channels optical potentials and gamma-ray strength functions for the deformed nuclei. Also, the problem of collective enhancement of level densities should be addressed in more detail in order to provide a reliable prescription for calculating level densities in deformed nuclei. The latter are often needed for ADS and new reactor concepts.
- RIPL-2 concentrated on incident energies below 20 MeV, a typical limit for standard nuclear data files. However, new applications such as ADS, medical radioisotope production and radiation treatment need data at much higher energies (up to 1.5 GeV in the case of ADS). Most of the parameters available from RIPL-2 can not be extrapolated to such high energies (e.g., temperature dependence of the GDR width). In particular, there should be consistency between statistical model calculations at low energies and the intranuclear cascade model commonly used at high energies.
- Special techniques should be applied for the determination of the parameters for nuclei far from the stability line for which there are usually no experimental data available. These nuclei are important for ADS and astrophysics.
- Use of the results obtained in heavy ion induced reactions could be helpful in determining model parameters, especially for nuclei far from the stability line.
- Medical applications require charged particle reactions, which should be better represented in the parameter library.
- New experimental data from the recently initiated projects (HINDAS and NTOF at CERN) should become available within a year or two, offering good possibilities for the testing of RIPL-2 parameters.

The participants concurred that these concerns should be addressed by a new CRP.

International Atomic Energy Agency
Third Research Co-ordination Meeting on
Nuclear Model Parameter Testing for Nuclear Data Evaluation
(Reference Input Parameter Library: Phase II)

IAEA Headquarters
Vienna, Austria
3 - 7 December 2001

AGENDA

Monday, 3 December

09:30 - 10:00 Opening
10:00 - 12:00 Status reports (10 minutes/person)
12:00 - 12:30 Review of actions
14:00 - 15:30 Segment III (Resonances)
15:30 - 17:00 Segment IV (Optical)

Tuesday, 4 December

09:00 - 11:30 Segment IV (Optical cont.)
11:30 - 12:30 Segment I (Masses)
14:00 - 17:00 Segment II (Levels)

Wednesday, 5 December

09:00 - 12:30 Segment V (Densities)
14:00 - 15:00 Segment VII (Fission)
15:00 - 16:00 Segment VI (Gamma)
16:00 - 17:00 Global testing

Thursday, 6 December

09:00 - 10:30 Interfaces and retrieval tools
10:30 - 12:30 Group reports
14:00 - 17:00 Group reports cont.

Friday, 7 December

09:00 - 10:00 Library structure and names
10:00 - 12:00 Discussion of the TECDOC
12:00 - 13:00 Recommendations for RIPL-III and cooperation with WPEC subgroup

International Atomic Energy Agency
Third Research Co-ordination Meeting on
Nuclear Model Parameter Testing for Nuclear Data Evaluation
(Reference Input Parameter Library: Phase II)

IAEA Headquarters

Vienna, Austria

3 - 7 December 2001

LIST OF PARTICIPANTS

BELGIUM

Stephane Goriely

Institut d'Astrophysique, CP-226

Campus de la Plaine

Université Libre de Bruxelles

Boulevard du Triomphe

B-1050 Brussels

Tel.: +32-2-650-2843

Fax: +32-2-650-4226

E-mail: sgoriely@astro.ulb.ac.be

FRANCE

Olivier Bersillon

Service de Physique Nucléaire

Centre d'Etudes Nucléaires de

Bruyères-le-Châtel

B.P. No. 12

F-91680 Bruyeres-le-Châtel

Tel.: +33-1-6926-5414

Fax: +33-1-6926-7063

E-mail: olivier.bersillon@cea.fr

CHINA

Ge Zhigang

China Nuclear Data Center

China Institute of Atomic Energy

P.O. Box 275 (41)

102413 Beijing

Tel.: +86-10-6935-7275

Fax: +86-10-6935-7008

E-mail: gezg@iris.ciae.ac.cn

HUNGARY

Tamas Belgya

Nuclear Physics Department

Institute of Isotope and Surface Chemistry

Chemical Research Center

P.O. Box 77

H-1525 Budapest

Tel.: +36-1-392-2539

Fax: +36-1-392-2584

E-mail: belgya@alpha0.iki.kfki.hu

CUBA

Roberto Capote Noy

Centro de Estudios Aplicados al

Desarrollo Nuclear

Calle 30 #502 e/5ta y 7ma

Miramar, Playa

11300 Ciudad de la Habana

Tel.: +34-954-550924

E-mail: rcapotenoy@yahoo.com

INDIA

Swaminathan Kailas

Nuclear Physics Division

Bhabha Atomic Research Centre

Trombay, Mumbai 400 085

Tel.: +91-22-559-3883

Fax: +91-22-550-5151

E-mail: kailas@magnum.barc.ernet.in

JAPAN

Tokio Fukahori

Nuclear Data Center
Department of Nuclear Energy System
Japan Atomic Energy Research Institute
Tokai-mura, Naka-gun
Ibaraki-ken 319-1195
Tel.: +81-29-282-5907
Fax: +81-29-282-6216
E-mail: fukahori@ndc.tokai.jaeri.go.jp

NETHERLANDS

Arjan Koning

Fuels Actinides and Isotopes
NRG Nuclear Research and
Consultancy Group
Westerduinweg 3
P.O. Box 25
NL-1755 ZG Petten
Tel.: +31-22456-4051
Fax: +31-22456-3490
E-mail: koning@nrg-nl.com

RUSSIA

Anatoly V. Ignatyuk

Institute for Physics and Power
Engineering
Bondarenko Sq. 1
249020 Obninsk, Kaluga Region
Tel.: +7-084-399-8035
Fax: +7-095-230-2326
E-mail: ignatyuk@ippe.obninsk.ru

UKRAINE

Vladimir Plujko

Nuclear Physics Department
Faculty of Physics
Taras Shevchenko National University
Prospect Acad. Glushkova 2, Bldg. 11
03022 Kiev-22
Tel.: +380-44-261-34-94
Fax: +380-44-265-44-63
E-mail: plujko@mail.univ.kiev.ua

UNITED STATES OF AMERICA

Richard A. Meyer

RAME Inc. & Clark University
129 Maravista Avenue
East Falmouth, MA 02536
E-mail: ramuth@adelphia.net

Pavel Obložinský

National Nuclear Data Center
Bldg. 197D
Brookhaven National Laboratory
P.O. Box 5000
Upton, NY 11973-5000
Tel.: +1-631-344-2814
Fax: +1-631-344-2806
E-mail: oblozinsky@bnl.gov

Phillip G. Young

T-16, MS B-243
Los Alamos National Laboratory
Los Alamos, NM 87545
Tel.: +1-505-667-7670
Fax: +1-505-667-9671
E-mail: pgy@lanl.gov

IAEA

Michal Herman (Scientific Secretary)

Nuclear Data Section
Wagramer Strasse 5
A-1400 Vienna
Tel.: +43-1-2600-21713
Fax: +43-1-26007
E-mail: herman@iaeand.iaea.or.at

Alan Nichols

Nuclear Data Section
Wagramer Strasse 5
A-1400 Vienna
Tel.: +43-1-2600-21709
Fax: +43-1-26007
E-mail: a.nichols@iaea.org

Technical input

1.	Work Report <i>S. Goriely</i>	31
2.	Los Alamos Progress Report for RIPL-II <i>P.G. Young and M.B. Chadwick</i>	39
3.	Status of Japanese Contribution to RIPL-2 <i>T. Fukahori</i>	53
4.	New Neutron and Proton Optical Models <i>A.J. Koning and J.P. Delaroche</i>	55
5.	Global Alpha – Nucleus Optical Model Potential <i>A. Kumar and S. Kailas</i>	77
6.	The Testing of Koning’s Global Potential <i>Ge Zhigang and Sun Zhengjun</i>	81
7.	Testing and Improvements of Dipole Radiative Strength Functions for Gamma Segment of the RIPL-II <i>V.A. Plujko</i>	85
8.	Test of RIPL-2 Cross Section Calculations <i>M. Herman</i>	95
9.	The UNF Code and its Interface PREUNF <i>Zhang Jingshang, Ge Zhigang and Sun Zhengjun</i>	109
10.	The Basic Testing of RIPL with UNF Code <i>Ge Zhigang, Zhang Jingshang and Sun Zhengjun</i>	111
11.	Comparison of Phenomenological and Microscopic Level Densities in Nuclear Reaction Calculations <i>A. Koning</i>	117

**Readers, please note:
The attachments were prepared by CRP members
before the meeting – subsequent discussions
have resulted in modifications to recommendations
that are NOT reflected in these texts.**

Work Report

Stephane Goriely
Institut d'Astronomie et d'Astrophysique
Université Libre de Bruxelles, Belgium

November 23, 2001

1 Improvements and extensions

1.1 Segment 1: Atomic Masses

New files have been added to Segment 1 in agreement with the Varenna meeting (2000, INDC(NDS)-416). These concern

- goriely-frdm95.dat and goriely-frdm95.readme: properly (i.e as agreed) formatted file with FRDM (version 1995) ground state properties (masses, microscopic corrections and β -deformations including Audi & Wapstra 1995 experimental and recommended masses when available).
- goriely-etfsi00.dat and goriely-etfsi00.readme: properly (i.e as agreed) formatted file with ETFSI (version 2) ground state properties (masses, deformations, density distribution and shell correction energies, including Audi & Wapstra 1995 experimental and recommended masses).
- goriely-expdef01.dat and goriely-expdef01.readme: experimental β -deformations from Raman et al. (2001).
- goriely-dz96.f and goriely-dz96.readme: original Duflo & Zuker (1996) fortran subroutine to estimate nuclear masses

Some Comments: We propose to replace in this Segment the ETFSI mass table by the newly-derived HFB mass table (Samyn et al. 2001). The HFB predictions have a sounder theoretical basis than ETFSI, especially in the extrapolation towards the exotic neutron-rich nuclei. Both the corresponding .dat and .readme files are ready. This is a suggestion open to further discussions.

In addition, it was decided in Varenna to include experimental masses within the theoretical files (and include a flag to distinguish the origin). However, in this case, at the interface between experimental and theoretical masses, it will not be possible for users to estimate mass differences within the same set. Remember the Ripl-1 warning to users: "When calculating Q-values, one should use atomic masses from the same source to avoid systematic errors. This means that one should use consistently either experimental values, or calculated values". Shouldn't we provide separately the theoretical and experimental atomic masses (for example in two columns) within the frdm95.dat and etfsi2.dat (or hfb01.dat) files ?

1.2 Segment 5: Densities - Total

- nld.zxxx and goriely-nld.readme: Nuclear Level Densities derived for some 8000 nuclei (with $8 \leq Z \leq 110$ and lying between the neutron and the proton driplines) from the microscopic statistical approach based on a HF+BCS single-particle level scheme. The nuclear level densities are given in a table format (one file per isotopic chain Z) for excitation energies from $0.25 \leq U[\text{MeV}] \leq 150$ and for spin ranging from $J=0$ ($1/2$) to $J=29$ ($59/2$). In addition, to the spin-dependent level density, are also provided the nuclear temperature, the cumulative number of level, the total level and state densities. The spin-cut-off factors are not provided. The microscopic HFBCS-based NLDs have been renormalized on experimental data (278 neutron resonance spacings and 1287 low-lying level schemes) to account for the available experimental information. All the details are published in Demetriou and Goriely(2001, Nucl. Phys. A695, 3)
- nmax_umax.hfbcs file: For completeness, in addition to the nuclear level density, the cumulative number of low-lying levels N_{max} (and corresponding energy U_{max}) up to which the experimental set of levels is complete can be found in the "nmax_umax.hfbcs" file (including some 1220 nuclei for which more than 20 excited levels are known experimentally).
- Z_xxx.dat and goriely-spletfsi00.readme: ETFSI single-particle level scheme including for about 8000 nuclei the deformation and for both the neutron and proton systems, the pairing strength and cut-off energies, and the single-particle level scheme (energy, parity, spin). All the data files are provided in a format identical to the files including the FRDM single-particle levels.

Comment: We propose to replace in this Segment the ETFSI single-particle levels and pairing strength by the HF-BCS predictions (Goriely et al. 2001) used to derive the nuclear level density tables (see above). The HFBCS predictions have a sounder theoretical basis than ETFSI, and the pairing strength is better suited for nuclear level density calculations. Both the corresponding .dat and .readme files are ready. This is a suggestion open to further discussions.

- As requested during the Varenna meeting, a new BSFG formula with all the required input fitted on the RIPL-2 D_{exp} compilation has been developed. A simple shell-dependent BSFG formula has been derived successfully and fitted to the 278 D_{exp} values from the RIPL compilation with a final $f_{rms} = 1.78$.

It corresponds to the classical BSFG approximation of the state density $\rho(U)$ and level density $\rho(U, J)$ of a nucleus (Z, A) with a given angular momentum J and excitation energy U , i.e

$$\rho(U) = \frac{\sqrt{\pi}}{12a^{1/4}(U - \delta)^{5/4}} e^{2\sqrt{a(U - \delta)}} \quad (1)$$

$$\rho(U, J) = \frac{2J + 1}{2\sqrt{2\pi}\sigma^3} \rho(U) e^{-(J + 1/2)^2/2\sigma^2} \quad (2)$$

where microscopic (shell, pairing and deformation) corrections to the binding energy are introduced in the U -dependent NLD parameter a through the semi-classical approximation (Goriely, 1996, Nucl. Phys. A605, 28)

$$a(U) = \tilde{a}[1 + 2 \gamma E_{mic} e^{-\gamma(U - \delta)}] \quad (3)$$

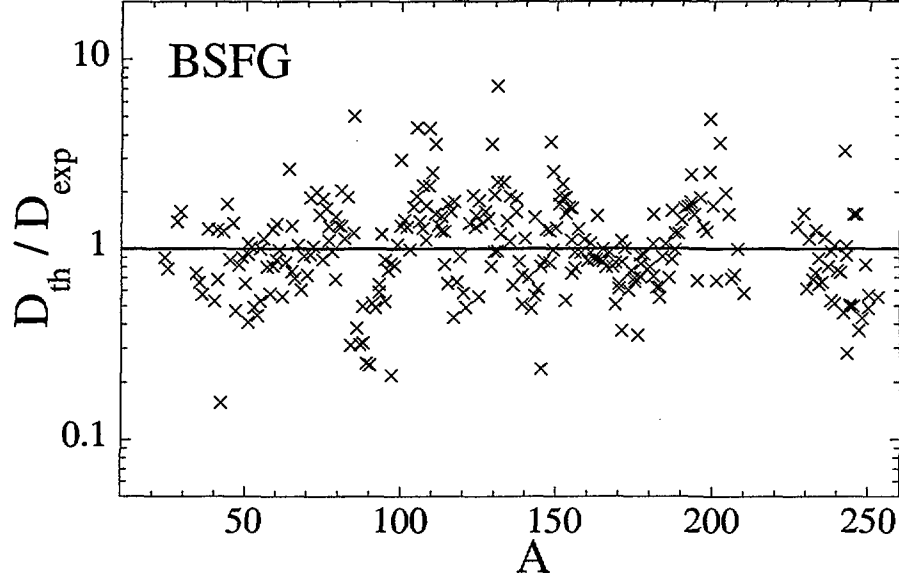


Figure 1: Comparison between theoretical BSGF (D_{th}) and experimental (D_{exp}) values of the s-neutron resonance spacings.

The microscopic energy $E_{mic} = E_{tot} - E_{LD}$ is derived from the experimental (or theoretical) binding energy $E_{tot} = M_{tot} - N M_n - Z M_H + B_e Z^{2.39}$ (where $M_n = 8.07132281$ MeV, $M_H = 7.2889694$ MeV, and $B_e = 1.433 \cdot 10^{-5}$ MeV; see Segment 1) and the simple spherical liquid drop formula

$$E_{LD} = a_v A + a_s A^{2/3} + (a_{sym} + a_{ss} A^{-1/3}) A I^2 + a_c \frac{Z^2}{A^{1/3}} \quad (4)$$

where $I = (N - Z)/A$. A fit to the 1888 $N, Z \geq 8$ experimental masses of Audi & Wapstra 1995 (with a final rms deviation of 3 MeV) leads to the liquid drop parameters (in MeV) $a_v = -15.6428$, $a_s = 17.5418$, $a_{sym} = 27.9418$, $a_{ss} = -25.3440$ and $a_c = 0.70$. Concerning the NLD parameters, a fit to the RIPL-2 experimental s-neutron resonance spacings D_{exp} gives $\tilde{a} = 0.1012A + 0.036A^{2/3}$ MeV $^{-1}$, $\gamma = 0.03$, $\sigma^2 = 0.0194A^{5/3} \sqrt{U/a}$ and $\delta = 0.5, 0, -0.5$ MeV for even-even, odd-mass and odd-odd nuclei, respectively. This global parametrization predicts the experimental D_{exp} of RIPL-2 with a rms deviation $f_{rms} = 1.78$ (Fig. 1) and those of compilation of Iljinov et al. (1992, NPA543, 517) with $f_{rms} = 1.50$. The formula is published in the ND2001 conference proceedings.

1.3 Segment 5: Densities - Fission

New files have been added in agreement with the Varenna meeting (2000, INDC(NDS)-416).

- goriely-fisbar00.dat and goriely-fisbar00.readme: properly (i.e as agreed) formatted file including the predictions of the fission barriers and saddle point deformations obtained within the ETFSI method for some 2301 nuclei with $78 \leq Z \leq 120$ up to the neutron-drip line.

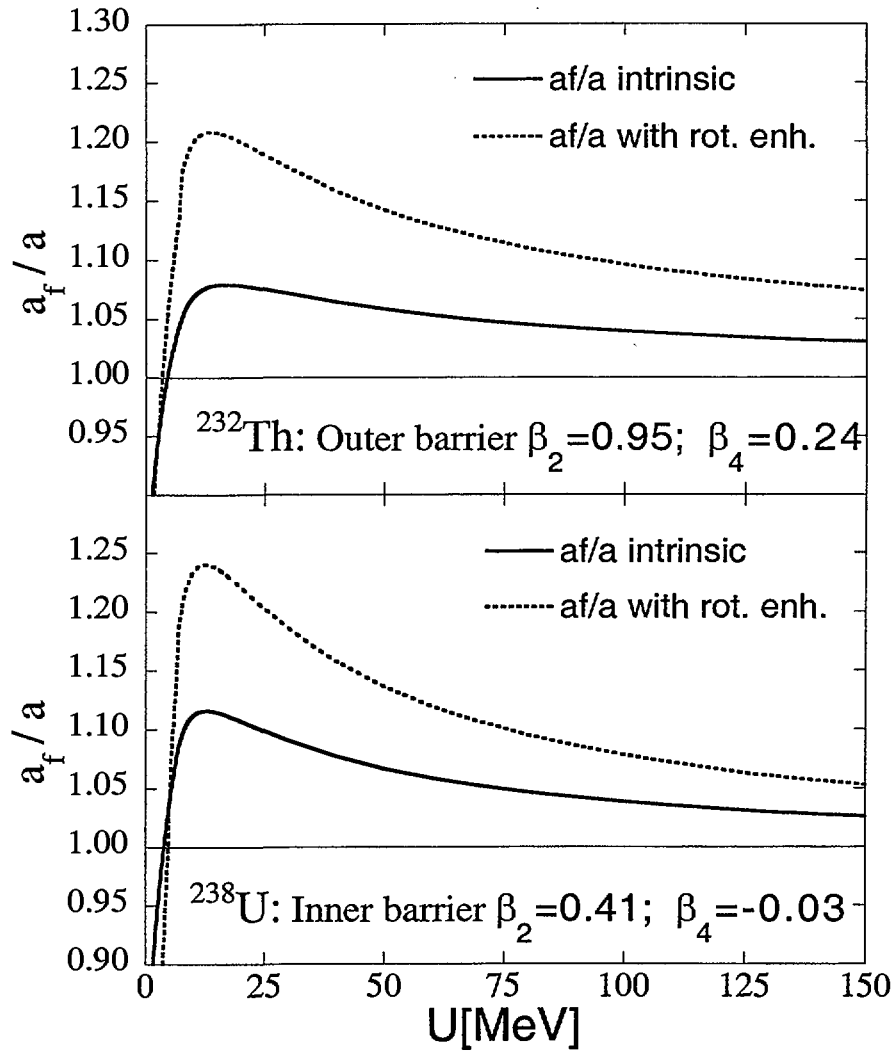


Figure 2: a_f/a ratios with or without rotational enhancement as a function of the excitation energy for ^{232}Th and ^{238}U predicted by the HFBCS-based nuclear level density.

Comment: Recent developments brought to our deformed Hartree-Fock code, in particular with the introduction a left-right asymmetry, give us the possibility to determine nuclear structure properties (and in particular single-particle level densities) at the saddle point with constrained quadrupole, octupole and hexadecapole deformations. This also enables us now to estimate the NLD of any heavy nucleus at the saddle point deformation, and consequently the a_f/a ratio of the NLD a -parameter at the saddle point corresponding to the (inner or outer) fission barrier to the value in the equilibrium ground-state configuration. Two examples are displayed in Fig.2 for the ^{232}Th outer barrier and the ^{238}U inner barrier. The saddle point deformations correspond to the values determined by the ETFSI model (see above). The ground-state properties (single-particle level density, pairing corrections) are determined within the constrained Hartree-Fock BCS model at the saddle point deformation with the MSk7 Skyrme force. The nuclear level density is estimated within the microscopic statistical approach (Demetriou and Goriely, 2001, Nucl. Phys. A695, 3) based the Hartree-Fock ingredients at the saddle point deformation, assuming no damping of the collective degrees of freedom. Figure 2 gives two estimates of the a_f/a ratios. The first one corresponds to the intrinsic a_f/a ratio, i.e the entropy S_f/S ratio (note that in the microscopic approach, $a = U/T^2$ differs from $a = S/2T$, and consequently the entropy ratio must be considered to estimate the traditionally a -ratio used in practical applications). The second gives the equivalent a -ratio when the rotational enhancement factor is implicitly included in the a -parameter. In the latter case, the equivalent a -value is determined from

$$\rho(U) = \frac{\sqrt{\pi}}{12 a^{1/4} U^{5/4}} e^{2\sqrt{a} U} \quad (5)$$

where ρ correspond to the total nuclear level density with the collective contribution of the rotational band. The a_f/a to be adopted in reaction cross-section calculation obviously depends on the nuclear level density formula considered, and more specifically if the collective enhancement factors are explicitly taken into account.

The ratio of the NLD at the ground-state deformation to the NLD at the saddle point deformation of the inner and outer fission barriers has been determined for a grid of some 2000 heavy nuclei corresponding to the fisbar00.dat compilation of fission barriers. The ratio a_f/a with and without collective enhancement is tabulated on an energy grid in the range $0 \leq U$ [MeV] ≤ 150 . The RIPL-2 meeting should consider the relevancy of the present data for reaction calculation and decide if it would be worth or not including this data in the present compilation !

1.4 Segment 6: γ -ray strength function

1.4.1 GDR energy and width files

New files have been added in agreement with the Varenna meeting (2000, INDC(NDS)-416), namely **goriely-gdr00.dat** and **goriely-gdr00.readme**, corresponding to properly (i.e as agreed) formatted file including the predictions of the GDR energies and shell-dependent widths for about 6000 nuclei. The ground-state properties (i.e nucleon density distribution, ground-state deformation and shell correction) are taken from the ETFSI mass model. Note that in contrast to the previously described quantities, HF calculations do not provide estimate of the (pure) shell correction, and can therefore not replace the ETFSI prediction.

In addition, it was decided to include in Segment 6 of the TECDOC (Coordinator: M.

Herman), details about the hybrid formula for the $E1$ -strength function, please find them below.

1.4.2 The hybrid formula for the $E1$ -strength function

The total photon transmission coefficient from a CN excited state is normally dominated by the $E1$ transition which is classically estimated within the Lorentzian representation of the GDR, at least for medium- and heavy-mass nuclei. Reaction theory relates the γ -transmission coefficient for excited states to the ground state photoabsorption assuming the giant resonance to be built on each excited state. Experimental photoabsorption data confirms the simple semi-classical prediction of a Lorentzian shape at energies around the resonance energy E_{GDR} . However, the more detailed description of the $E1$ strength function at energies below the neutron separation energy S_n of Kadenskii et al. (1983, Sov. J. Nucl. Phys. 37, 165) is known to improve significantly the predictions of the experimental radiation widths and gamma-ray spectra (J. Kopecky, M. Uhl, 1990, Phys. Rev. C41, 1941). A unified approach between the low-energy description and the Lorentzian high-energy shape can be achieved in the hybrid formula for the γ -ray strength function (Goriely 1998, Phys. Lett. B436, 10)

$$f_{E1}(\varepsilon_\gamma) = 8.68 \cdot 10^{-8} [\text{mb}^{-1} \text{MeV}^{-2}] \frac{\sigma_0 \varepsilon_\gamma \Gamma_{GDR} \Gamma(\varepsilon_\gamma)}{(\varepsilon_\gamma^2 - E_{GDR}^2)^2 + \Gamma_{GDR} \Gamma(\varepsilon_\gamma) \varepsilon_\gamma^2} \quad (6)$$

The energy-dependent width is given by

$$\Gamma(\varepsilon_\gamma) = \sqrt{\frac{1 + \frac{2}{3}F'}{1 + 2F}} \Gamma_{GDR} \frac{\varepsilon_\gamma^2 + 4\pi^2 T_n^2}{\varepsilon_\gamma E_{GDR}} \quad (7)$$

T_n is the nuclear temperature of the final state and F, F' the Migdal constants related to the nuclear matter incompressibility modulus K_∞ , symmetry energy J_∞ , and Fermi energy ε_F . Typically, $\sqrt{(1 + 2/3F')/(1 + 2F)} \simeq 0.7$. Eq. (6) has the advantage of fitting relatively well both the high-energy Lorentzian (of energy E_{GDR} and width Γ_{GDR}) and the theoretical energy dependence of the low-energy tail (below the neutron separation energy) as prescribed by Kadenskii et al. (1983). In particular, the nonzero $\varepsilon_\gamma \rightarrow 0$ limit of the $E1$ -strength function $f_{E1} \propto T_{E1}/\varepsilon_\gamma^3$ is included in Eq. (6) and improves the predictions of low-energy experimental data (Kopecky & Uhl 1990). The reduced $E1$ -strength around the neutron binding energy also agrees well with empirical corrections brought to the Lorentzian GDR to explain the measured strength functions and γ -ray intensities.

2 Testing

Only the files available have been tested.

2.1 Segment 2: Levels

A systematic testing of the cumulative number N_m up to the energy U_{max} has been achieved by comparing N_m derived by the constant- T formula (and provided by T. Belgia) in Segment 2 and the value obtained by the microscopic HF-based NLD formula (all details are given in Demetriou & Goriely, 2001, Nucl. Phys. A695, 3). The results are presented in Fig. 3.

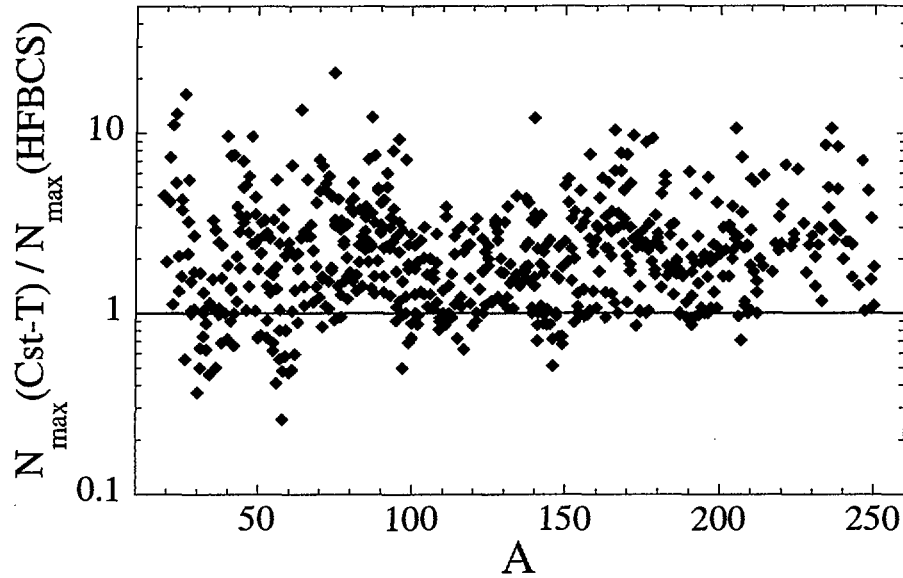


Figure 3: Comparison between the constant- T and HFBCS-based predictions of the number of levels up to which the level scheme is complete.

On the 613 entries shown in Fig. 3, the N_{max} predicted by the RIPL-2 constant- T formula is roughly up to a factor of 10 higher than the value predicted by the microscopic HF-BCS formula. This result has to be kept in mind by the reaction modellers.

In addition, some specific problems have been found in the Levels Z_XXX.DAT files and the corresponding PARALL.DAT file for the N_m determination:

- ^{86}Sr : $nlev = 82$ and $N_m = 79$. However, the last 6 levels (levels 77-82) are not ordered and are identified as *unc=SP+*. What is the meaning of "SP+". Since the last 6 levels have unknown energies and can hardly be included in the level scheme as known level, how comes that $N_m > 76$ (Note that in this case the HFBCS predictions is $N_m = 11$). Where the SP+, +X, +Y levels systematically included in the N_m fit ? How comes, if we do not know the absolute energies ?
- ^{89}Nb : the first 2 levels have a zero energy with a +X and +Y assignment. The other 23 excited levels have no +X or +Y assignment. Should we understand that the assigned level energies are absolute values, while the ground-state energy is not known ? It looks like the +X have been dropped from all the excited levels !
- ^{165}Lu : all levels are assigned +X,+Y, ... for unknown absolute values of the level energy, except the last level ($N_l=84$) at 4.4839 MeV, which I suppose should be within the +Y band !
- ^{214}Fr : $nlev = 59$ and $N_m = 33$. However, out of the 59 known levels, 14 have an absolute energy assignment, and 45 are assigned to +X and +Y bands. The estimated $N_m = 33$ is consequently based on many levels of unknown energies. How is it possible ? Were absolute energies given to the X and Y-values ?

- ^{213}Rn : $nlev = 54$ and $N_m = 24$. Same as for ^{214}Fr : out of the 54 known levels, 22 have an absolute energy assignment, and 32 are assigned to +X and +Y bands. The estimated $N_m = 24$ is consequently based on many levels of unknown energies. How is it possible? Were absolute energies given to the X and Y-values?
- Among the numerous cases for which 2 levels are known ($nlev = 2$), many have $N_m = 2$, in particular in the actinides region. Some of these nuclei have their second excited states assigned with +X, some others have excited states as large as 3-4 MeV. For example, $^{234,235}\text{Pu}$ have their second excited states (supposed to be complete) at 3 and 4 MeV, respectively. Shouldn't we be more careful and assign $N_m = 1$ to these nuclei? Note that there are in the full compilation about 59 $nlev = N_m = 2$ cases with a second excited states either +X assigned (33 cases) or with an energy larger than 1 MeV (26 cases).
- About the PARALL.DAT file: the worst fits ($\chi > 0.05$) should be flagged to warn the users about the situation. The last columns flagged by a "*" should be clarified ("the record comes from the main fit format"). What is the main fit, and what does it mean if it is not?
- About the file format, I thought we decide to harmonize the Element symbols by a first capital letter and a second small letter (e.g Fe and not FE). At least, Neutrons (N) should be distinguished from Nitrogen (N). Also note that Z=105 is Db, Z=106 is Sg, Z=107 is Bh, Z=108 is Hs and Z=109 is Mt!
- Another detail: the same quantity is called N_m in the PARALL.DAT file and $nmax$ in the Z_XXX readme file. Same for $nlev$ and nlv . Maybe, it would be better to use only one notation.

In summary, apart from the minor above-cited problems found in the Levels files, we would like to stress one major concern: how comes that levels with unknown energies (the +X, +Y cases) are considered for the estimate of N_m ?

2.2 Segment 3: Resonances

With respect to the latest file including the RIPL-2 resonance spacings D_0 provided by A. Ignatyuk at the IAEA meeting in November 2000, some questions arise for

1. ^{33}S . The D_0 value has been changed from 150 keV down to 15 keV with respect to the RIPL-1 compilation. Note that the Beijing, Iljinov et al. (1992) and Rohr's compilations give 28 keV, 150 keV and 150 keV, respectively.
2. ^{42}K for which $D_0 = 25$ keV. It would be nice to have a confirmation of this rather high value compared with Iljinov et al. (1992) of $D_0 = 4.8$ keV, since NLD systematics largely underpredict the value too (see Fig. 1).

2.3 Segment 5: Level Densities

no file available

Los Alamos Progress Report for RIPL-II
P. G. Young and M. B. Chadwick
December 3, 2001

Summary

Since the RIPL-II CRP meeting at Varenna, we have continued development of the RIPL-2 optical model parameter database. We have extended the format for optical potentials and have made major extensions to the optical model parameter file. The parameter file has been divided into archival and user versions. We have continued development of the code, OMINPUT, which retrieves potentials from the parameter file and formats them for the SCAT2000 and ECIS96 computer codes. We are coordinating our work with A. Koning in his development of the PREGNASH code and have assisted with coding for interfacing the optical model parameter file and for calculating transmission coefficients with deformed optical potentials.

I. Format of the Optical Model Parameter File (RIPL-2)

The format for compiling optical model potentials in the RIPL-2 library was modified and is described in the file omformat.readme. Major changes to the format are summarized below.

1. The ordering of potentials has been changed to follow ECIS96:

- real volume potential
- imaginary volume potential
- real surface derivative potential
- imaginary surface derivative potential
- real spin-orbit potential
- imaginary spin-orbit potential

2. The number of terms possible in the potential strengths has been increased from 21 to 24. The special case potentials are now:

- pot(i,j,22).ne.0 - Smith et al. , OMP reference # 118
- pot(i,j,23).ne.0 - Varner et al., OMP reference # 2100, 5100
- pot(i,j,24).ne.0 - Koning potentials, reference # 2404, 2405, 5404, 5405

3. The option activated when pot(i,j,24).ne.0 has been generalized to accommodate Koning's global neutron and proton potentials as well as his earlier ⁹⁰Zr potential.
4. The format has been extended to accommodate additional variables for dispersive potentials. That is, locations are specified to save the average energy of particle states (EP) and the energy at which non-locality is assumed (EA). Note that there was already a spot for the Fermi energy (EF).

5. An additional relativistic potential option has been added, i.e., $irel=2$, to indicate that the potentials must be multiplied by a factor, γ , required for the Madland Paris potential and for certain potentials from R. Capote. The factor is: $\gamma = 1 + E/(E+2*mc**2)$ where m is the mass of the incident particle and E is the center-of-mass kinetic energy.

II. Content of the Optical Model Parameter File (RIPL-2)

A new version of the OMP library has been constructed, following the format summarized above (omformat.readme). The number of potentials in the complete library has been increased from the 293 in RIPL-1 to 414 in the present RIPL-2 library. Additions to the library since the original RIPL library include:

1. A set of potentials from the Chinese Nuclear Data Center has been added.
2. Additional potentials from JENDL (Fukahori) have been added.
3. Koning's new global neutron and proton potential has been added.
4. Several miscellaneous potentials have been added, mainly from Bruyeres-le-Chatel, LANL, and A.B. Smith.
5. R. Capote has provided five dispersive optical model (DOM) parameterizations.

The RIPL-2 library is available in two versions. The complete or archival library (omparameter.adat) contains all optical model potentials compiled thus far, a total of 414 entries. A second shorter version of the file, a user library (omparameter.udat), is a subset of the archival library and is constructed by eliminating all potentials defined for only a single energy. The user library is constructed from the archival library by setting a simple flag in the RIPLMOD code, described below. The existing user library contains 291 potentials.

III. Retrieval Code for RIPL-2 Optical Parameters

A new version of the code, OMINPUT12, has been developed for retrieving optical model potentials from the RIPL-2 optical model parameter library and formatting the potentials for input into either the SCAT2000 or ECIS96 optical model codes.

The input required for the code is the energy grid for the calculations (or a default grid can be used), the Z and A of the target nucleus, and the optical model potential number in the RIPL-2 library. In addition, the RIPL-2 optical parameter file (omparameter.dat) and the ground-state mass/spin/parity file (gs-masssp.dat) are required. At present the code works for spherical, vibrational, rotational band potentials. The code has been extensively tested for spherical and

rotational model potentials, as well as for the special Smith, Varner, and Koning potentials described above.

The present code is available in the `ominput12.for` and `ominput12.cmb` files. The input and output files are described in Appendix I. The code differs from the previous version (OMINPUT11) in that it contains additions from R. Capote to handle dispersive potentials as well as coding that permits automatic application of the gamma factor for relativistic calculations, referred to by D. G. Madland in OMP references #2001 and 5001. (See Section I.5 above.) Concerning the gamma factor, we have investigated whether the factor is required for relativistic calculations when using the Madland potentials with the SCAT2000 and ECIS96 codes.

We compared calculations with SCAT2000 and ECIS96, both with and without applying the gamma factor to the potential well depths, to results provided by D. G. Madland. Madland's calculations were performed with his SNOOPY code, which was used in the analysis leading to his global potential. The comparisons for the integrated cross sections for $n + {}^{208}\text{Pb}$ interactions at 100 and 400 MeV are given in Table 1. The results shown in Table 1 show reasonable agreement between the ECIS96, SCAT2000, and SNOOPY codes when gamma is set to unity. While this comparison is very limited, it does provide strong evidence that the gamma factor should *not* be applied when performing relativistic calculations with SCAT2000 and ECIS96. Accordingly, we have set the gamma factor to unity in the OMINPUT12 code. However, we have preserved the coding for calculating the gamma factor, in case we wish to broaden OMINPUT12 to handle other optical model codes in the future.

Table 1. Comparison of Optical Model Calculations of Integrated Cross Sections with the SNOOPY, SCAT2000, and ECIS96 Codes for $n + {}^{208}\text{Pb}$ Reactions

CODE	100 MeV			400 MeV		
	TOTAL (mb)	REACT (mb)	ELAS (mb)	TOTAL (mb)	REACT (mb)	ELAS (mb)
SNOOPY Benchmark	4585.0	2029.6	2555.4	2816.1	1761.5	1054.6
SCAT2000 without gamma factor	4591.0	2028.6	2562.4	2802.3	1752.2	1050.1
SCAT2000 with gamma factor	4671.8	2070.4	2601.3	2996.1	1832.6	1163.4
ECIS96 without gamma factor	4581.7	2029.1	2552.6	2816.0	1760.2	1055.8
ECIS96 with gamma factor	4663.4	2070.9	2592.5	3011.3	1841.5	1169.8

IV. Utility Codes for Processing the OMP library

Three utility codes are available for managing and using the OMP library. The codes are the following:

1. OMSUMMARY11 – a code that produces a summary of all the potentials in the OMP library (omparameter.dat). The reference number, the author, the citation or reference, the descriptive comments, the Z- and A-ranges of the potential, and the type of potential are listed for each potential. A sample of the SUMMARY output is included in Appendix II.
2. OMTABLE11 – a concise table, one line per entry, is produced describing the essential features of each potential (type potential, Z- and A-ranges, lead author, etc.) A sequential (local) reference number is assigned to each potential and a separate reference list is produced in addition to the table. The TABLE and REFERENCES files produced for the current OMP user's library are given in Appendix III.
3. RIPLMOD11 – a code that can be used to add or delete references from an input OMP file. By setting an appropriate flag, the code will eliminate all single-energy potentials, that is, it will produce a "user" library from the inputted "archival" library.

The OMSUMMARY and OMTABLE codes only require an input of the OMP library (omparameter.dat) and a file of common variable information (omp.cmb). The input for RIPLMOD is slightly more complicated and is described in Appendix IV.

V. Interfacing the GNASH Code with RIPL-2 Libraries.

The interfacing of the GNASH code with RIPL-2 libraries will be accomplished with the PREGNASH code, which is being developed by A. Koning. At Los Alamos, we developed a temporary, local version of PREGNASH that includes coding for accessing the RIPL-2 OMP libraries. This coding was provided to Koning to assist in his development of the final RIPL-2 version of PREGNASH.

Appendix II. Sample output from the OMSUMMARY11 Code.

```
IREF= 2 Neutron incident, vibrational model
      Potential is non-relativistic and non-dispersive.
      Z-Range= 82-82 A-Range= 208-208 E-Range= 0-200 MeV
      Author(s)=
      H.Vonach,A.Pavlik,M.B.Chadwick,R.C.Haight,R.O.Nelson,S.A.Wender,P.G.
      Young
      Reference= Phys. Rev. C 50, 1952 (1994)
      Summary= Based on detailed fits to neutron data 8.5-10 MeV, simply
      extrapolated to lower energies and extended to higher energies.
      Reaction cross section deficient above 100 MeV.

+++++
IREF= 410 Neutron incident, coupled-channels rotational model
      Potential is non-relativistic and non-dispersive.
      Z-Range= 92-92 A-Range= 238-238 E-Range= 0- 20 MeV
      Author(s)= Ch.Lagrange
      Reference= NEANDC (E)228 "L", INDC(FR) 56/L (1982)
      Summary= Results of Coupled-Channels Calculations for the Neutron Cross
      Sections of a Set of Actinide Nuclei. Included are parameters for
      230,232Th, 234,238U, 242Pu, 246Cm, 252Cf.

+++++
IREF= 418 Neutron incident, spherical nucleus model
      Potential is relativistic and dispersive.
      Z-Range= 13-13 A-Range= 27- 27 E-Range= 0-250 MeV
      Author(s)= Molina A., Capote R., Quesada J.M., Lozano M., Universidad de
      Seville
      a
      Reference= Phys.Rev.C, submitted on October,2001 [nucl-th/0111048 preprint]
      Summary= A relativistic dispersive OMP for Al-27. Nonlocality in the volume
      absorption was included. Requires OM code with relativistic
      kinematics & total pot must be multiplied by  $1 + E/(E+2*mc**2)$ 
      where E,m are for incident particle and E is th e total cm kinetic
      energy

+++++
IREF= 2001 Neutron incident, spherical nucleus model
      Potential is relativistic and non-dispersive.
      Z-Range= 6-82 A-Range= 12-208 E-Range= 50-400 MeV
      Author(s)= D.G.Madland
      Reference= OECD/NEA Specialists Mtg. on Opt.Mod.to 200 MeV,Paris,1997
      Summary= Update of Semmering potential [NEANDC-245 U (1988)] to include
      generalized imag. diff. parameter. Global pot for incid. neutrs and
      prots. Requires OM code with relativistic kine. & total pot must
      be
      multiplied by  $1 + E/(E+2*mc**2)$  where E,m are for incident
      particle
      and E = total cm kinetic energy.

+++++
IREF= 2405 Neutron incident, spherical nucleus model
      Potential is relativistic and non-dispersive.
      Z-Range= 13-83 A-Range= 27-209 E-Range= 0-200 MeV
      Author(s)= A.J.Koning, J.P.Delaroche
      Reference= Phys. Rev. C, submitted for publication, July,2001
      Summary= A new global neutron optical model potential for incident energies
      between 1 keV and 200 MeV and valid for Al through Bi. The
      potential is based on detailed fits of neutron total and elastic
      cross sections and elastic angular distributions with the ECISVIEW
      interactive code.
```

Appendix III. The TABLE and REFERENCES Files Created by the OMTABLE11 Code from the User Version of the OMP Library.

Lib. No.	Inc. Part.	Model Type	Z-Range	A-Range	E-Range (MeV)	Ref. No.	First Author
1	n	CC rot.	93-93	237-237	0.0- 30.0	1	P.G.Young
2	n	vibra.	82-82	208-208	0.0-200.0	2	H.Vonach
3	n	CC rot.	92-92	235-235	0.0- 30.0	1	P.G.Young
4	n	CC rot.	92-92	237-237	0.0- 30.0	3	P.G.Young
5	n	CC rot.	92-92	238-238	0.0- 30.0	3	P.G.Young
6	n	CC rot.	94-94	242-242	0.0- 20.0	4	D.G.Madland
7	n	CC rot.	94-94	239-239	0.0- 30.0	3	P.G.Young
8	n	CC rot.	95-95	241-243	0.0- 30.0	5	P.G.Young
9	n	spher.	90-95	230-250	0.0- 10.0	6	D.G.Madland
10	n	spher.	26-26	54- 56	0.0- 52.0	7	E.D.Arthur
11	n	spher.	27-27	59- 59	0.0- 27.5	8	E.D.Arthur
12	n	spher.	30-30	57- 81	0.0- 20.0	9	P.G.Young
13	n	spher.	39-39	89- 89	0.0- 21.0	10	E.D.Arthur
14	n	spher.	40-40	90- 90	0.0- 20.0	11	E.D.Arthur
15	n	spher.	6- 6	12- 12	0.0- 65.0	12	M.B.Chadwick
16	n	spher.	7- 7	14- 14	0.0- 60.0	12	M.B.Chadwick
17	n	spher.	8- 8	16- 16	0.0- 50.0	12	M.B.Chadwick
18	n	spher.	13-13	27- 27	0.0- 20.0	13	R.C.Harper
19	n	spher.	28-28	58- 58	0.0- 20.0	13	R.C.Harper
20	n	spher.	41-41	93- 93	0.0- 20.0	13	R.C.Harper
21	n	spher.	79-79	197-197	0.0- 20.0	13	R.C.Harper
100	n	spher.	20-92	40-238	10.0- 50.0	14	F.D.Becchetti
101	n	spher.	12-83	24-209	11.0- 11.0	15	J.C.Ferrer
102	n	spher.	82-82	206-208	5.0- 50.0	16	R.W.Finlay
103	n	spher.	26-26	56- 56	0.0-100.0	17	A.Prince
104	n	spher.	26-26	54- 54	0.0-100.0	17	A.Prince
105	n	spher.	26-26	57- 57	0.0-100.0	17	A.Prince
106	n	spher.	26-26	58- 58	0.0-100.0	17	A.Prince
107	n	spher.	28-28	58- 58	0.0-100.0	17	A.Prince
108	n	spher.	28-28	60- 60	0.0-100.0	17	A.Prince
109	n	spher.	28-28	61- 61	0.0-100.0	17	A.Prince
110	n	spher.	28-28	62- 62	0.0-100.0	17	A.Prince
111	n	spher.	28-28	64- 64	0.0-100.0	17	A.Prince
112	n	spher.	24-24	50- 50	0.0-100.0	17	A.Prince
113	n	spher.	24-24	53- 53	0.0-100.0	17	A.Prince
114	n	spher.	24-24	52- 52	0.0-100.0	17	A.Prince
115	n	spher.	24-24	54- 54	0.0-100.0	17	A.Prince
116	n	spher.	20-83	40-209	0.0- 5.0	18	P.A.Moldauer
117	n	spher.	13-13	27- 27	0.0- 60.0	19	J.Petler
118	n	spher.	39-51	85-125	0.0- 5.0	20	A.B.Smith
119	n	CC rot.	67-67	165-165	0.0- 30.0	21	A.B.Smith
120	n	CC rot.	67-67	165-165	0.0- 30.0	21	A.B.Smith
121	n	spher.	82-82	208-208	0.0- 80.0	22	Weisel
122	n	spher.	83-83	209-209	0.0- 80.0	22	Weisel
200	n	spher.	0-69	0-146	0.0- 20.0	23	S.Igarasi
201	n	spher.	69-95	147-999	0.0- 20.0	23	S.Igarasi
202	n	spher.	33-37	61-107	0.0- 20.0	24	Japan
203	n	spher.	38-42	69-116	0.0- 20.0	24	Japan
204	n	spher.	43-45	80-125	0.0- 20.0	24	Japan
205	n	spher.	46-48	89-134	0.0- 20.0	24	Japan
206	n	spher.	49-51	97-141	0.0- 20.0	24	Japan
207	n	spher.	52-54	103-150	0.0- 20.0	24	Japan
208	n	spher.	55-55	111-153	0.0- 20.0	24	Japan
209	n	spher.	56-56	112-154	0.0- 20.0	24	Japan
210	n	spher.	57-58	117-156	0.0- 20.0	24	Japan
211	n	spher.	59-59	119-160	0.0- 20.0	24	Japan

212	n	spher.	60-60	141-143	0.0- 20.0	24	Japan
213	n	spher.	60-60	144-148	0.0- 20.0	24	Japan
214	n	spher.	60-60	150-999	0.0- 20.0	24	Japan
215	n	spher.	61-61	147-999	0.0- 20.0	24	Japan
216	n	spher.	62-62	144-144	0.0- 20.0	24	Japan
217	n	spher.	62-62	147-147	0.0- 20.0	24	Japan
218	n	spher.	62-62	148-148	0.0- 20.0	24	Japan
219	n	spher.	62-62	149-149	0.0- 20.0	24	Japan
220	n	spher.	62-62	150-150	0.0- 20.0	24	Japan
221	n	spher.	63-63	151-999	0.0- 20.0	24	Japan
222	n	spher.	64-64	133-171	0.0- 20.0	24	Japan
223	n	spher.	65-65	138-175	0.0- 20.0	24	Japan
240	n	spher.	0-69	0-146	0.0- 20.0	25	S.Igarasi
241	n	spher.	69-95	147-999	0.0- 20.0	25	S.Igarasi
242	n	spher.	13-13	27- 27	0.0-250.0	26	Lee
400	n	CC rot.	79-79	197-197	0.0- 57.0	27	J.P.Delaroche
401	n	spher.	20-92	40-238	0.0- 25.0	28	D.Wilmore
402	n	spher.	83-83	209-209	0.0- 30.0	29	O.Bersillon
403	n	spher.	74-74	182-186	0.0- 30.0	30	J.P.Delaroche
404	n	spher.	23-41	50- 95	0.0- 30.0	31	B.Strohmaier
406	n	CC rot.	94-94	236-244	0.0- 20.0	32	Ch.Lagrange
408	n	CC rot.	90-90	230-232	0.0- 20.0	33	Ch.Lagrange
409	n	CC rot.	92-92	234-234	0.0- 20.0	33	Ch.Lagrange
410	n	CC rot.	92-92	238-238	0.0- 20.0	33	Ch.Lagrange
411	n	CC rot.	94-94	242-242	0.0- 20.0	33	Ch.Lagrange
412	n	CC rot.	96-96	246-246	0.0- 20.0	33	Ch.Lagrange
413	n	CC rot.	98-98	252-252	0.0- 20.0	33	Ch.Lagrange
414	n	CC rot.	90-90	232-232	0.0- 20.0	34	G.Haouat
415	n	CC rot.	92-92	235-235	0.0- 20.0	34	G.Haouat
416	n	CC rot.	92-94	238-239	0.0- 20.0	34	G.Haouat
417	n	CC rot.	94-94	242-242	0.0- 20.0	34	G.Haouat
418	n	spher.	13-13	27- 27	0.0-250.0	35	Molina
419	n	spher.	13-13	27- 27	0.0-150.0	35	Molina
500	n	spher.	31-31	69- 69	0.1- 20.0	36	Zhang
501	n	spher.	36-36	83- 83	0.1- 20.0	37	Cai
502	n	spher.	36-36	86- 86	0.1- 20.0	38	Cai
503	n	spher.	37-37	85- 85	0.1- 20.0	37	Cai
504	n	spher.	38-38	88- 88	0.1- 20.0	37	Cai
505	n	spher.	39-39	89- 89	0.1- 20.0	37	Cai
506	n	spher.	39-39	91- 91	0.1- 20.0	39	Cai
507	n	spher.	41-41	93- 93	0.1- 20.0	40	Rong
508	n	spher.	41-41	95- 95	0.1- 20.0	40	Rong
509	n	spher.	42-42	95- 95	0.1- 20.0	41	Cai
510	n	spher.	42-42	97- 97	0.1- 20.0	42	Cai
511	n	spher.	42-42	98- 98	0.1- 20.0	42	Cai
512	n	spher.	42-42	100-100	0.1- 20.0	38	Cai
513	n	spher.	43-43	99- 99	0.1- 20.0	39	Cai
514	n	spher.	44-44	99- 99	0.1- 20.0	43	Zhang
515	n	spher.	44-44	100-100	0.1- 20.0	43	Zhang
516	n	spher.	44-44	101-101	0.1- 20.0	44	Zhang
517	n	spher.	44-44	102-102	0.1- 20.0	43	Zhang
518	n	spher.	44-44	103-103	0.1- 20.0	44	Zhang
519	n	spher.	44-44	104-104	0.1- 20.0	43	Zhang
520	n	spher.	44-44	105-105	0.1- 20.0	43	Zhang
521	n	spher.	45-45	103-103	0.1- 20.0	43	Zhang
522	n	spher.	45-45	105-105	0.1- 20.0	43	Zhang
523	n	spher.	46-46	105-105	0.1- 20.0	45	Zhang
524	n	spher.	46-46	108-108	0.1- 20.0	45	Zhang
525	n	spher.	48-48	113-113	0.1- 20.0	46	Zhang
526	n	spher.	49-49	115-115	0.1- 20.0	46	Zhang
527	n	spher.	51-51	121-121	0.1- 20.0	46	Zhang
528	n	spher.	51-51	123-123	0.1- 20.0	46	Zhang
529	n	spher.	52-52	130-130	0.1- 20.0	45	Zhang
530	n	spher.	53-53	127-127	0.1- 20.0	45	Zhang

531	n	spher.	53-53	135-135	0.1- 20.0	45	Zhang
532	n	spher.	54-54	123-123	0.1- 20.0	47	Shen
533	n	spher.	54-54	124-124	0.1- 20.0	47	Shen
534	n	spher.	54-54	129-129	0.1- 20.0	48	Shen
535	n	spher.	54-54	131-131	0.1- 20.0	48	Shen
536	n	spher.	54-54	132-132	0.1- 20.0	48	Shen
537	n	spher.	54-54	134-134	0.1- 20.0	48	Shen
538	n	spher.	54-54	135-135	0.1- 20.0	48	Shen
539	n	spher.	54-54	136-136	0.1- 20.0	48	Shen
540	n	spher.	55-55	133-133	0.1- 20.0	43	Zhang
541	n	spher.	55-55	134-134	0.1- 20.0	43	Zhang
542	n	spher.	55-55	135-135	0.1- 20.0	43	Zhang
543	n	spher.	55-55	137-137	0.1- 20.0	43	Zhang
544	n	spher.	56-56	135-135	0.1- 20.0	43	Zhang
545	n	spher.	56-56	136-136	0.1- 20.0	43	Zhang
546	n	spher.	56-56	137-137	0.1- 20.0	43	Zhang
547	n	spher.	56-56	138-138	0.1- 20.0	43	Zhang
548	n	spher.	57-57	139-139	0.1- 20.0	43	Zhang
549	n	spher.	58-58	140-140	0.1- 20.0	43	Zhang
550	n	spher.	58-58	141-141	0.1- 20.0	43	Zhang
551	n	spher.	58-58	142-142	0.1- 20.0	43	Zhang
552	n	spher.	58-58	144-144	0.1- 20.0	43	Zhang
553	n	spher.	59-59	141-141	0.1- 20.0	47	Shen
554	n	spher.	60-60	142-142	0.1- 20.0	47	Shen
555	n	spher.	60-60	143-143	0.1- 20.0	47	Shen
556	n	spher.	60-60	144-144	0.1- 20.0	47	Shen
557	n	spher.	60-60	145-145	0.1- 20.0	47	Shen
558	n	spher.	60-60	146-146	0.1- 20.0	47	Shen
559	n	spher.	60-60	147-147	0.1- 20.0	47	Shen
560	n	spher.	60-60	148-148	0.1- 20.0	47	Shen
561	n	spher.	60-60	150-150	0.1- 20.0	47	Shen
562	n	spher.	61-61	147-147	0.1- 20.0	47	Shen
563	n	spher.	61-61	148-148	0.1- 20.0	47	Shen
564	n	spher.	61-61	149-149	0.1- 20.0	47	Shen
565	n	spher.	62-62	144-144	0.1- 20.0	47	Shen
566	n	spher.	62-62	147-147	0.1- 20.0	47	Shen
567	n	spher.	62-62	148-148	0.1- 20.0	47	Shen
568	n	spher.	62-62	149-149	0.1- 20.0	47	Shen
569	n	spher.	62-62	150-150	0.1- 20.0	47	Shen
570	n	spher.	62-62	151-151	0.1- 20.0	47	Shen
571	n	spher.	62-62	152-152	0.1- 20.0	47	Shen
572	n	spher.	62-62	154-154	0.1- 20.0	47	Shen
573	n	spher.	63-63	151-151	0.1- 20.0	49	Ge
574	n	spher.	63-63	153-153	0.1- 20.0	49	Ge
575	n	spher.	63-63	154-154	0.1- 20.0	49	Ge
576	n	spher.	63-63	155-155	0.1- 20.0	49	Ge
577	n	spher.	64-64	152-152	0.1- 20.0	47	Shen
578	n	spher.	64-64	154-154	0.1- 20.0	47	Shen
579	n	spher.	64-64	155-155	0.1- 20.0	47	Shen
580	n	spher.	64-64	156-156	0.1- 20.0	47	Shen
581	n	spher.	64-64	157-157	0.1- 20.0	47	Shen
582	n	spher.	64-64	158-158	0.1- 20.0	47	Shen
583	n	spher.	64-64	160-160	0.1- 20.0	47	Shen
584	n	spher.	66-66	164-164	0.1- 20.0	50	Ge
585	n	spher.	69-69	169-169	0.1- 20.0	50	Ge
586	n	spher.	71-71	174-174	0.1- 20.0	51	Han
587	n	spher.	71-71	175-175	0.1- 20.0	51	Han
600	n	CC rot.	90-103	227-260	0.0- 20.0	52	G.Vladuca
800	n	spher.	20-83	40-210	0.0-155.0	53	C.A.Engelbrecht
2001	n	spher.	6-82	12-208	50.0-400.0	54	D.G.Madland
2002	n	CC rot.	74-74	182-186	0.0-100.0	55	P.G.Young
2003	n	CC rot.	67-69	165-169	0.0-100.0	56	E.D.Arthur
2004	n	CC rot.	63-63	151-153	0.0- 20.0	57	R.Macklin
2005	n	CC rot.	75-75	185-187	0.0- 20.0	58	R.Macklin

2006	n	CC rot.	92-92	238-238	0.0-200.0	59	P.G.Young
2007	n	CC rot.	67-69	165-169	0.0- 30.0	60	P.G.Young
2100	n	spher.	20-83	40-209	10.0- 26.0	61	R.L.Varner
2101	n	spher.	26-82	54-208	10.0- 80.0	62	R.L.Walter
2404	n	spher.	40-40	90- 90	0.0-200.0	63	A.J.Koning
2405	n	spher.	13-83	27-209	0.0-200.0	64	A.J.Koning
4000	p	spher.	25-26	54- 56	0.0- 28.0	7	E.D.Arthur
4001	p	spher.	26-27	59- 59	0.0- 23.0	65	E.D.Arthur
4002	p	spher.	38-38	88- 89	0.0- 21.0	10	E.D.Arthur
4003	p	spher.	39-39	89- 89	0.0- 21.0	10	E.D.Arthur
4004	p	CC rot.	79-79	197-197	0.0- 57.0	66	P.G.Young
4015	p	spher.	6- 6	12- 12	0.0- 65.0	67	M.B.Chadwick
4016	p	spher.	7- 7	14- 14	0.0- 70.0	67	M.B.Chadwick
4017	p	spher.	8- 8	16- 16	0.0- 50.0	67	M.B.Chadwick
4018	p	spher.	13-13	27- 27	0.1- 20.0	13	R.C.Harper
4019	p	spher.	28-28	58- 58	0.1- 20.0	13	R.C.Harper
4020	p	spher.	41-41	93- 93	0.1- 20.0	13	R.C.Harper
4100	p	spher.	16-49	30-100	0.0- 22.0	68	F.G.Perey
4101	p	spher.	20-83	40-209	10.0- 50.0	69	F.D.Becchetti
4102	p	spher.	6-82	12-208	30.0- 60.0	70	J.J.H.Menet
4108	p	spher.	20-82	48-208	25.0- 45.0	71	D.M.Patterson
4109	p	spher.	39-39	89- 89	1.0- 7.0	72	C.H.Johnson
4110	p	spher.	41-41	93- 93	1.0- 7.0	72	C.H.Johnson
4111	p	spher.	45-45	103-103	1.0- 7.0	72	C.H.Johnson
4112	p	spher.	46-46	105-105	1.0- 7.0	72	C.H.Johnson
4113	p	spher.	47-47	107-107	1.0- 7.0	72	C.H.Johnson
4114	p	spher.	47-47	109-109	1.0- 7.0	72	C.H.Johnson
4115	p	spher.	48-48	110-110	1.0- 7.0	72	C.H.Johnson
4116	p	spher.	48-48	111-111	1.0- 7.0	72	C.H.Johnson
4117	p	spher.	48-48	113-113	1.0- 7.0	72	C.H.Johnson
4118	p	spher.	48-48	114-114	1.0- 7.0	72	C.H.Johnson
4119	p	spher.	49-49	115-115	1.0- 7.0	72	C.H.Johnson
4120	p	spher.	50-50	116-116	1.0- 7.0	72	C.H.Johnson
4121	p	spher.	50-50	122-122	1.0- 7.0	72	C.H.Johnson
4122	p	spher.	50-50	124-124	1.0- 7.0	72	C.H.Johnson
4123	p	spher.	52-52	128-128	1.0- 7.0	72	C.H.Johnson
4124	p	spher.	52-52	130-130	1.0- 7.0	72	C.H.Johnson
4125	p	spher.	40-40	92- 92	2.0- 7.0	73	D.S.Flynn
4126	p	spher.	40-40	94- 94	2.0- 7.0	73	D.S.Flynn
4127	p	spher.	40-40	96- 96	2.0- 7.0	73	D.S.Flynn
4128	p	spher.	42-42	95- 95	2.0- 7.0	73	D.S.Flynn
4129	p	spher.	42-42	98- 98	2.0- 7.0	73	D.S.Flynn
4130	p	spher.	42-42	100-100	2.0- 7.0	73	D.S.Flynn
4650	p	spher.	21-21	45- 45	3.0- 5.0	74	S.Kailas
4651	p	spher.	20-20	48- 48	3.0- 5.0	74	S.Kailas
4652	p	spher.	23-23	51- 51	3.0- 5.0	74	S.Kailas
4653	p	spher.	24-24	54- 54	3.0- 5.0	74	S.Kailas
4654	p	spher.	27-27	59- 59	3.0- 5.0	74	S.Kailas
4655	p	spher.	28-28	61- 61	3.0- 5.0	74	S.Kailas
4656	p	spher.	29-29	65- 65	3.0- 5.0	74	S.Kailas
4657	p	spher.	31-31	71- 71	3.0- 5.0	74	S.Kailas
4658	p	spher.	33-33	75- 75	3.0- 5.0	74	S.Kailas
4659	p	spher.	34-34	80- 80	3.0- 5.0	74	S.Kailas
4660	p	spher.	19-19	41- 41	1.0- 7.0	75	Y.P.Viyogi
4661	p	spher.	21-21	45- 45	1.0- 7.0	75	Y.P.Viyogi
4662	p	spher.	20-20	48- 48	1.0- 7.0	75	Y.P.Viyogi
4663	p	spher.	22-22	49- 49	1.0- 7.0	75	Y.P.Viyogi
4664	p	spher.	23-23	51- 51	1.0- 7.0	75	Y.P.Viyogi
4665	p	spher.	25-25	55- 55	1.0- 7.0	75	Y.P.Viyogi
4666	p	spher.	27-27	59- 59	1.0- 7.0	75	Y.P.Viyogi
4667	p	spher.	28-28	61- 61	1.0- 7.0	75	Y.P.Viyogi
4668	p	spher.	29-29	65- 65	1.0- 7.0	75	Y.P.Viyogi
4669	p	spher.	30-30	68- 68	1.0- 7.0	75	Y.P.Viyogi
4670	p	spher.	31-31	71- 71	1.0- 7.0	75	Y.P.Viyogi

4671	p	spher.	33-33	75- 75	1.0- 7.0	75	Y.P.Viyogi
4672	p	spher.	34-34	80- 80	1.0- 7.0	75	Y.P.Viyogi
4673	p	spher.	39-39	89- 89	1.0- 7.0	75	Y.P.Viyogi
4674	p	spher.	41-41	93- 93	1.0- 7.0	75	Y.P.Viyogi
4675	p	spher.	42-42	96- 96	1.0- 7.0	75	Y.P.Viyogi
4676	p	spher.	42-42	98- 98	1.0- 7.0	75	Y.P.Viyogi
4677	p	spher.	45-45	103-103	1.0- 7.0	75	Y.P.Viyogi
4678	p	spher.	46-46	105-105	1.0- 7.0	75	Y.P.Viyogi
4679	p	spher.	47-47	107-107	1.0- 7.0	75	Y.P.Viyogi
4680	p	spher.	47-47	109-109	1.0- 7.0	75	Y.P.Viyogi
4681	p	spher.	48-48	110-110	1.0- 7.0	75	Y.P.Viyogi
4682	p	spher.	49-49	115-115	1.0- 7.0	75	Y.P.Viyogi
4683	p	spher.	50-50	120-120	1.0- 7.0	75	Y.P.Viyogi
4684	p	spher.	50-50	124-124	1.0- 7.0	75	Y.P.Viyogi
4685	p	spher.	52-52	128-128	1.0- 7.0	75	Y.P.Viyogi
4686	p	spher.	52-52	130-130	1.0- 7.0	75	Y.P.Viyogi
5001	p	spher.	6-82	12-208	50.0-400.0	54	D.G.Madland
5002	p	CC rot.	74-74	182-186	0.0-100.0	55	P.G.Young
5003	p	CC rot.	67-69	165-169	0.0-100.0	56	E.D.Arthur
5004	p	CC rot.	63-63	151-153	0.0- 20.0	57	R.Macklin
5005	p	CC rot.	75-75	185-187	0.0- 20.0	58	R.Macklin
5006	p	CC rot.	92-92	238-238	0.0-200.0	59	P.G.Young
5100	p	spher.	20-83	40-209	16.0- 65.0	61	R.L.Varner
5101	p	spher.	26-82	54-208	10.0- 80.0	76	R.L.Walter
5404	p	spher.	40-40	90- 90	0.0-200.0	63	A.J.Koning
5405	p	spher.	13-83	27-209	0.0-200.0	64	A.J.Koning
6001	d	spher.	20-82	40-208	11.0- 27.0	77	C.M.Perey
6100	d	spher.	20-83	40-209	8.0- 13.0	78	J.M.Lohr
6400	d	spher.	6-82	12-208	20.0-100.0	79	J.Bojowald
7100	t	spher.	20-82	40-208	1.0- 40.0	80	F.D.Becchetti
8100	3He	spher.	20-82	40-208	1.0- 40.0	80	F.D.Becchetti
8101	3He	spher.	20-20	40- 40	21.0- 84.0	81	H.H.Chang
8102	3He	spher.	28-28	58- 58	22.0- 84.0	81	H.H.Chang
9000	4He	spher.	13-26	27- 56	1.0-100.0	82	E.D.Arthur
9001	4He	spher.	27-27	59- 59	1.0-100.0	83	E.D.Arthur
9018	4He	spher.	13-13	27- 27	0.1- 20.0	13	R.C.Harper
9019	4He	spher.	28-28	58- 58	0.1- 20.0	13	R.C.Harper
9020	4He	spher.	41-41	93- 93	0.1- 20.0	13	R.C.Harper
9100	4He	spher.	8-82	16-208	1.0- 25.0	84	L.McFadden
9101	4He	spher.	10-92	20-235	1.0- 46.0	85	J.R.Huizenga
9400	4He	spher.	20-45	40-100	1.0- 30.0	86	B.Strohmaier
9401	4He	spher.	22-30	37- 86	20.0- 30.0	87	O.F.Lemos
9600	4He	spher.	8-96	16-250	1.0- 73.0	88	V.Avrigeanu

REFERENCES

1. P.G.Young and E.D.Arthur, Proc.Int.Conf.Nucl.Data Sci.and Tech., Ju lich (1992) p894
2. H.Vonach,A.Pavlik,M.B.Chadwick,R.C.Haight,R.O.Nelson,S.A.Wender,P. G.Young, Phys. Rev. C 50, 1952 (1994)
3. P.G.Young and E.D.Arthur, LANL Report LA-UR-91-1424,894(1992)
4. D.G.Madland and P.G.Young, Report LA-7533-MS (1978)
5. P.G.Young and E.D.Arthur, LANL Report LA-UR-95-3654, paper at RIPL CRP Mtg., Vienna, Oct.30-Nov.3,1995.
6. D.G.Madland and P.G.Young, Int. Conf. ,Harwell ,UK ,Sept. 25-29,1 978
7. E.D.Arthur and P.G.Young, LA-UR-95-3654 (1995),BNL-NCS-51245 (1980) p.731, LA-8626-MS (1980)
8. E.D.Arthur, P.G.Young, and W.Matthes, BNL-51245,p.751 (1980); Nucl .Sci.Eng.124,271(1996)
9. P.G.Young and D.Rutherford, Report IAEA-TECDOC-483,167 (1988)
10. E.D.Arthur, Nucl.Sci.Eng. 76,137 1980)

11. E.D.Arthur, Nucl.Sci.Eng. 76,137(1980); LA-UR-94-3104 (1994)
12. M.B.Chadwick and P.G.Young, Nucl.Sci.Eng. 123, 17 (1996)
13. R.C.Harper and W.L.Alford, J.Phys.G:Nucl.Phys. 8, 153(1982)
14. F.D.Becchetti, Jr. and G.W.Greenlees, Phys. Rev. 182,1190 (1969)
15. J.C.Ferrer,J.D.Carlson, and J.Rapaport, Nucl. Phys. A275,325 (1977)
16. R.W.Finlay et al., Phys. Rev. C 30, 796 (1984)
17. A.Prince, Int. Conf. on Nucl. Data, Antwerp ,1982
18. P.A.Moldauer, Nucl. Phys. 47,65(1963)
19. J.Petler,M.S.Islam, and R.W.Finlay, Phys. Rev. C 32 ,673 (1985)
20. A.B.Smith,P.T.Guenther,J.F.Whalen, Nucl. Phys. A415,1 (1984)
21. A.B.Smith, Report ANL/NDM-151 (December, 2000)
22. Weisel G. J., Tornow W et al, Phys.Rev.C54 (1996) 2410-2428
23. S.Igarasi, Japan At.Ener.Res. Insti. 1228 , 41 (1973)
24. Japan At.Ener.Res. Insti., JNDC FP Nucl. Data WG
25. S.Igarasi, JAERI-M 5752 (1974)
26. Lee Y.O. et al., J. Nucl. Sci. Eng. 36 (1999) 1125-1134
27. J.P.Delaroche, Proc.Int.Conf.on Neut.Phys. for Reactors, Harwell(1978)
28. D.Wilmore and P.E.Hodgson, Nucl. Phys. 55,673 (1964)
29. O.Bersillon, CEA Report CEA-N-2284 (1982) p.130; see also NEANDC-2 22U
30. J.P.Delaroche et al., Int. Conf. on Nucl. Data, Knoxville,TN,1979
31. B.Strohmaier et al, IAEA Advisory Group Meeting, Rad. Damage ,1981
32. Ch.Lagrange, CEA-N-1970, NEANDC(E) 179 "L", INDC(FR) 16/L (1977)
33. Ch.Lagrange, NEANDC(E)228 "L", INDC(FR) 56/L (1982)
34. G.Haouat,J.Lachkar,Ch.Lagrange, Nucl.Sci.Engr.81,491(1982)
35. Molina A., Capote R., Quesada J.M., Lozano M., Universidad de Sevilla, Phys.Rev.C, submitted on October,2001
36. Zhang Songbai (China Nuclear Data Center), Communication of Nuclear Data Progress, No.21(1999)52
37. Cai Chonghai (Nankai University, Tianjin, P.R.China), Communication of Nuclear Data Progress, No.21(1999)40
38. Cai Chonghai (Nankai University, Tainjin, P.R.China), to be published
39. Cai Chonghai (Nankai University, Tianjin, P.R.China), to be published
40. Rong Jian, Zhang Zhengjun (China Nuclear Data Center), to be published
41. Cai Chonghai, to be published
42. Cai Chonghai, Ge Zhigang (China Nuclear Data Center), to be published
43. Zhang Zhengjun (Phys. Dept. of Northwest Univ., Xian), to be published
44. Zhang Zhengjun, Ge Zhigang (China Nuclear Data Center), to be published
45. Zhang Zhengjun et al., to be published
46. Zhang Zhengjun et al., Communication of Nuclear Data Progress, No. 20(1998)77.
47. Shen Qingbiao (China Nuclear Data Center), to be published
48. Shen Qingbiao, Zhang Zhengjun (China Nuclear Data Center), to be published
49. Ge Zhigang (China Nuclear Data Center), Communication of Nuclear Data Progress, No.21(1999)35
50. Ge Zhigang (China Nuclear Data Center), to be published
51. Han Yinlu (China Nuclear Data Center), to be published
52. G.Vladuca, A.Tudora, and M.Sin, Rom. J. Phys.,tome 41, no. 7-8 (1996) 515-526
53. C.A.Engelbrecht and H.Fiedeldej, Ann. Phys. 42,262-295 (1967)
54. D.G.Madland, OECD/NEA Specialists Mtg. on Opt.Mod.to 200 MeV,Paris ,1997
55. P.G.Young,E.D.Arthur,M.Bozian,T.R.England,G.M.Hale,R.J.LaBauve,R.C.Little,et al., LANL Report LA-11753-MS (1990); see also LA-8630-P R,p2 (1980)

56. E.D.Arthur and C.Philis, Report LA-8630-PR,p2 (1980)
57. R.Macklin and P.G.Young, Nucl.Sci.Eng. 95,189(1987)
58. R.Macklin and P.G.Young, Nucl.Sci.Eng. 97,239(1987)
59. P.G.Young, LANL Progress Report LA-11972-PR (1990) p.9
60. P.G.Young, Report LA-UR (1997)
61. R.L.Varner,W.J.Thompson,T.L.McAbee,E.J.Ludwig,T.B.Clegg, Phys. Rep . 201,57 (1991)
62. R.L.Walter and P.P.Guss, Rad. Effects 92, 1079 (1985) [1985 Santa Fe Conf. Proc.]
63. A.J.Koning, J.J.van Wijk, J.P.Delaroche, OECD/NEA Specialists Mtg. on Opt.Mod.to 200 MeV,Paris,1997
64. A.J.Koning, J.P.Delaroche, Phys. Rev. C, submitted for publication , July,2001
65. E.D.Arthur,P.G.Young,W.Matthes, BNL-51245,p.751 (1980); Nucl.Sci.Eng.124,271(1996)
66. P.G.Young and E.D.Arthur, LA-UR-84-2767 (1984); LA-UR-94-3104 (1994)
67. M.B.Chadwick and P.G.Young, Proc.Int. Particle Therapy Mtg. and PT COG XXIV, 24-26 Apr. 1996,Detroit,Mich.
68. F.G.Perey, Phys. Rev. 131,745 (1963)
69. F.D.Becchetti Jr. and G.W.Greenlees, Phys. Rev. 182,1190 (1969)
70. J.J.H.Menet,E.E.Gross,J.J.Malanify, and A.Zucker, Phys. Rev. C4,114 (1971)
71. D.M.Patterson et al, Nucl. Phys. A263,261 (1976)
72. C.H.Johnson et al, Phys. Rev. Lett.39,1604(1977); Phys. Rev. C20,2052(1979)
73. D.S.Flynn et al, Phys. Rev. C. 31, 87 (1985)
74. S.Kailas et al, Phys. Rev. C 20, 1272(1979); Pramana.J.Phys.27, 139(1986)
75. Y.P.Viyogi, Ph.D Thesis (Calcutta University 1983)
76. R.L.Walter and P.P.Guss, Rad. Effects 92, 1079 (1985) [1985 Santa Fe Conf. Proc.]
77. C.M.Perey and F.G.Perey, Phys. Rev. 132,755 (1963)
78. J.M.Lohr and W.Haerberli, Nucl. Phys. A232,381(1974)
79. J.Bojowald et al, Phys. Rev. C 38,1153(1988)
80. F.D.Becchetti Jr. and G.W.Greenlees, Ann. Rept. J.H.Williams Lab., Univ. Minnesota (1969)
81. H.H.Chang et al, Nucl. Phys. A297,105 (1978)
82. E.D.Arthur and P.G.Young, Report LA-8636-MS(ENDF-304) (1980)
83. E.D.Arthur,P.G.Young,W.Matthes, Report BNL-51245,751(1980)
84. L.McFadden and G.R.Satchler, Nucl. Phys. 84, 177 (1966)
85. J.R.Huizenga and G.Igo, Nucl. Phys. 29,462 (1962)
86. B.Strohmaier et al, Paper at the IAEA Advisory Group Meeting ,1981
87. O.F.Lemos, Orsay, Series A ,No.136 (1972)
88. V.Avrigeanu,P.E.Hodgson, and M.Avrigeanu, Report OUNP-94-02 (1994) , Phys. Rev. C49,2136 (1994)

Status of Japanese Contribution to RIPL-2

Tokio FUKAHORI

Nuclear Data Center, Tokai-mura, Naka-gun, Ibaraki-ken 319-1195, Japan

e-mail: fukahori@ndc.tokai.jaeri.go.jp

1. Deformation Parameter Retrieve from ENSDF and Literature

The deformation parameter has been retrieved from ENSDF and Literature. They are summarized in Table 1. The deformation parameters, such as quadrupole moment (Q), BE2 and BE3 have been pick up from ENSDF. The deformation parameter, β_2 , was derived from Q by using the equation;

$$Q = Q_0 \frac{3K^2 - I(I+1)}{(I+1)(2I+3)} \quad (1)$$

$$Q_0 = \frac{3}{\sqrt{5\pi}} ZR_0^2 \beta(1 + 0.16\beta + \dots) \quad (2)$$

$$R_0^2 = 0.0144A^{2/3} \text{ [b]} \quad (3)$$

where K , I were assumed to equal to ground and excited state spins, and Z , A atomic and mass number, respectively.

The deformation parameters, $B(E2; 0^+ \rightarrow 2^+)$ and $B(E3; 0^+ \rightarrow 3^-)$, were compiled from the Ref. [1,2]. The parameters can be converted to β_2 and β_3 by using appropriate equations [1,2];

$$B(E2) \uparrow = \left(\frac{3}{4\pi} R_0^2 Z e \beta_2 \right)^2 \text{ [e}^2\text{b}^2\text{]} \quad (4)$$

$$B(E3) \uparrow = \left(\frac{3}{4\pi} R_0^3 Z e \beta_3 \right)^2 \text{ [e}^2\text{b}^3\text{]} \quad (5)$$

2. WWW Page Preparation

We have tried to prepare WWW page related to the RIPL-2 File. Prepared were the pages for mass and giant dipole resonance parameters. The pages for the other segments are under preparation. They will be finished soon. For example, RIPL-2 home page is shown in Fig.1.

References

- [1] S. Raman, C.W. Nestor, Jr., S. Kahane and K.H. Bhatt; Atomic Data and Nuclear Data Tables 42, 1-54 (1989).
- [2] R.H. Spear; Atomic Data and Nuclear Data Tables 42, 55-104 (1989).

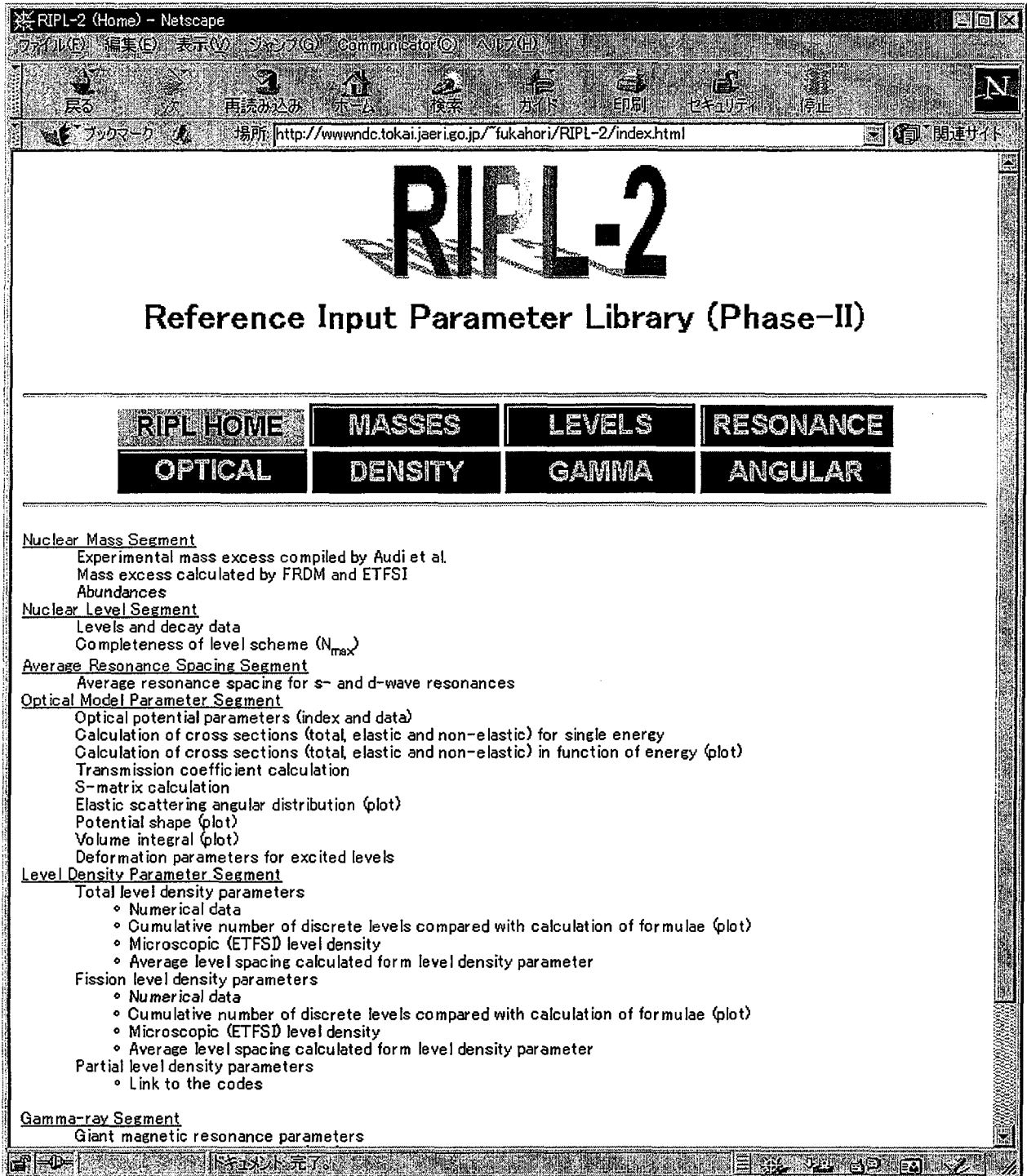


Fig. 1 The example of "Mass Page"

New neutron and proton optical models

A. J. Koning

*Nuclear Research and Consultancy Group NRG,
P.O. Box 25, 1755 ZG Petten, The Netherlands*

J. P. Delaroche

*Commissariat à l'Energie Atomique,
Service de Physique Nucléaire, Boîte Postale 12,
91680 Bruyères-le-Châtel, France
(November 30, 2001)*

I. INTRODUCTION

We present a new global optical model parameterization for neutrons and protons with energies from a few keV up to 200 MeV, for (near-)spherical nuclides in the mass range $A > 24$. It is based on a unique functional form for the energy dependence of the potential depths, and physically constrained geometry parameters. For the first time, this enables to predict basic scattering observables over a very broad energy and mass range, thereby removing the necessity to use different optical models in different energy regions. Using extensive grid searches and a new computational steering technique, we first obtained optical model parameters for each nucleus separately. From this, we have constructed a global optical model which is shown to be superior to all other existing phenomenological global optical models, while the latter moreover apply in much more restricted energy regions. To constrain our parameterization as much as possible, we have used an extensive data set of resonance parameters, total and non-elastic cross sections, elastic scattering angular distributions and analyzing powers, to assess the performance of our potential.

II. THEORY

A. The optical model potential

The optical model potential \mathcal{U} is defined as:

$$\mathcal{U}(r, E) = -\mathcal{V}_V(r, E) - i\mathcal{W}_V(r, E) - i\mathcal{W}_D(r, E) + \mathcal{V}_{SO}(r, E) + i\mathcal{W}_{SO}(r, E) + \mathcal{V}_C(r), \quad (2.1)$$

where $\mathcal{V}_{V,SO}$ and $\mathcal{W}_{V,D,SO}$ are the real and imaginary components of the volume-central (V), surface-central (D) and spin-orbit (SO) potentials, respectively. When treating the optical model phenomenologically, all components are separated in energy-dependent well depths, V_V, W_V, W_D, V_{SO} and W_{SO} , and radial-dependent parts f ,

$$\begin{aligned}
\mathcal{V}_V(r, E) &= V_V(E)f(r, R_V, a_V) \\
\mathcal{W}_V(r, E) &= W_V(E)f(r, R_V, a_V) \\
\mathcal{W}_D(r, E) &= -4a_D W_D(E) \frac{d}{dr} f(r, R_D, a_D) \\
\mathcal{V}_{SO}(r, E) &= V_{SO}(E) \left(\frac{\hbar}{m_\pi c} \right)^2 1. \sigma \frac{1}{r} \frac{d}{dr} f(r, R_{SO}, a_{SO}) \\
\mathcal{W}_{SO}(r, E) &= W_{SO}(E) \left(\frac{\hbar}{m_\pi c} \right)^2 1. \sigma \frac{1}{r} \frac{d}{dr} f(r, R_{SO}, a_{SO})
\end{aligned} \tag{2.2}$$

As usual, the form factor $f(r, R_i, a_i)$ is given by the Woods-Saxon shape

$$f(r, R_i, a_i) = \frac{1}{1 + \exp((r - R_i)/a_i)}, \tag{2.3}$$

where the geometry parameters are the radius $R_i = r_i A^{1/3}$, with A the nuclear mass number, and the diffuseness a_i for each component of the potential. For charged projectiles the Coulomb term \mathcal{V}_C is given by

$$\begin{aligned}
\mathcal{V}_C(r) &= \frac{Zze^2}{2R_C} \left(3 - \frac{r^2}{R_C^2} \right), \quad \text{for } r \leq R_C \\
&= \frac{Zze^2}{r}, \quad \text{for } r \geq R_C
\end{aligned} \tag{2.4}$$

with $Z(z)$ the charge of the target (projectile).

It is important to note that the real and imaginary potentials of each component V , and SO share the same form factors, i.e. we assume the same geometry parameters for the pair $(\mathcal{V}_V, \mathcal{W}_V)$ and for the pair $(\mathcal{V}_{SO}, \mathcal{W}_{SO})$, while \mathcal{W}_D has its own geometry parameters. Moreover, we take each r_i and a_i independent of energy. These constraints allow us less parameter freedom than allowed in most existing phenomenological optical models, but it is physically better justified in the light of dispersion relations. The dispersive corrections themselves are not included, in this paper, which is indicated by the absence of a real surface term \mathcal{V}_D or, equivalently, an effective energy-dependent radius of the real volume potential in (2.1).

All functional forms for the potential depths depend on $E - E_f$ where E is the laboratory energy of the incident particle, and E_f is the Fermi energy. The latter is defined as the energy halfway the last occupied and the first unoccupied shell of the nucleus. For incident neutrons, it is given by

$$E_f({}^N_Z A) = -\frac{1}{2}[S_n({}^N_Z A) + S_n({}^{N+1}_Z A + 1)] \tag{2.5}$$

with S_n the neutron separation energy for a nucleus ${}^N_Z A$, and for incident protons by

$$E_f({}^N_Z A) = -\frac{1}{2}[S_p({}^N_Z A) + S_p({}^N_{Z+1} A + 1)] \tag{2.6}$$

with S_p the proton separation energy.

Our optical model parameterization is given by

$$\begin{aligned}
 V_V(E) &= v_1[1 - v_2(E - E_f) + v_3(E - E_f)^2 - v_4(E - E_f)^3] + \epsilon \cdot 0.42Z/A^{1/3} \\
 W_V(E) &= w_1 \frac{(E - E_f)^2}{(E - E_f)^2 + w_2^2} \\
 r_V &= \text{constant} \\
 a_V &= \text{constant} \\
 W_D(E) &= d_1 \exp(-d_2(E - E_f)) \frac{(E - E_f)^2}{(E - E_f)^2 + d_3^2} \\
 r_D &= \text{constant} \\
 a_D &= \text{constant} \\
 V_{so}(E) &= v_{so1} \exp[-v_{so2}(E - E_f)] \\
 W_{so}(E) &= w_{so1} \frac{(E - E_f)^2}{(E - E_f)^2 + w_{so2}^2} \\
 r_{so} &= \text{constant} \\
 a_{so} &= \text{constant} \\
 r_C &= \text{constant}, \tag{2.7}
 \end{aligned}$$

where $\epsilon = 0$ for neutrons and $\epsilon = 1$ for protons.

B. Compound nucleus contribution and relativistic correction

A good analysis of scattering observables at low energies requires the inclusion of a compound nucleus contribution. For this, we use the width fluctuation correction model by Moldauer [1], coupled with the Blatt-Biedenharn formalism for angular distributions. For a particular incident energy, all channels that are open to compound nucleus emission are included. We include the first several discrete states as competing channels and complement this, for higher excitation energies, by a continuum described by the Gilbert-Cameron level density formula. The level density parameters are taken from Mengoni's RIPL table. The analysis of shape + compound elastic scattering is done iteratively, since the transmission coefficients required for the compound nucleus cross section are the same as those that describe the shape elastic part.

For a consistent analysis at all energies we have used the relativistic Schrödinger equation throughout. In practice, this means that if one would apply our results in a non-relativistic calculation, significant deviations from the correct result should be expected above several tens of MeV.

III. GLOBAL OPTICAL MODEL

Our methodology to obtain our global optical models will not be described here. We merely mention that it was obtained using a combination of automatic optimization around the ECIS-code [2] and a novel interactive visualisation technique, enabled by the ECISVIEW software package. With the general parameterization (2.7), we have obtained dedicated

optical models for virtually every (near-)spherical nucleus separately. These more extensive results will be reported in a following publication. Important here is that each parameter follows a clear trend as a function of mass, enabling us to construct the following global optical model. The mass dependence of all parameters is for neutrons:

$$\begin{aligned}
 v_1 &= 59.30 - 21.0(N - Z)/A - 0.024A \text{ MeV} \\
 v_2 &= 0.007228 - 1.48 \cdot 10^{-6} A \text{ MeV}^{-1} \\
 v_3 &= 1.994 \cdot 10^{-5} - 2.0 \cdot 10^{-8} A \text{ MeV}^{-2} \\
 v_4 &= 7 \cdot 10^{-9} \text{ MeV}^{-3} \\
 w_1 &= 12.195 + 0.0167A \text{ MeV} \\
 w_2 &= 73.55 + 0.0795A \text{ MeV} \\
 r_V &= 1.3039 - 0.4054A^{-1/3} \text{ fm} \\
 a_V &= 0.6778 - 1.487 \cdot 10^{-4} A \text{ fm} \\
 d_1 &= 16.0 - 16.0(N - Z)/A \text{ MeV} \\
 d_2 &= 0.0180 + 0.003802/(1 + \exp[(A - 156.)/8.]) \text{ MeV}^{-1} \\
 d_3 &= 11.5 \text{ MeV} \\
 r_D &= 1.3424 - 0.01585A^{1/3} \text{ fm} \\
 a_D &= 0.5446 - 1.656 \cdot 10^{-4} A \text{ fm} \\
 v_{so1} &= 5.922 + 0.0030A \text{ MeV} \\
 v_{so2} &= 0.0040 \text{ MeV}^{-1} \\
 w_{so1} &= -3.1 \text{ MeV} \\
 w_{so2} &= 160. \text{ MeV} \\
 r_{so} &= 1.1854 - 0.647A^{-1/3} \text{ fm} \\
 a_{so} &= 0.59 \text{ fm} \\
 r_C &= 0. \text{ fm} \\
 E_f &= -11.2814 + 0.02646A \text{ MeV}
 \end{aligned} \tag{3.1}$$

and for protons:

$$\begin{aligned}
 v_1 &= 59.30 + 21.0(N - Z)/A - 0.024A \text{ MeV} \\
 v_2 &= 0.007067 + 4.36 \cdot 10^{-6} A \text{ MeV}^{-1} \\
 v_3 &= 1.747 \cdot 10^{-5} + 1.5 \cdot 10^{-8} A \text{ MeV}^{-2} \\
 w_1 &= 14.336 + 0.0189A \text{ MeV} \\
 d_1 &= 14.3 + 20.0(N - Z)/A \text{ MeV} \\
 a_d &= 0.5413 + 3.963 \cdot 10^{-4} A \text{ fm} \\
 r_C &= 1.198 + 0.697A^{-2/3} + 12.994A^{-5/3} \text{ fm} \\
 E_f &= -8.4075 + 0.01378A \text{ MeV}
 \end{aligned} \tag{3.2}$$

with the other parameters the same as for neutrons. Note that E_f is given by a simple form here.

Several conclusions can be drawn from this parametrization. First, by including the isovector term in v_1 and d_1 , we automatically take it energy-dependent and moreover assume

this dependence is equal to that of the isoscalar term. Our grid search clearly indicates that r_v increases with mass. To compensate for this effect, V contains a term that decreases linearly with A , in addition to the asymmetry term. Note that this linear term does not change sign for protons. We had to adopt a surface diffuseness a_d that is bigger for protons than for neutrons, in order to get a satisfactory fit of the proton reaction cross sections. This means that we can not yet accomplish a Lane-consistent model with our parametrization.

IV. RESULTS

The present paper covers our results for neutrons only. Table I shows a comparison of our global neutron potential with some well-known other global optical models, on a χ^2/N (per point) basis. The results are based on about 800 angular distributions and 120 total cross sections sets, covering measurements over the whole range of interest. When judged with this numerical criterion, our global optical model appears to perform better than each of the listed models in their own energy range, even though ours covers a wider energy range. Only angular distributions predicted by the Walter-Guss model are close to our performance.

As a first illustration, we compare our global optical model with measured resonance information in Fig. 1, for S_0, S_1 and R' respectively.

Figs. 2-3 show calculated and measured neutron total cross sections, for various nuclides and a wide energy range. Results are given for both the particular optical model (i.e. parameter set per nucleus) and the global optical model. The general agreement is excellent, both at low and high energies. The recent total cross section measurements, performed at WNR in Los Alamos, for energies between 5 MeV and several hundreds of MeV [3], are generally predicted within 1-2 % by our global optical model.

Figs. 4-23 show the neutron elastic angular distributions for many nuclides, again for both the particular and the global optical model.

V. CONCLUSIONS

Among the notorious problems which have *not* been solved by our new approach are:

- A description of the total cross section below 3 MeV in the Cr-Ni region. The measurements suggest a low-energy resonance, whereas this is not predicted by our (or any other) global model. Dispersion relations and a coupled-channels approach only partially solve this problem and so far only an optical model with a contribution from selected partial waves has been successful in this respect.
- An underestimation of R' and an overestimation of S_1 in the $90 < A < 120$ mass range. Even though the optical model yields the correct total cross sections in the keV region, its division into a shape-elastic and a reaction part may be incorrect.
- Problems with the phasing of forward angle proton angular distributions above 150 MeV (not shown here). This is where the validity of the Woods-Saxon form factors and/or its energy-independent geometry parameters begins to break down.

- Our global optical model is preliminary. Two minor adjustments are foreseen. The isovector term in v_1 , 21.0, is considered to be a bit small, and should be around 24. Also, there is probably a little bit too much surface absorption for light nuclides, which is exhibited by a slight underestimation of angular distributions at backward angles. These are however, minor modifications.

Nevertheless, we think the results reported in this paper are valuable for the following reasons:

- A physically constrained set of optical model parameters, obtained by simultaneously analyzing all different types of observables at widely varying energies.
- The first global optical model that is obtained from a grid search.
- An optical model that is applicable at *any* energy up to 200 MeV, and that compares favorably to other global optical models.

The figures obviously indicate that the global optical model itself is outperformed by dedicated parameters per nucleus. These will be reported in a following paper.

REFERENCES

- [1] P.A. Moldauer, *Nuc. Phys.* **A344** 185 (1980).
- [2] J. Raynal, *Notes on ECIS94*, CEA Saclay report CEA-N-2772 (1994).
- [3] F. Dietrich, *Phys. Rev. C* ?? (2001).
- [4] S.F. Mughabghab, *Neutron cross sections*, Academic Press (1984).

TABLES

TABLE I. Comparison of our neutron potential ($0.001 < E < 200$ MeV, $24 < A < 209$) with other global potentials. The χ^2 per point is given for elastic scattering angular distributions and total cross sections separately, in the mass and energy range for which the older optical models were claimed to be valid.

OMP	A	E (MeV)	χ_{ad}^2/N	χ_{ad}^2/N (This)	χ_{tot}^2/N	χ_{tot}^2/N (This)
Wilmore-Hodgson	40-208	0 - 15	11.2	7.4	9.2	6.7
Rapaport	40-208	7 - 26	10.0	7.0	4.1	1.8
Varner	40-208	7 - 26	8.3	7.0	4.7	1.8
Walter-Guss	53-208	10- 80	6.3	6.1	2.3	1.3
Madland	40-208	50-200	8.6	4.5	6.9	1.2

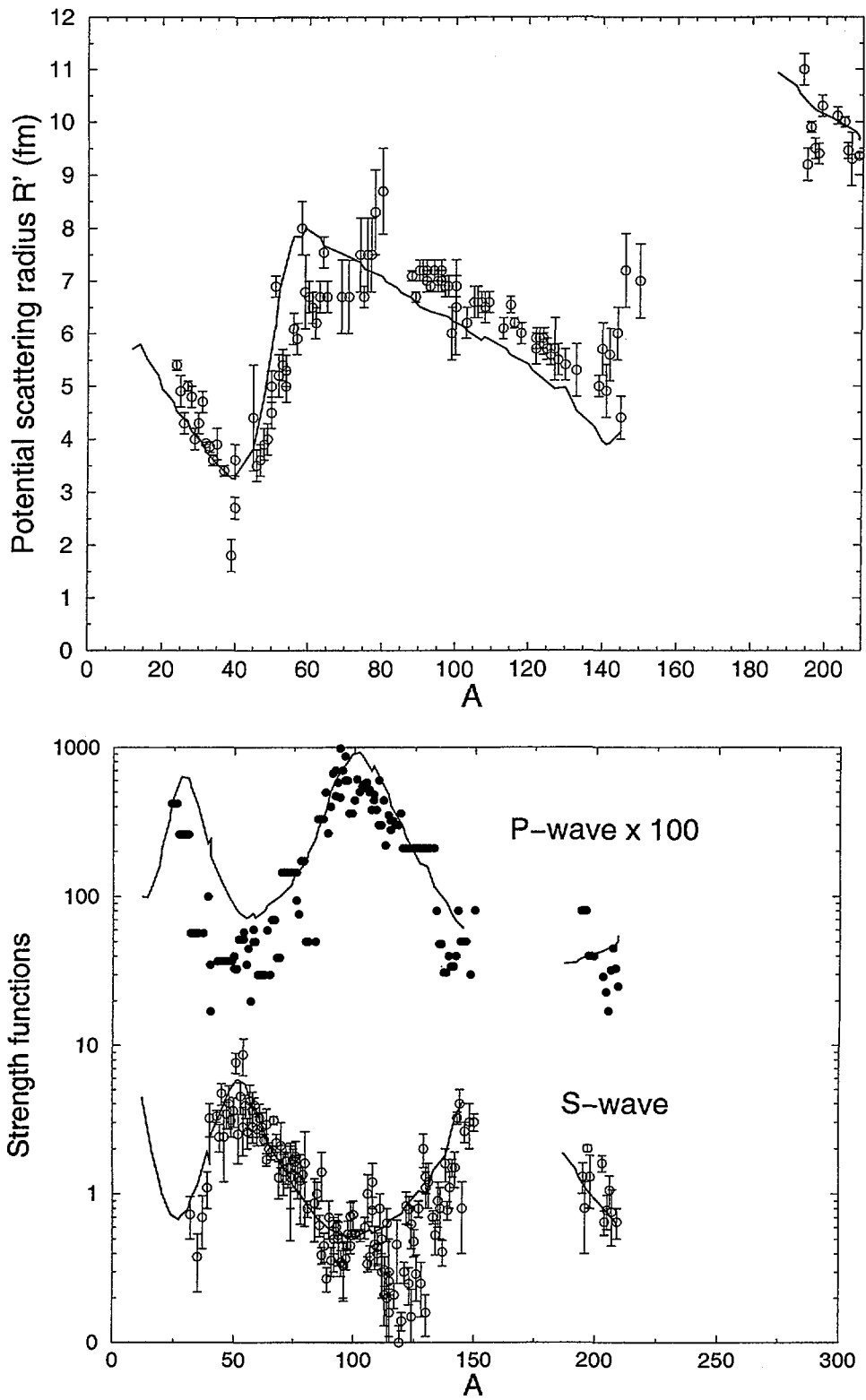


FIG. 1. S-wave, P-wave strength functions and potential scattering radius R' . The experimental data were taken from Ref. [4].

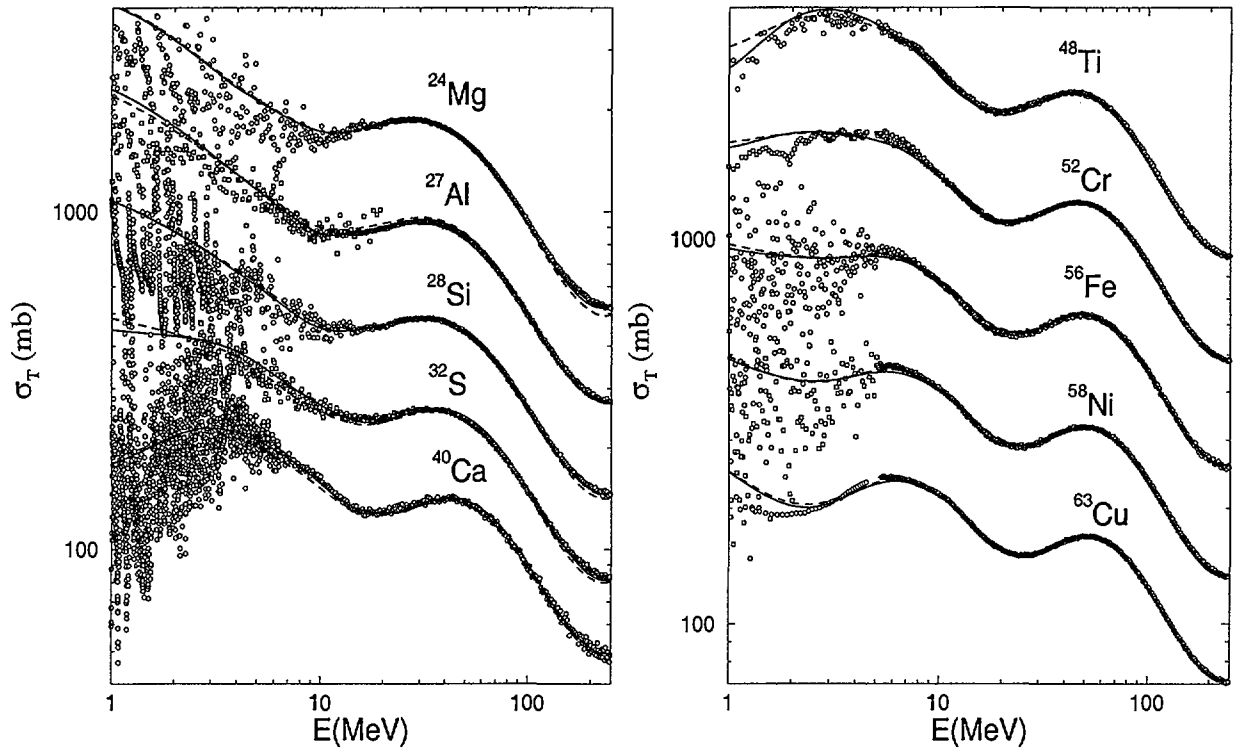


FIG. 2. Comparison of predicted neutron total cross sections and experimental data, for nuclides in the Mg-Ca and Ti-Cu mass ranges, for the energy range 1-250 MeV. The solid line represents calculations with the particular optical model per nucleus, while the dashed line represents the global optical model. The curves and data points at the top represent true values, the others are offset by a factor of 2.

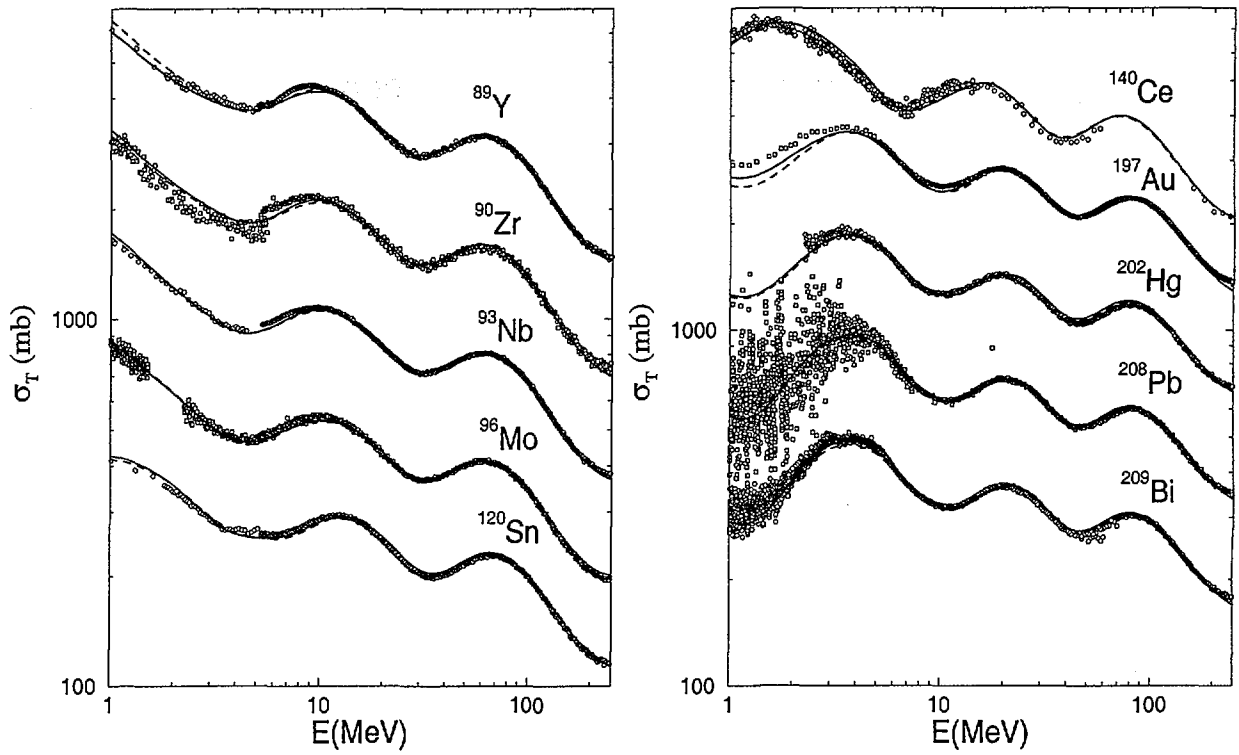


FIG. 3. Comparison of predicted neutron total cross sections and experimental data, for nuclides in the Y-Sn and Ce-Bi mass ranges, for the energy range 1-250 MeV. For more details, see the caption of Fig. 2

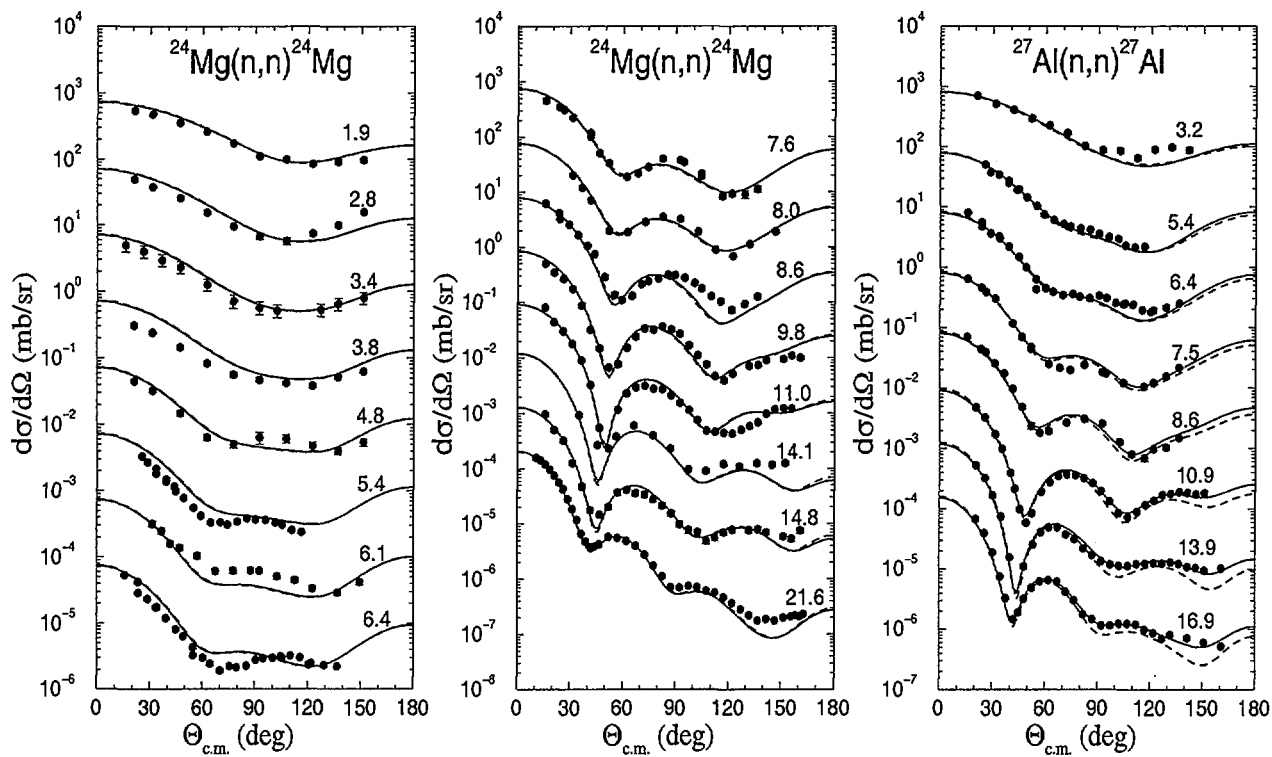


FIG. 4. Comparison of predicted differential cross sections and experimental data, for neutrons scattered from ^{24}Mg and ^{27}Al . The solid line represents calculations with the particular optical model per nucleus, while the dashed line represents the global optical model. The incident energies are given in MeV. The differential cross sections are offset by factors of 10.

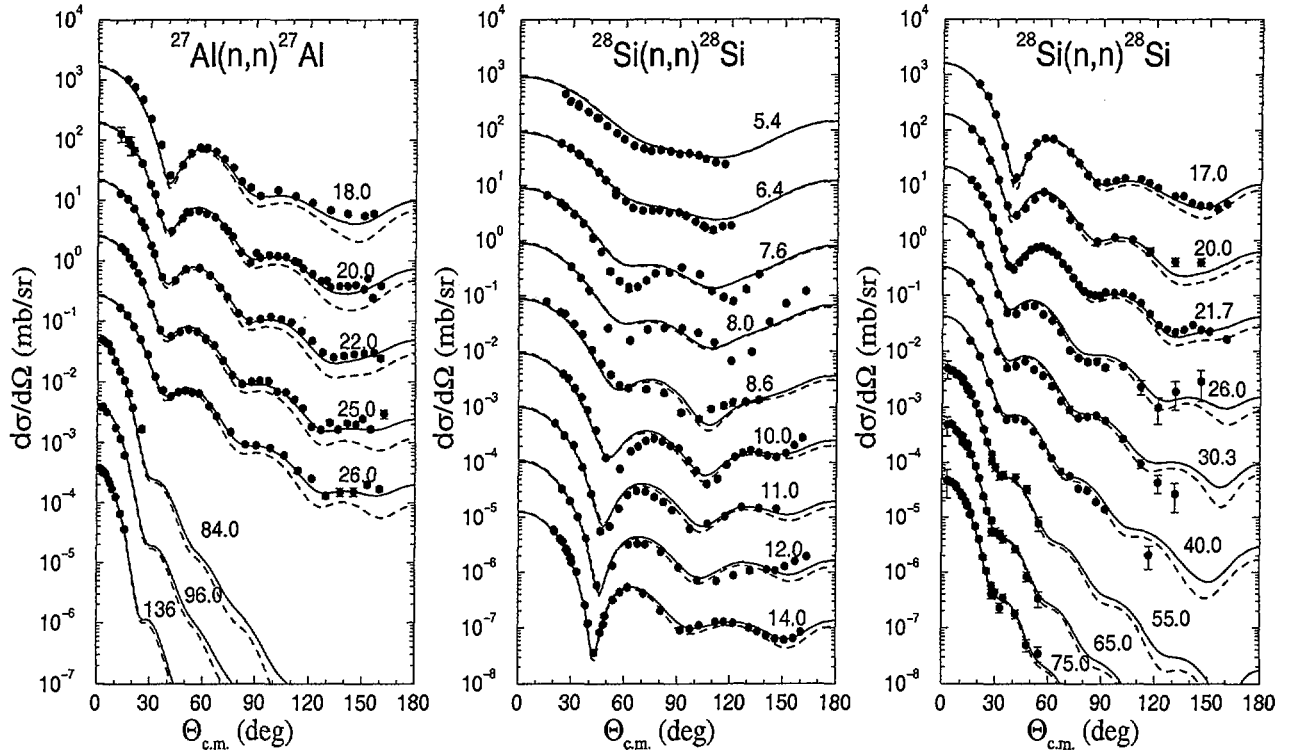


FIG. 5. Comparison of predicted differential cross sections and experimental data, for neutrons scattered from ^{27}Al and ^{28}Si . For more details, see the caption of Fig. 4

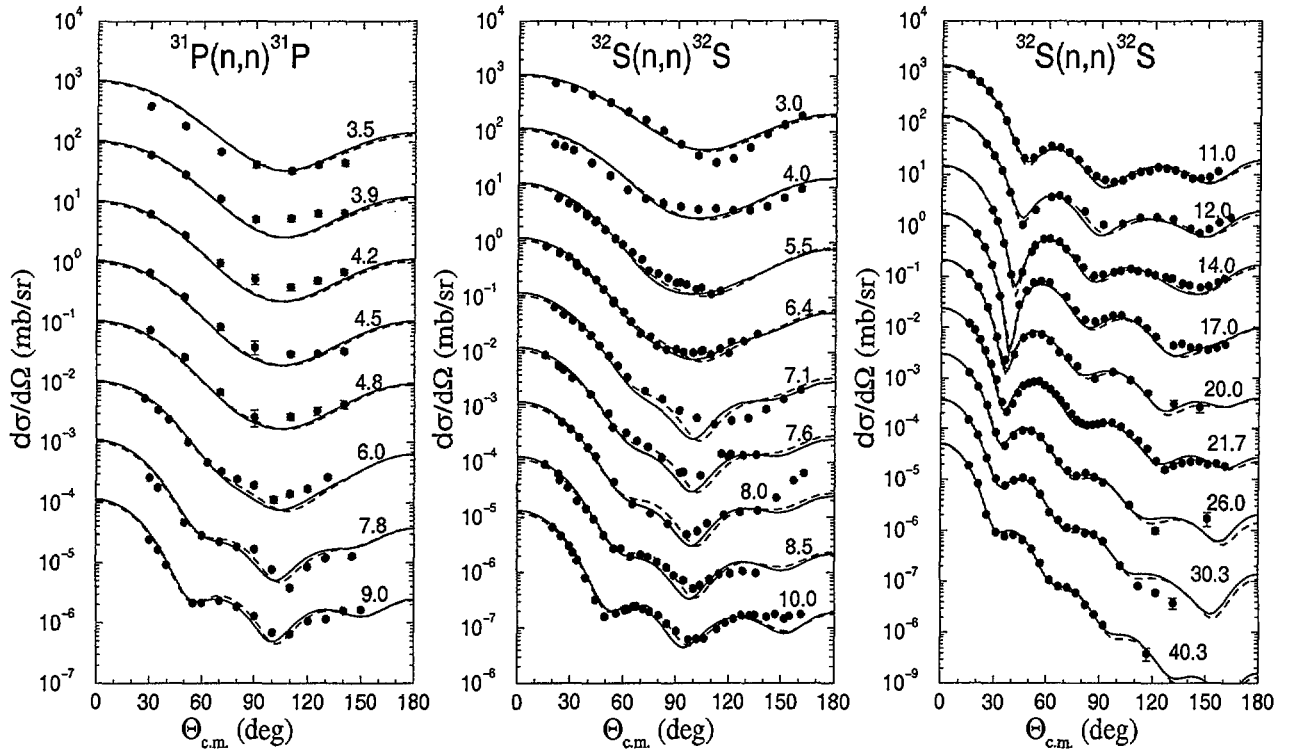


FIG. 6. Comparison of predicted differential cross sections and experimental data, for neutrons scattered from ^{31}P and ^{32}S . For more details, see the caption of Fig. 4

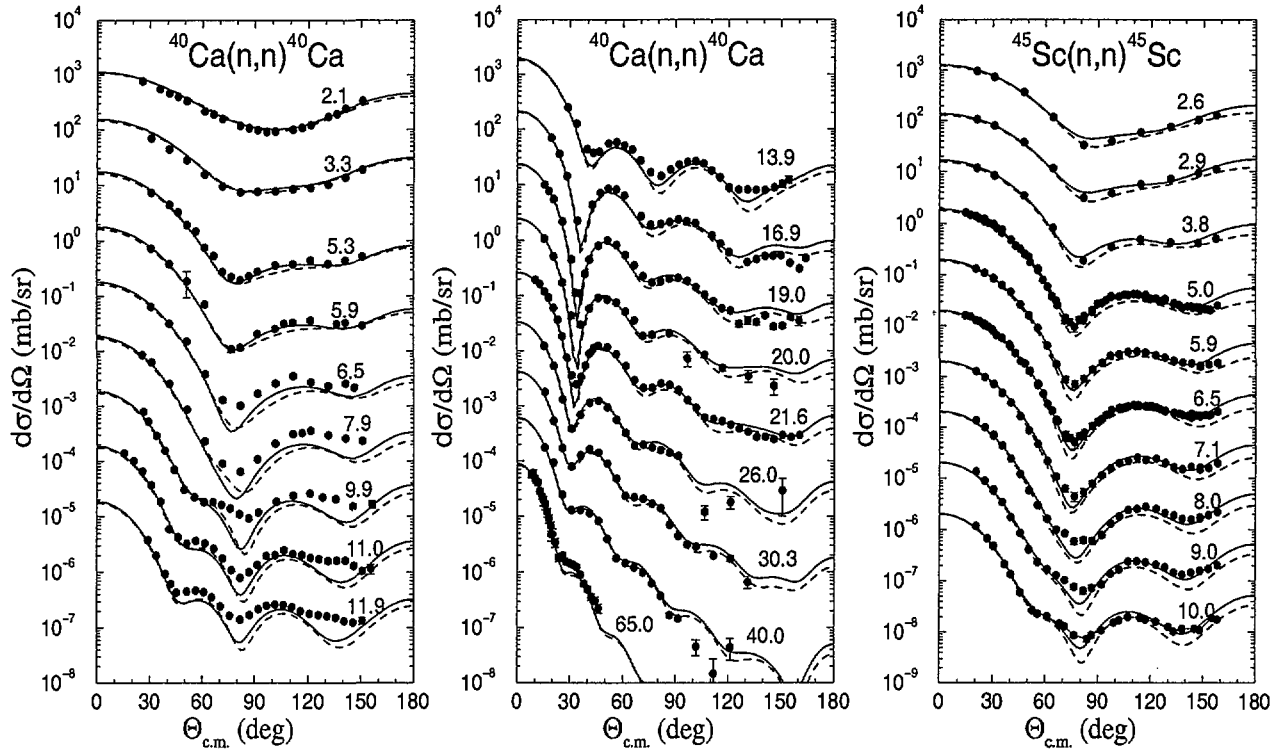


FIG. 7. Comparison of predicted differential cross sections and experimental data, for neutrons scattered from ^{40}Ca and ^{45}Sc . For more details, see the caption of Fig. 4

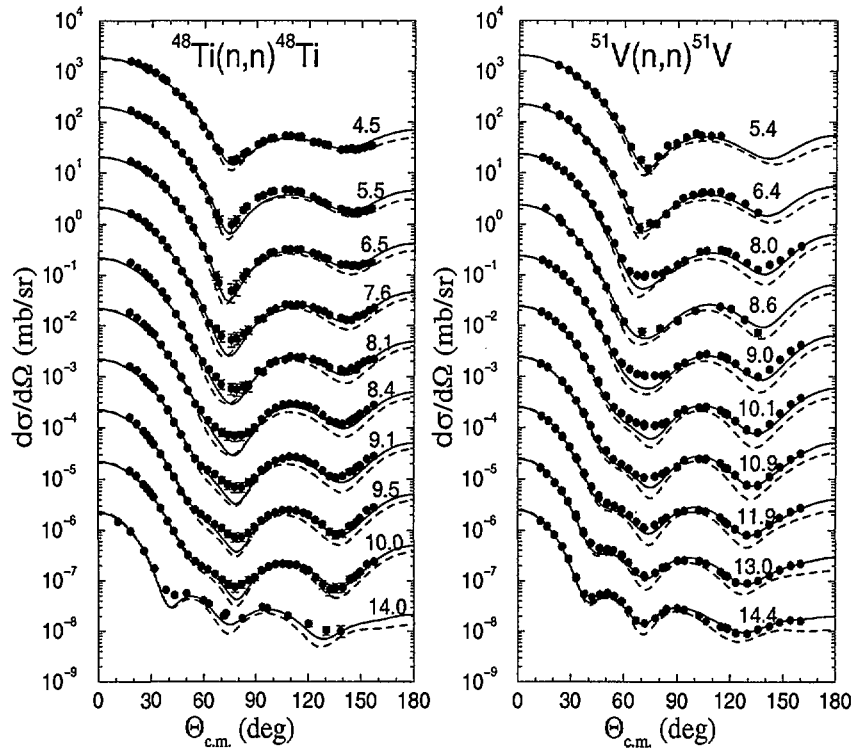


FIG. 8. Comparison of predicted differential cross sections and experimental data, for neutrons scattered from ^{48}Ti and ^{51}V . For more details, see the caption of Fig. 4

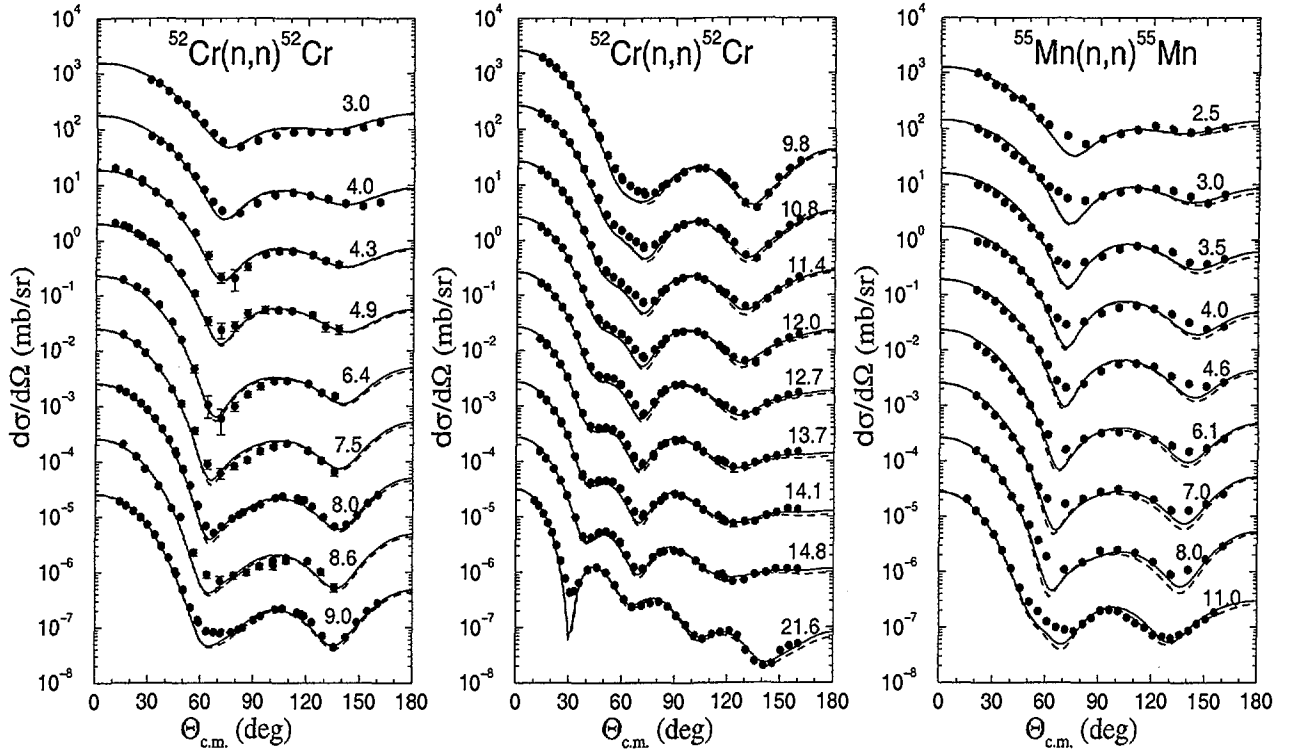


FIG. 9. Comparison of predicted differential cross sections and experimental data, for neutrons scattered from ^{52}Cr and ^{55}Mn . For more details, see the caption of Fig. 4

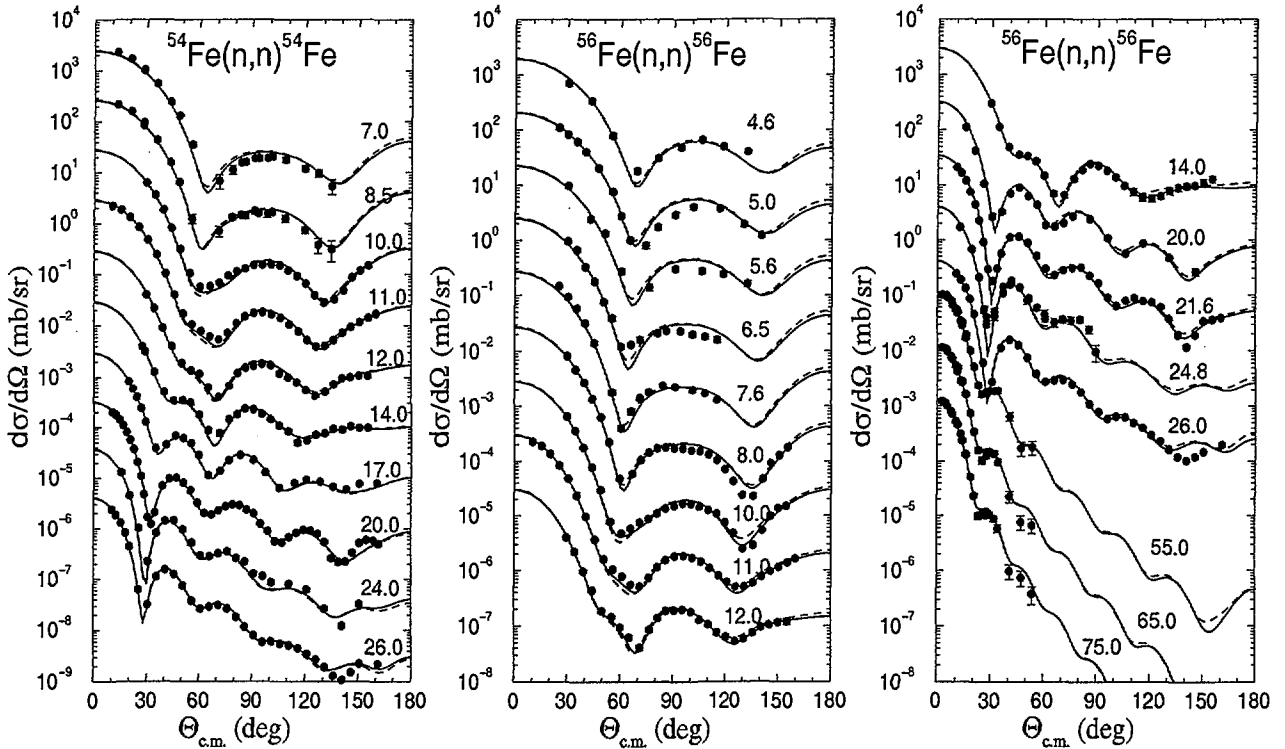


FIG. 10. Comparison of predicted differential cross sections and experimental data, for neutrons scattered from ^{54}Fe and ^{56}Fe . For more details, see the caption of Fig. 4

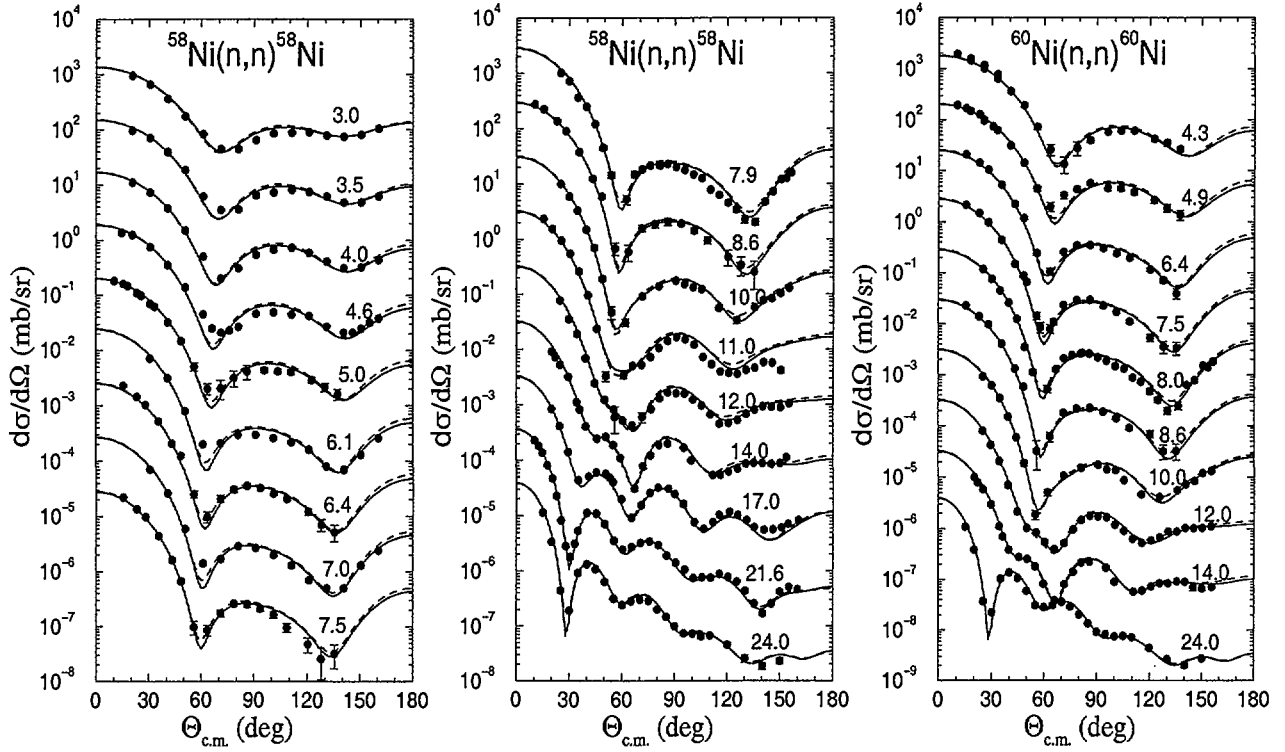


FIG. 11. Comparison of predicted differential cross sections and experimental data, for neutrons scattered from ^{58}Ni and ^{60}Ni . For more details, see the caption of Fig. 4

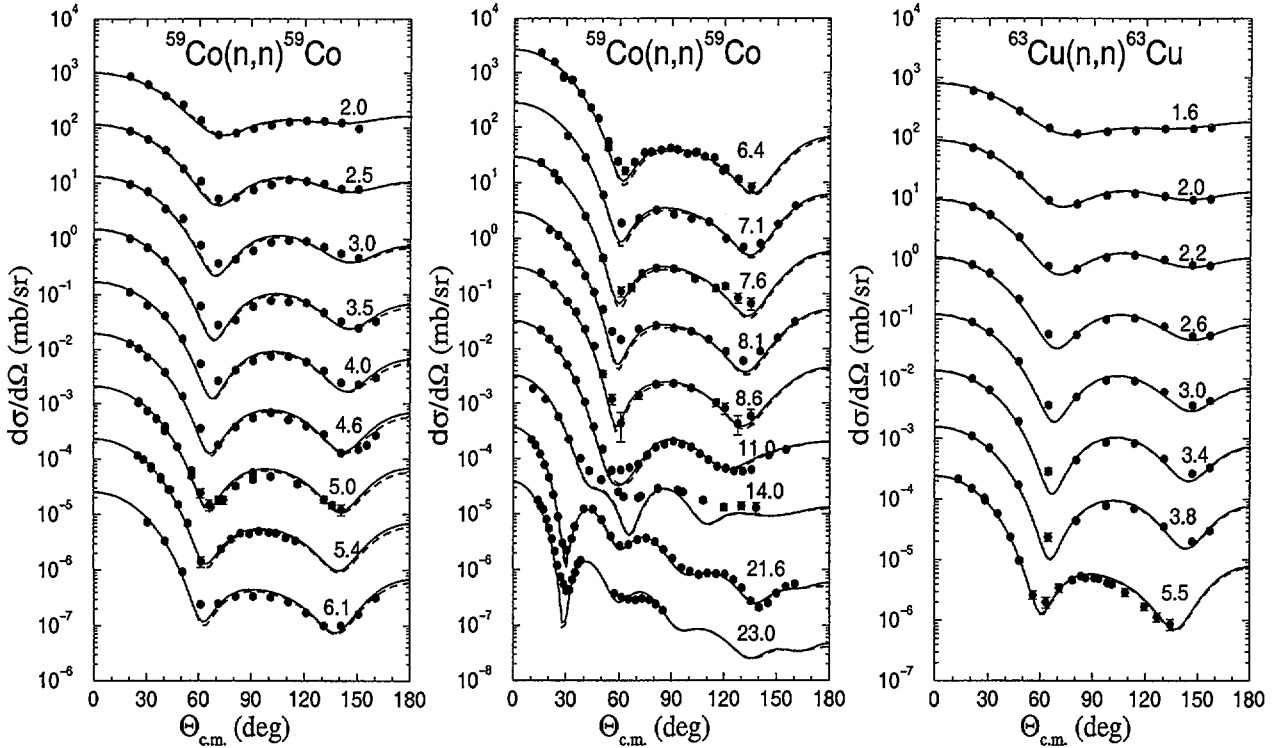


FIG. 12. Comparison of predicted differential cross sections and experimental data, for neutrons scattered from ^{59}Co and ^{63}Cu . For more details, see the caption of Fig. 4

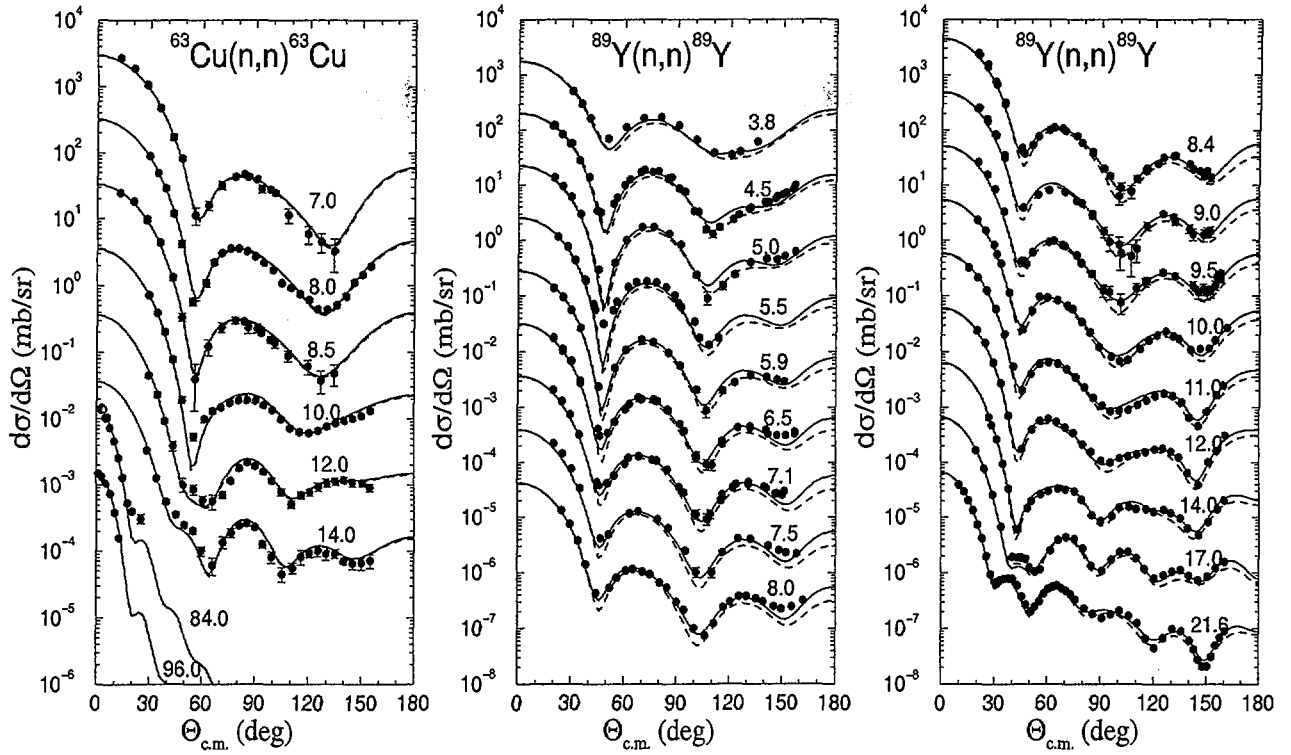


FIG. 13. Comparison of predicted differential cross sections and experimental data, for neutrons scattered from ^{63}Cu and ^{89}Y . For more details, see the caption of Fig. 4

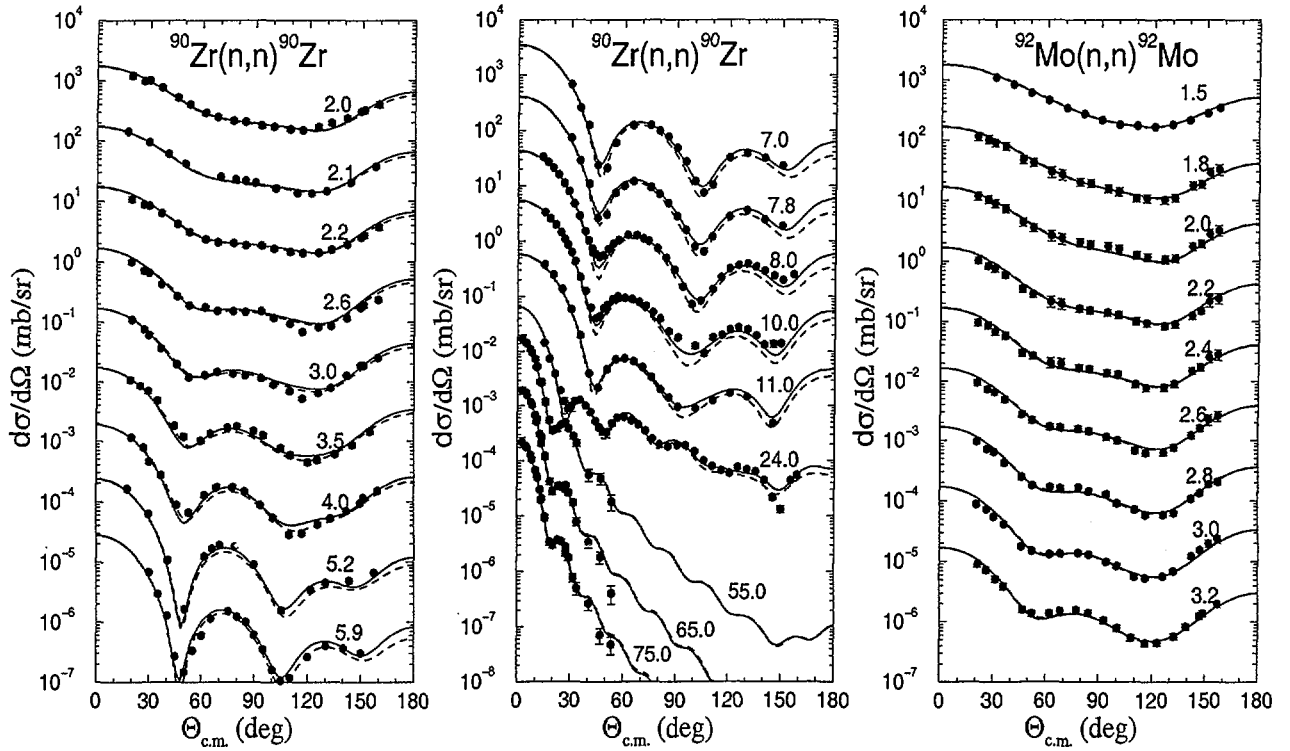


FIG. 14. Comparison of predicted differential cross sections and experimental data, for neutrons scattered from ^{90}Zr and ^{92}Mo . For more details, see the caption of Fig. 4

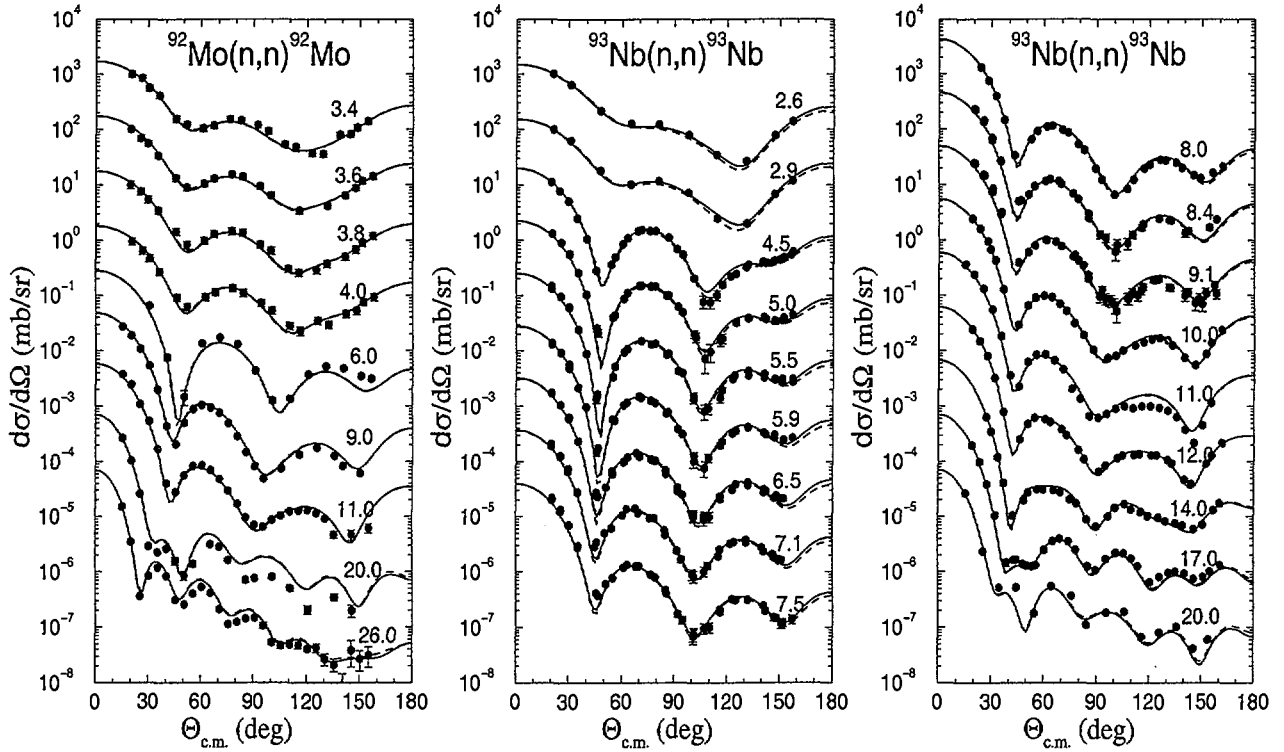


FIG. 15. Comparison of predicted differential cross sections and experimental data, for neutrons scattered from ^{92}Mo and ^{93}Nb . For more details, see the caption of Fig. 4

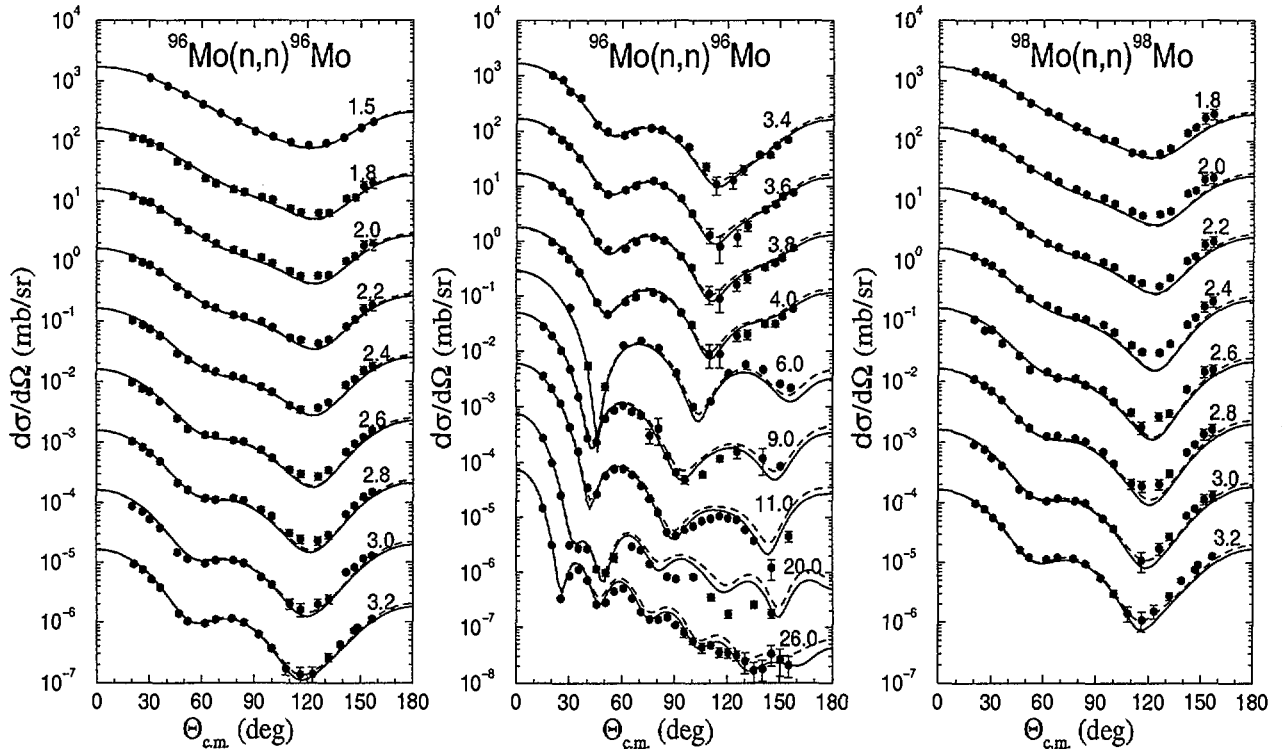


FIG. 16. Comparison of predicted differential cross sections and experimental data, for neutrons scattered from ^{96}Mo and ^{98}Mo . For more details, see the caption of Fig. 4

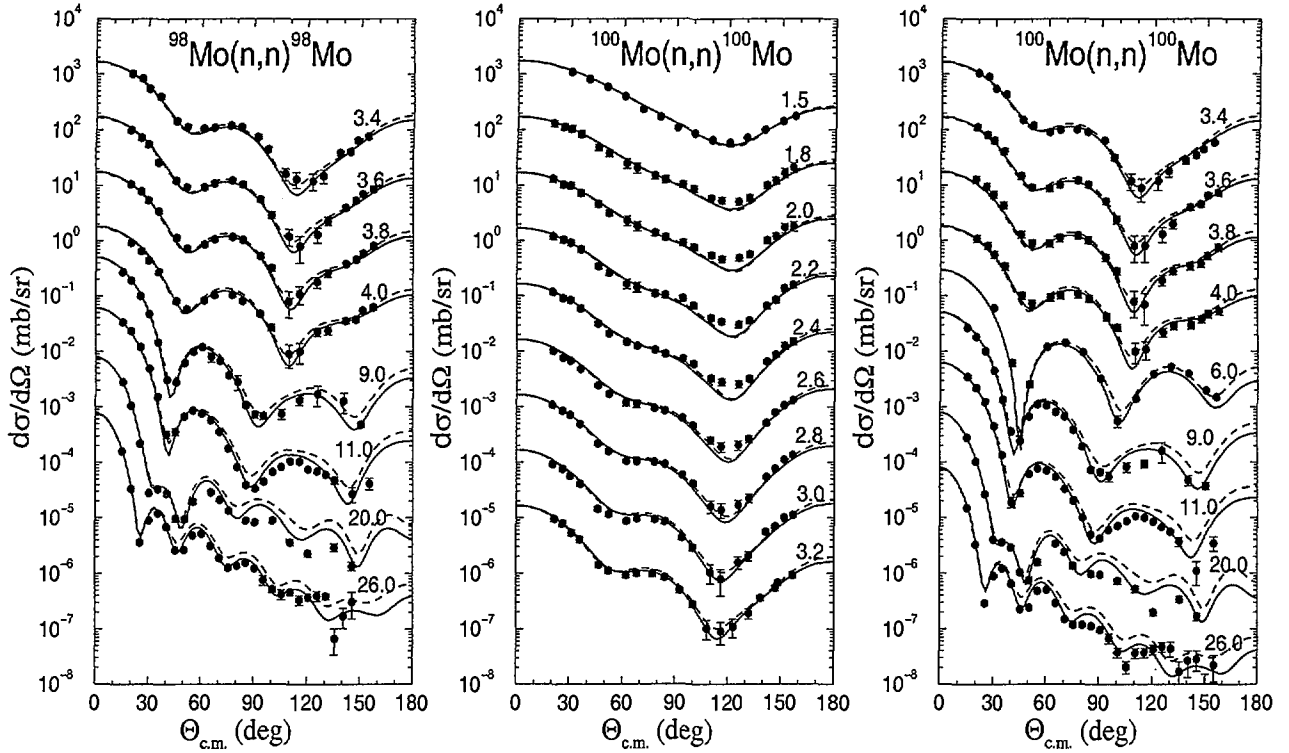


FIG. 17. Comparison of predicted differential cross sections and experimental data, for neutrons scattered from ^{98}Mo and ^{100}Mo . For more details, see the caption of Fig. 4

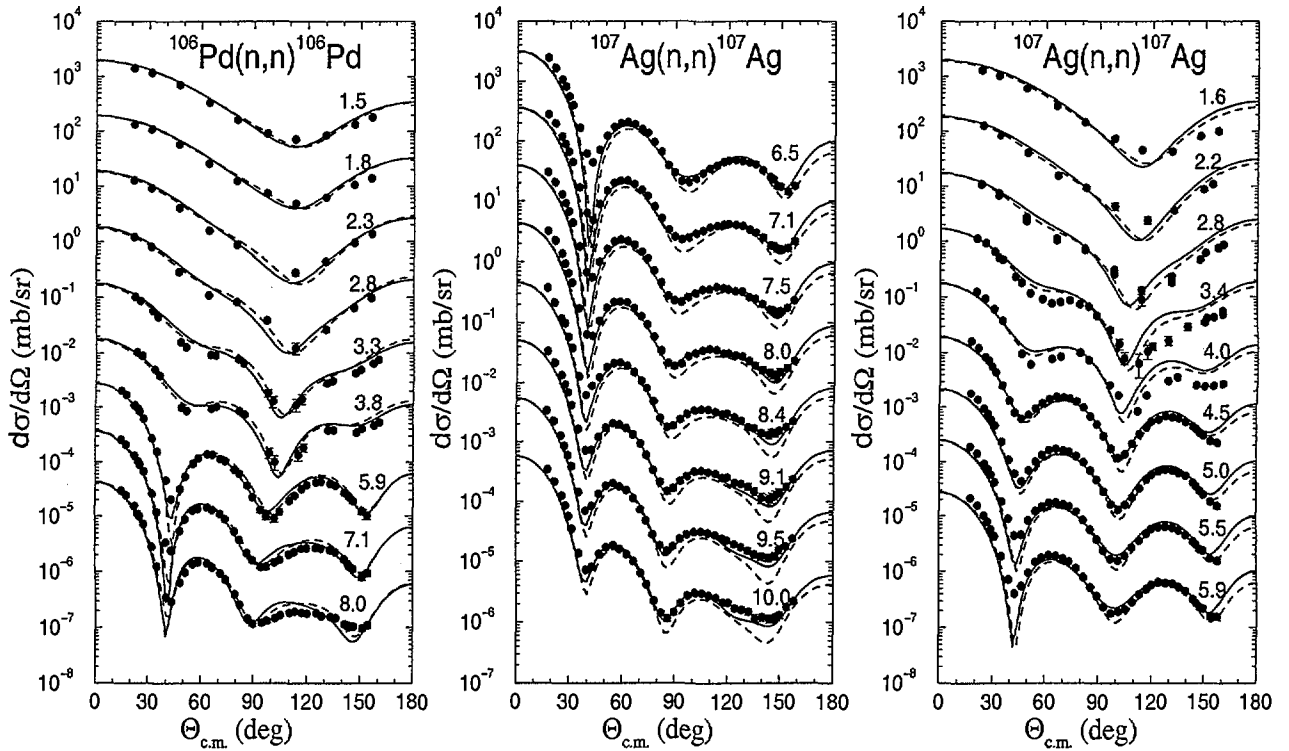


FIG. 18. Comparison of predicted differential cross sections and experimental data, for neutrons scattered from ^{106}Pd and ^{107}Ag . For more details, see the caption of Fig. 4

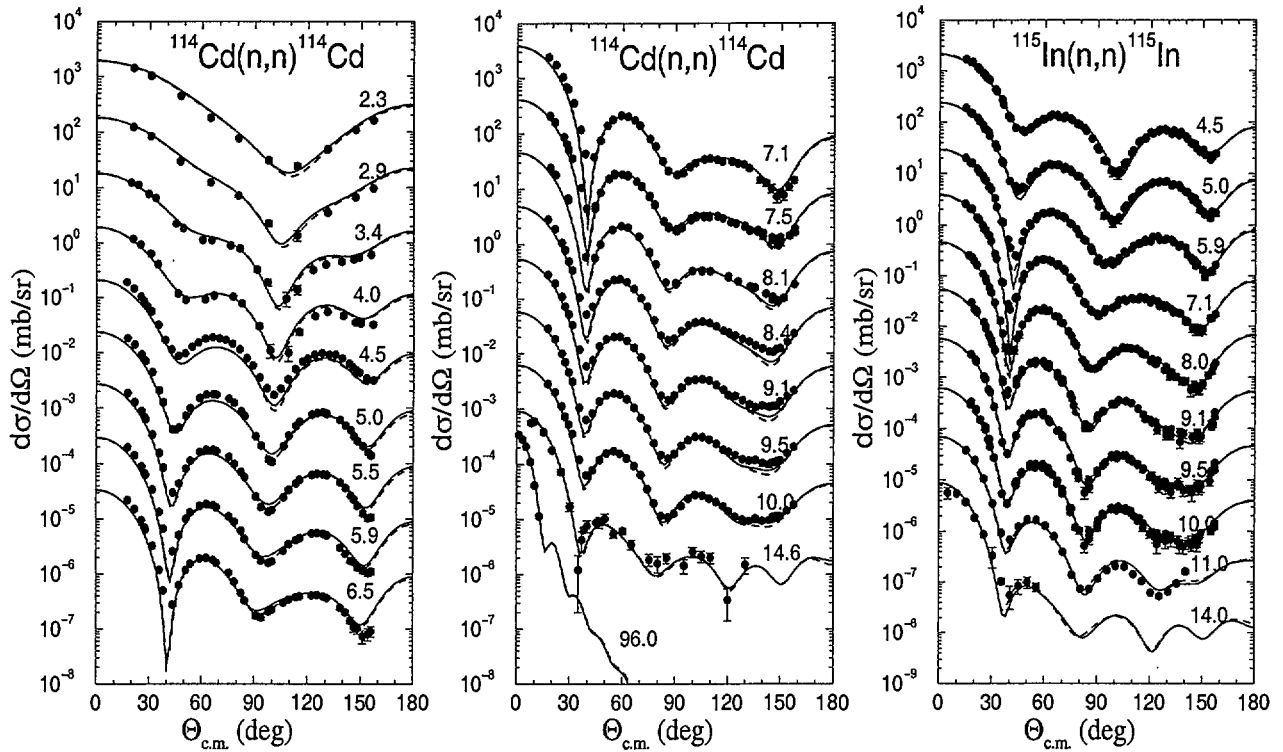


FIG. 19. Comparison of predicted differential cross sections and experimental data, for neutrons scattered from ^{114}Cd and ^{115}In . For more details, see the caption of Fig. 4

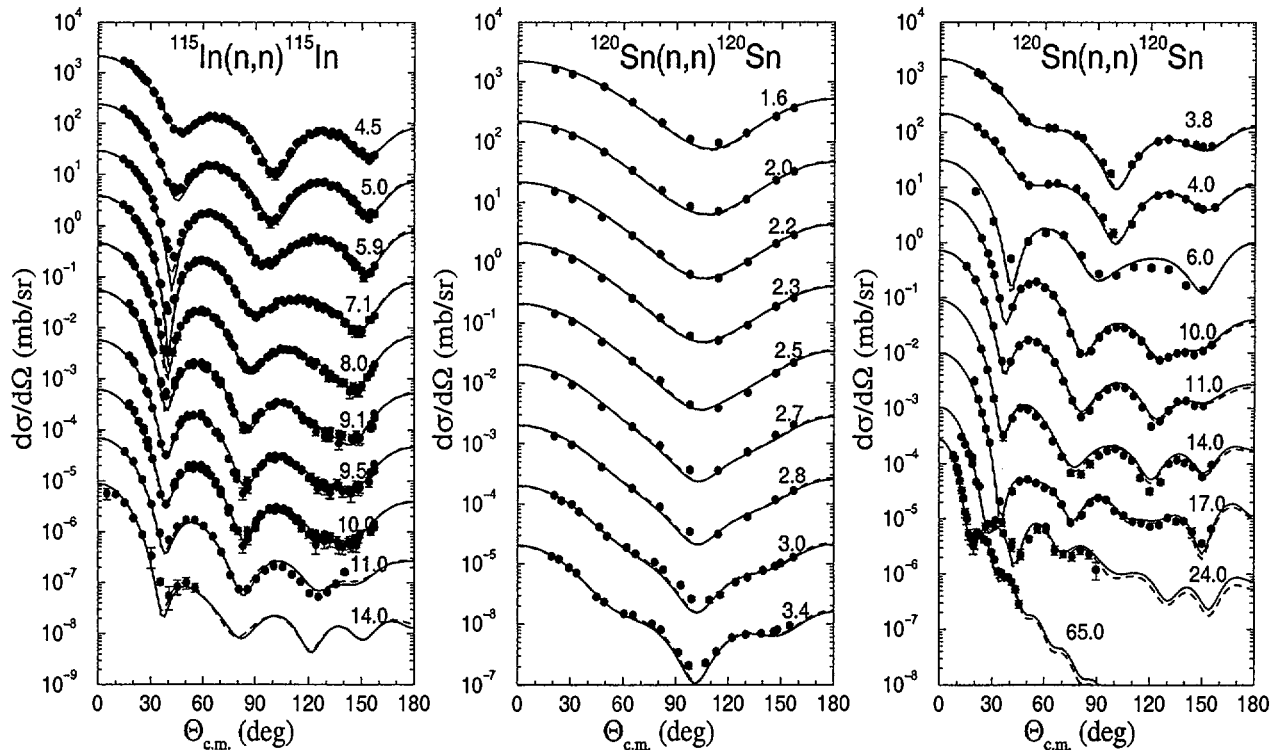


FIG. 20. Comparison of predicted differential cross sections and experimental data, for neutrons scattered from ^{116}Sn and ^{120}Sn . For more details, see the caption of Fig. 4

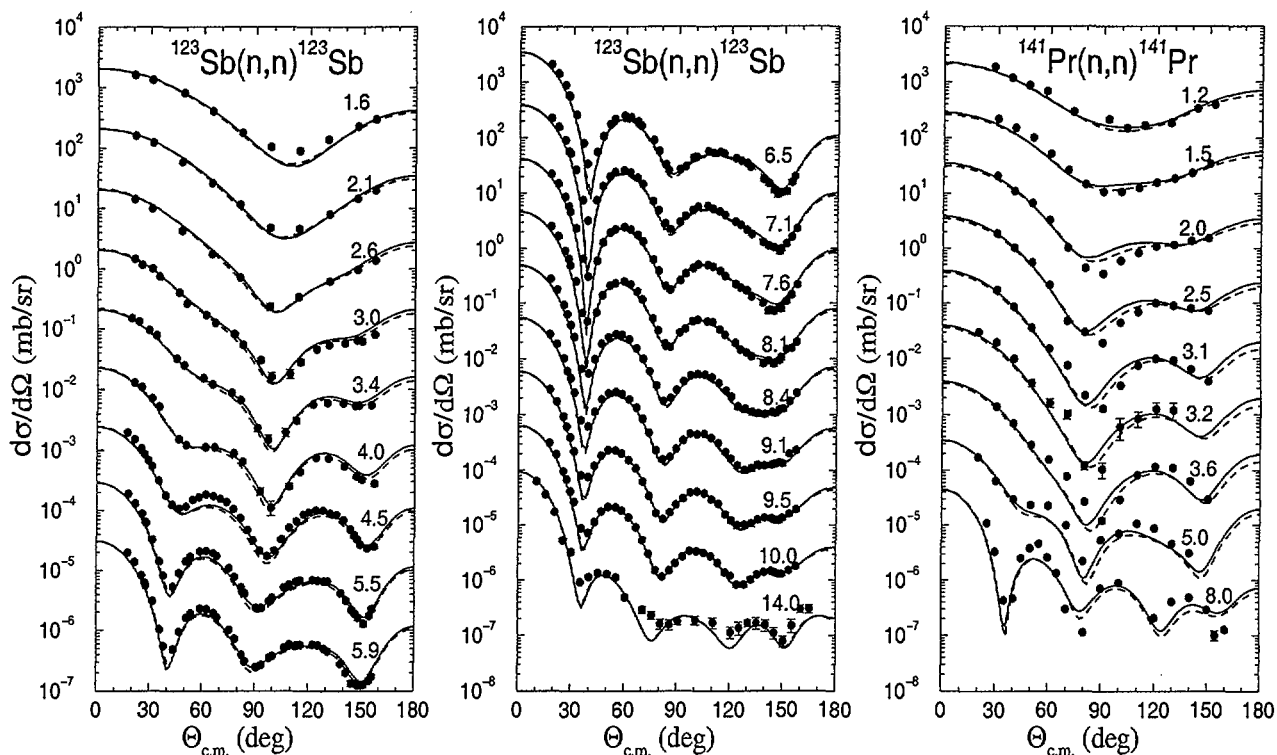


FIG. 21. Comparison of predicted differential cross sections and experimental data, for neutrons scattered from ^{123}Sb and ^{141}Pr . For more details, see the caption of Fig. 4

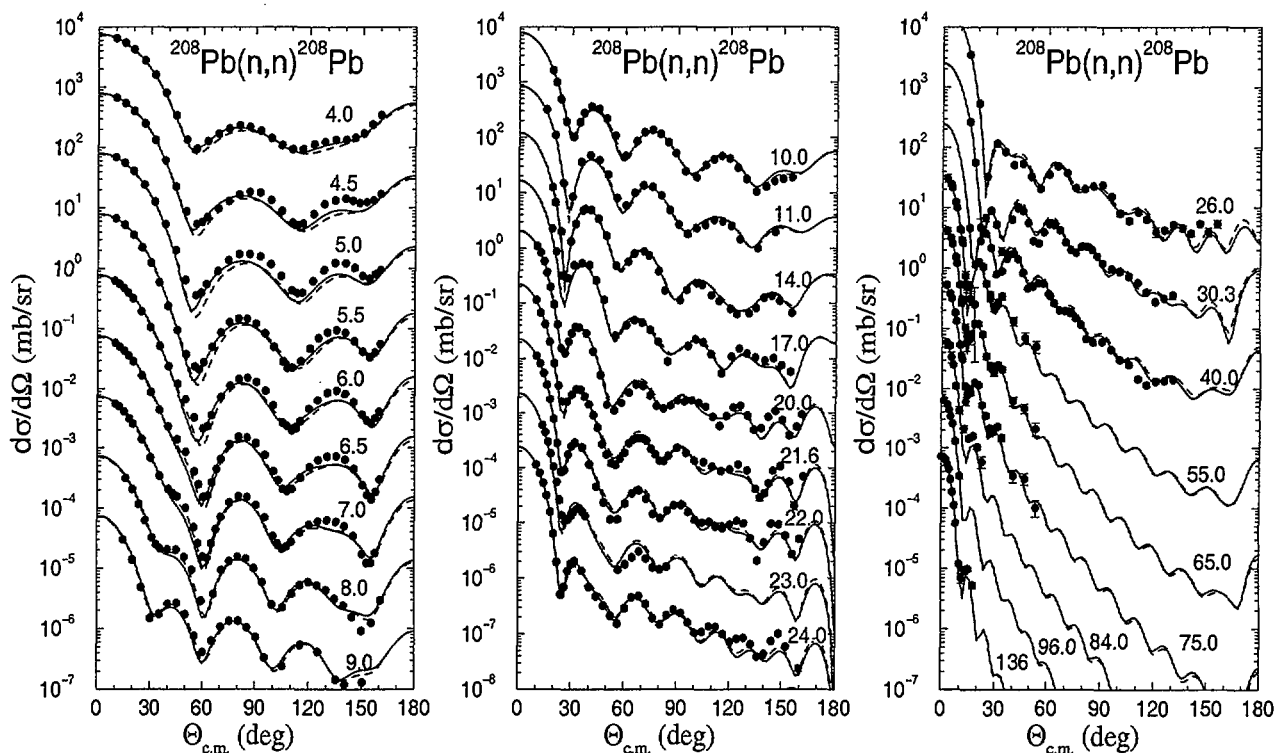


FIG. 22. Comparison of predicted differential cross sections and experimental data, for neutrons scattered from ^{208}Pb . For more details, see the caption of Fig. 4

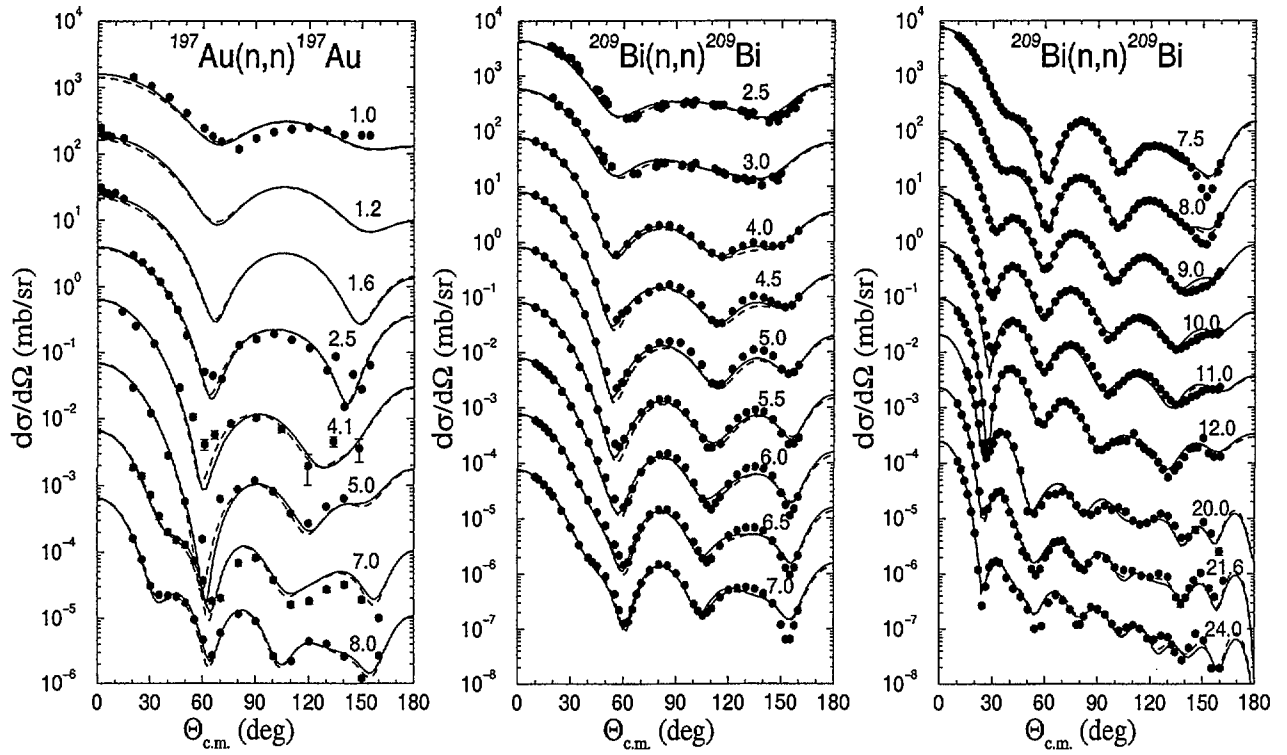


FIG. 23. Comparison of predicted differential cross sections and experimental data, for neutrons scattered from ^{197}Au and ^{209}Bi . For more details, see the caption of Fig. 4

Global Alpha-Nucleus Optical Model Potential

Ashok Kumar* and S. Kailas**

*Theoretical Physics Division, B.A.R.C., Mumbai 400 085

**Nuclear Physics Division, B.A.R.C., Mumbai 400 085

Introduction:

It is of interest to determine the global alpha-nucleus optical model potential as knowledge of this is important for understanding many nuclear and astrophysical processes, involving alphas in the entrance and the exit channels.

Several attempts have been made to determine alpha-nucleus optical potential (both phenomenological and microscopic) in the last four decades. In one of the earliest works, Huizinga and Igo [1] using a complex potential calculated reaction cross sections for about 20 target nuclei for energies up to ~ 45 MeV. Mc Fadden and Satchler [2] did an extensive optical model analysis of elastic scattering of 24.7 MeV alpha particles for nuclei ranging from O to U. A comprehensive review of alpha-nucleus optical model was made by Singh and Schwandt [3]. They discussed in detail the various approaches followed and some systematics of the potential with respect to E and A. Nolte et al. [4] proposed a global optical model potential for $E \geq 80$ MeV starting from Put and Paans's [5] extensive analysis for ^{90}Zr . Essentially the energy independent geometry parameters were similar to the ones of Put and Paans. Only the depths of the potentials systematized with respect to E and A. Avrigeanu et.al. [6] extended this to lower energies, by varying only the imaginary potential depth to fit E dependence of this part from the values of Put and Paans. They calculated with this potential a number of (n, α) reactions. Interestingly they found that the cross sections in the exit channel are rather strongly related to σ_{fus} and σ_{el} at $E \geq 80$ MeV but much less to σ_{el} at lower energies. The BARC group [7] has followed an entirely different approach to determine α -nucleus potential. They have used volume integral systematics and the proton-nucleus potential behaviour to obtain the correct energy dependence of the potential. Further, they found that the radius at which the potential is 2.4 MeV ($R_{2.4}$) (Related to Strong Absorption Radius) and the slope of potential at this radius ($S_{2.4}$) are well behaved with respect to E and A. They have provided a prescription to determine α -nucleus optical potential from J, $R_{2.4}$ and $S_{2.4}$ systematics, both for the real and the imaginary parts.

There have been several attempts to obtain alpha - nucleus potential following a microscopic approach. Atzrott et al. [8] have analysed a large body of alpha elastic scattering data using a microscopic prescription. They have shown consistency between the real and the imaginary potential volume integrals. Mohr [9] has obtained alpha - Nucleus potential using a microscopic approach similar to the above but also used alpha -decay rates to obtain potential at low energies.

Methodology:

In the present work, we have taken the real potential microscopic volume integrals from Atzrott et al. available between 30-150 MeV as the most reliable and used $R_{2.4}$, $S_{2.4}$ and $\langle r^2 \rangle$ systematics to obtain phenomenological optical model potential. Further, the energy dependence of the imaginary part of the potential has been suitably adjusted so that the corresponding real part satisfied the dispersion relation connecting the two parts. The

quantities J , $R_{2.4}$, $S_{2.4}$ and $\langle r^2 \rangle$ are defined as:

$$J_R = (\pi/3A) V_R R_R^3 (1 + (\pi a_R / R_R)^2), \quad (1)$$

$$R_{2.4} = R_R + a_R \ln ((V_R - 2.4)/2.4), \quad (2)$$

$$\langle r^2 \rangle_R = 0.6 R_R^2 (1 + (7 (\pi a_R / R_R)^2 / 3)), \quad (3)$$

$$S_{2.4} = (1/a_R) [1 + \exp(-(R_{2.4} - R_R)/a_R)]^{-1}. \quad (4)$$

For the present analysis we considered results both from phenomenological and microscopic approaches. It is found that the $\langle r^2 \rangle_R$ for the real part of the potential for a given nucleus is energy independent over a large range of energies and it is possible to parametrise this as a function of A of the target as $\langle r^2 \rangle_R = (A^{1/3} + 0.8)^2 \text{ fm}^2$. Similarly, the radius at which the potential becomes 2.4 MeV, is also energy independent and can be represented as $R_{2.4} = 1.35 A^{1/3} + 2.55 \text{ fm}$. The volume integrals for nuclei ^{16}O , ^{24}Mg , ^{40}Ca , ^{58}Ni , ^{90}Zr and ^{208}Pb have been parametrised as

$$J_R = (224 - 0.98 E / A^{0.184} + 2.57 Z / A^{1/3}) (1 + 2.05 / A^{1/3}) \quad (5)$$

(E is in c.m. and in the E (lab) range 30 to 140 MeV).

It is also observed that the slope of the Woods - Saxon potential at $R_{2.4}$, is nearly the same for many nuclei at the higher energies. From the average value of this quantity it is possible to deduce a value for the diffuseness parameter a_R to be 0.76 fm. Treating this quantity to be energy independent (as implied from microscopic analysis) and making use of $\langle r^2 \rangle_R^{1/2}$, $R_{2.4}$ and J_R systematics and the analytical expressions for these quantities connecting V_R , R_R and a_R , the real potential parameters have been determined. As $R_{2.4}$ varies slowly with V_R (see expression (2)), we solved for V_R and R_R using expressions (1) and (2) at an energy between 80 and 100 MeV and kept this value of R_R as energy independent. The energy dependence is kept only for the depth of the potential. It is found that the $\langle r^2 \rangle_I^{1/2}$ and $R_{2.4}$ values for the imaginary part are also nearly energy independent in the energy region 70 to 140 MeV and can be represented as $A^{1/3} + 1.38 \text{ fm}$ and $1.35 A^{1/3} + 2.14 \text{ fm}$ respectively. From the slope of the potential at $R_{2.4}$ at the high energies, an average value of a_I valid for many nuclei has been deduced to be 0.60 fm. Again with the plausible assumption, that a_I is energy independent and making use of $\langle r^2 \rangle_I$, $R_{2.4}$ and J_I systematics and expressions (similar to the ones for the real part) the imaginary potential parameters have been obtained at the higher energies where J_I values have nearly saturated. The imaginary volume integral is parametrised as

$$J_I = JI (1 - \exp(-0.05*EF)) \quad (6)$$

where $EF = E - EB$, EB is the Coulomb barrier and E is in lab. Further, JI is given as

$$JI = 32.8 (1 + 7.1 / A^{1/3}) \quad (7)$$

For E lower than EB , a smooth exponential fall off is assumed. The dispersion relation between the real and the imaginary parts has been made use of to constrain the imaginary potentials and their energy dependence at the near barrier energies. The real potential values at lower energies are determined from the dispersion relation.

Results:

The final values of potentials are given in Table. I for the above systems.

The diffuseness parameters are: $a_R = 0.76$ fm. $a_I = 0.60$ fm.

^{16}O	^{40}Ca	^{58}Ni	^{90}Zr	^{208}Pb
$R_R = 1.180$ fm	$R_R = 1.220$ fm	$R_R = 1.230$ fm	$R_R = 1.250$ fm	$R_R = 1.265$ fm
$R_I = 1.746$ fm	$R_I = 1.622$ fm	$R_I = 1.589$ fm	$R_I = 1.568$ fm	$R_I = 1.515$ fm

E	V_R	V_I								
30.	142.5	11.2	144.5	12.2	146.5	11.8	143.6	10.4	145.0	5.0
65.	126.2	17.6	129.6	19.0	132.2	18.9	130.7	18.0	138.1	16.5
104.	114.8	18.8	119.2	20.3	122.1	20.2	121.2	19.4	128.6	18.6
140.	108.7	18.9	113.6	20.4	116.6	20.4	116.1	19.6	123.6	18.9

(Energy and potential depths are in MeV. E is in lab.)

Preliminary testing of the above parameters in terms of elastic and reaction cross sections calculations and comparison with the data are very encouraging. It is proposed to fine tune the parameters based on this comparison.

Conclusion:

A new method of obtaining global alpha - nucleus potentials valid for a range of energies from near Coulomb barrier to around 150 MeV and for a range of nuclei from $A = 16$ to 208 has been proposed. The cross sections calculated starting from these parameters provide satisfactory description of elastic and reaction cross section data. The cross sections for alphas in the exit channel need to be calculated for these global parameters. It is proposed to follow a similar procedure for the other light complex projectiles. Preliminary studies in this direction have given encouraging results.

References:

- [1] J.R. Huizenga and G. Igo, Nucl. Phys. 29,462 (1962).
- [2] L. Mcfadden and G.R.Satchler, Nucl. Phys. 84, 177 (1966).
- [3] P.P.Singh and P. Schwandt, Nukleonika 21, 451 (1976).
- [4] M. Nolte et al. Phys. Rev. C36, 1312 (1987).
- [5] L.W. Put and A. M.J. Panns, Nucl. Phys. A291, 93 (1977).
- [6] V. Avrigeanu et al. Phys. Rev. C49, 2136 (1994).
- [7] S.K. Gupta and K.H.N. Murthy, Z. Phys. A307, 187(1982); A. Shridhar et al. Phys. Rev. C30, 1760 (1984); A. Shridhar et al., Phys. Rev. C 31, 1965 (1985); S. Kailas et al. Pramana. J. Phys. 23, 495 (1984); A. Chatterjee et al. Phys. Rev. C37, 1420 (1988); S. Kailas, Phys. Rev. C 22, 1799 (1980) and references in these papers.
- [8] U. Atzrott et al., Phys. Rev. C 53, 13336 (1996).
- [9] P. Mohr, Phys. Rev. C61, 045802 (2000).

The Testing of Koning's Global Potential

Ge Zhigang Sun Zhengjun

China Nuclear Data Center, China Institute of Atomic Energy

P.O.Box 275-41, Beijing 102413, P.R.China

Tel:+86-10-69357275, Fax: +86-10-69377008, E-mail:gezg@iris.ciae.ac.cn

Introduction

A comparison of Koning's with other four global potentials of optical model (Wilmore-Hodgson, Bechetti-Greenless, Ferrer-Rapaport and Cindro-Bersillon) for the $n+^{56}\text{Fe}$ reaction has been performed at CNDC. 313 sets of elastic angular distributions of experimental values and 20 sets of total cross sections in energy region of 1-20 MeV are calculated and taken account into this work.

1. Calculation

The spherical optical model calculation includes only the ^{56}Fe ground state 0^+ . All optical model calculations are performed with code ECIS95.

The calculated χ_j^2 in this work is defined simply as following;

$$\chi_j^2 = \frac{1}{n} \sum_{i=1}^n \frac{[\sigma_{cang}(\theta_{ji}) - \sigma_{eang}(\theta_{ji})]^2}{\Delta \sigma_{eang}(\theta_{ji})^2} \quad (1)$$

where j is the number of the energy, i is the number of the angles at the energy E_j . $\sigma_{eang}(\theta_{ji})$ and $\Delta \sigma_{eang}(\theta_{ji})$ are experimental value and its error at angle θ_{ji} , respectively. $\sigma_{cang}(\theta_{ji})$ is the optical model calculated results. The average $\bar{\chi}^2$ for the angular distribution at energy E_j is obtained

$$\bar{\chi}^2 = \frac{1}{m} \sum_{j=1}^m \chi_j^2 \quad (2)$$

If a weight factor W (0.9 is used in this calculation) introduced to the $\bar{\chi}^2$ of the total cross sections and elastic angular distributions calculations, so the reduced $\tilde{\chi}^2$ for this reaction calculation can be defined as

$$\tilde{\chi}^2 = \frac{1}{m} \sum_{j=1}^m W \frac{[\sigma_{ctot}(E_j) - \sigma_{etot}(E_j)]^2}{[\Delta \sigma_{etot}(E_j)]^2} - \frac{1}{n} \sum_{j=1}^m \sum_{i=1}^n (1-W) \frac{[\sigma_{cang}(\theta_{ji}) - \sigma_{eang}(\theta_{ji})]^2}{[\Delta \sigma_{eang}(\theta_{ji})]^2} \quad (3)$$

2. Results

Fig 1. shows the χ^2 results of every energy for different global potentials, the calculation results of this work indicates that Koning's potential can reproduce the angular distributions better than other in this energy and angular region based on the same condition.

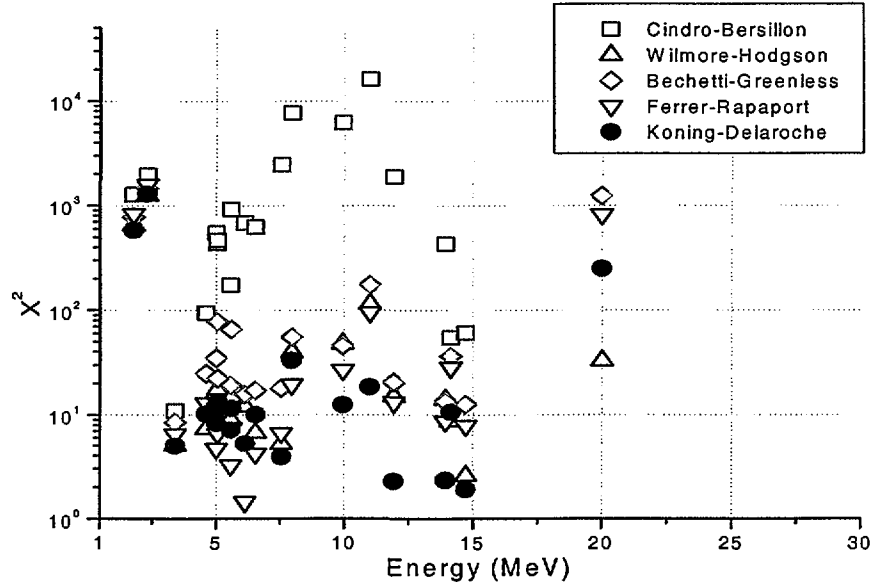


Fig.1 The χ^2 of angular distribution

Table 1. The average $\bar{\chi}^2$ of the elastic angular distributions

POT	Koning-Delaroche	Wilmore-Hodgson	Bechetti-Greenless	Ferrer-Rapaport	Cindro-Bersillon
$\bar{\chi}^2$	106.8	118.1	152.7	140.2	2202.8

The $\bar{\chi}^2$ of the total cross sections calculations is defined similar as the equation (1). Because there are a lot of experimental data for the ^{56}Fe and there are many resonance in the energy region less than 7 MeV for structure nuclei. And the theoretical OM calculation can not provide those resonances, so we have to do the evaluation for the experimental data and give an error for them in the region before the $\bar{\chi}^2$ account. In this work a smooth line with a certain error is introduced to describe the total cross sections' behavior and 3% is used as their error. Table 2 gives the average $\bar{\chi}^2$ of all 5 potentials for the total cross sections calculations. The reduced $\bar{\chi}^2$ for the all calculation are given by the Table 3. The results indicate that Koning's potential is also the best one in the total cross sections and angular distribution calculations.

Table 2. The average $\bar{\chi}^2$ of the total cross section

POT	Koning-Delaroche	Wilmore-Hodgson	Bechetti-Greenless	Ferrer-Rapaport	Cindro-Bersillon
$\bar{\chi}^2$	27.96	29.45	34.49	37.71	103.52

Table 3. The reduced average $\tilde{\chi}^2$ for the n+⁵⁶Fe

POT	Koning-Delaroche	Wilmore-Hodgson	Bechetti-Greenless	Ferrer-Rapaport	Cindro-Bersillon
$\tilde{\chi}^2$	35.84	38.32	46.31	47.96	313.45

3. Conclusions

From the optical model calculations mentioned above. A conclusion for n+⁵⁶Fe optical model calculation with the five global potentials and based on the same condition, can be obtained;

- All five global optical model potentials are better in describing the total cross sections than their elastic angular distributions calculations.
- Koning's global potential can repeat the behavior of experimental values both in the total cross sections and angular distributions better than others in the energy region of 1-20 MeV for the reaction n+⁵⁶Fe.

As ones knew that Koning's global potential can be used for a very wide mass region and higher incident energy region (up to 200 MeV). A gross view and comments for Koning's new global potential could be obtained when a test for a wide mass and energy region have been performed.

TESTING AND IMPROVEMENTS OF DIPOLE RADIATIVE STRENGTH FUNCTIONS FOR GAMMA SEGMENT OF THE RIPL II

V.A. PLUJKO

Nuclear Physics Department, Taras Shevchenko National University,
Pr. Acad. Glushkova, 2, bdg.11, 03022 Kiev, Ukraine
E-mail: plujko@mail.univ.kiev.ua

Abstract

The main results are summarized on development of a theory-supported practical method for calculations of the dipole radiative strength functions (RSF). The approach covers relatively wide interval of gamma-ray energy, ranging from zero to the values above the GDR energy and gives a rather accurate tool for description of the gamma-ray strength functions in the medium and heavy nuclei. The dependence of the deformation parameters in rotating spheroidal nuclei on angular momentum are also given in order to make possible the RSF calculations in rotating nuclei produced in heavy-ion reactions.

1 Introduction

The work deals with development of the theory-supported practical method for calculation of the average dipole radiative strength function for nuclear gamma-decay in a wide range of gamma-energies.

Gamma-emission is one of the most universal channel of the nuclear de-excitation processes which can accompany any nuclear reaction. It can be described through the use of the RSF[1, 2]. The photoabsorption and electron-positron decay are also described by these functions. The RSF include information on nuclear structure and they are widely used to study mechanisms of the nuclear processes and nuclear structure. In particular, the widths and energies of the giant multipole resonances and nuclear deformations are often extracted from experimental data by comparison of the experimental shape of the RSF with theoretical one.

The gamma-ray strengths are, as a rule, the auxiliary quantities in time-consuming calculations of different nuclear characteristics and processes and the simple closed-form expressions are preferable for these strengths. The theory-based approaches are also required to improve the reliability and accuracy of the RSF expressions.

According to the Brink hypothesis[3, 4], the Lorentzian line shape with the energy-independent width (SLO model) is used widely for calculations of the dipole ($E1$) radiative strength. This approach is probably the most appropriate simple method for a description of the photoabsorption data on medium-weight and heavy nuclei [2, 5, 6]. In the case of the gamma-emission, the SLO model strongly underestimates the gamma-ray spectra at low energies $\epsilon_\gamma \lesssim 1MeV$ [7]. A global description of the gamma-spectra by the Lorentzian is found as rather well in the range $1 \lesssim \epsilon_\gamma \lesssim 8MeV$ only when the giant dipole resonance (GDR) parameters are taken to be different from that ones for photoabsorption data. On the whole, the SLO approach overestimates the integral experimental data like the capture cross sections and the average radiative widths in heavy nuclei ([2],[8]-[10]).

The first model for correct description of the $E1$ strengths at the energies ϵ_γ near zero was proposed in Ref.[11]. An enhanced generalized Lorentzian model (EGLO) was developed and analyzed in Refs.[12, 13] for a unified description of the low-energetic and integral data. The EGLO radiative strength function consists of two components for spherical nuclei: the Lorentzian with the energy and temperature dependent width $\Gamma_k(\epsilon_\gamma, T)$, and term corresponding to zero value of γ - ray energy from Ref.[11]. An empirical expression for the width $\Gamma_k(\epsilon_\gamma, T)$ was used with two additional parameters. The mass-number dependence of the parameters was obtained to fit the EGLO calculations to the experimental data. The EGLO method was recommended in the RIPL I [13] as the best suited practical model to calculations of the dipole gamma-ray strength function if the experimental data are unavailable.

The SLO and EGLO expressions for the gamma-decay strength function of heated nuclei are in fact the parametrizations of the experimental data. They are also in contradiction with some aspect of recent theoretical studies, namely,

1) These expressions are not consistent with a general relation between the strength function and the imaginary part of the response function of heated nuclei [14];

2) The behaviour of the EGLO damping width Γ_k with γ -energy and temperature corresponds to the one of the zero sound damping in the infinite Fermi-liquid when the collisional (two-body) dissipation is taken into account only. It is well known that the important contribution to the total width in heavy nuclei is also given by the fragmentation (one - body) width arising from the nuclear mean field [15]. This kind of the width is almost independent of the nuclear temperature. The SLO-model width has properties of the fragmentation component of the width and does not account for collisional damping.

A closed-form model of the dipole RSF ([16]-[20]), which is briefly outlined here, avoids these defects at least in approximate way. It has the following main features:

1) spectral function expression is obtained from calculation of the average radiative widths for ensemble with microcanonically distributed initial states;

2) semiclassical analytical expression for nuclear response function in cold and heated nuclei with excitation of giant dipole resonance (GDR);

3) theory-reasonable expressions for damping width.

This method was named previously as the thermodynamic pole approximation, *TPA approach*. Here, as in Ref.([20]), we rename this approach and call it as *the modified Lorentzian (MLO) approach*, because the resulting expression see below Eq. (3) for the dipole RSF is a Lorentzian with energy-dependent width scaled by an enhanced factor.

2 General form of the average dipole RSF in the MLO approach

The dipole γ -ray emission is described by a gamma- decay (downward) strength function \overleftarrow{f}_{E1} . The average dipole radiative width Γ_{E1} per unit of the γ - ray energy interval and gamma- decay strength function are related to one another in the following way:

$$\overleftarrow{f}_{E1}(\epsilon_\gamma, T) \equiv \frac{\Gamma_{E1}(\epsilon_\gamma)}{3\epsilon_\gamma^3} \frac{\rho(U, Z, N)}{\rho(U - \epsilon_\gamma, Z, N)} = \mathcal{F}(\epsilon_\gamma, T_f), \quad (1)$$

where $\rho(U, Z, N)$ is the density of the initial states in nuclei at fixed initial excitation energy U (initial temperature T) and $\rho(U - \epsilon_\gamma, Z, N)$ is the density of the final states; T_f is the temperature of the final states which is a function of the γ - ray energy in contrast to the initial state temperature T . The spectral function $\mathcal{F}(\epsilon_\gamma, T)$ is introduced in Eq.(1) for further convenience.

The dipole transmission coefficient $T_{E1}(\epsilon_\gamma)$ is also determined by the RSF:

$$T_{E1}(\epsilon_\gamma) = 2\pi\epsilon_\gamma^3 \overleftarrow{f}_{E1}(\epsilon_\gamma, T) \equiv 2\pi\epsilon_\gamma^3 \mathcal{F}(\epsilon_\gamma, T_f). \quad (2)$$

It was shown in Refs.([16]-[19]) by quantum statistical calculation of the average gamma-decay width for microcanonically distributed initial states with the use of the saddle- point method for integrals appearing in the expression that the dipole spectral function $\mathcal{F}(\epsilon_\gamma, T)$ is proportional to the product of the strength function, $S_1(\omega)$, for nuclear response on dipole field with frequency $\omega = \epsilon_\gamma/\hbar$ and the scaling factor $\mathcal{L}(\epsilon_\gamma, T) = 1/[1 - \exp(-\epsilon_\gamma/T)]$. The factor \mathcal{L} determines the enhancement of magnitude of the radiative strength functions in heated nuclei with temperature T as compared to zero temperature case. This factor can be interpreted as the average number of the 1p-1h states excited by an external field. The strength function S_1 for nuclear response on dipole electric field is determined by imaginary part of the response function on the external potential with radial form factor of dipole multipolarity. We used linear response function of Ref.[21] within framework semiclassical Landau - Vlasov equation with collision term to obtain simple analytical expressions for strength function S_1 and radiative spectral function. The expression for dipole strength function has approximately the Lorentzian form when the strength is strongly concentrated near

collective (giant resonance) state. As a result the final analytical expression for dipole spectral function in spherical nuclei has the following form

$$\mathcal{F}(\epsilon_\gamma, \mathcal{T}) = 8.674 \cdot 10^{-8} \frac{\sigma_r \Gamma_r}{1 - \exp(-\epsilon_\gamma/\mathcal{T})} \frac{\epsilon_\gamma \Gamma(\epsilon_\gamma, \mathcal{T})}{(\epsilon_\gamma^2 - E_r^2)^2 + (\Gamma(\epsilon_\gamma, \mathcal{T}) \epsilon_\gamma)^2}, \quad MeV^{-3}, \quad (3)$$

where the quantity σ_r is taken in mb ; the values of the energies and widths are in MeV . Here, the E_r is the giant resonance energy and the width $\Gamma(\epsilon_\gamma, \mathcal{T})$ depends on the gamma-ray energy and the temperature:

$$\Gamma(\epsilon_\gamma, \mathcal{T}) = \tilde{\alpha} \cdot \bar{\Gamma}(\epsilon_\gamma, \mathcal{T}), \quad \bar{\Gamma}(\epsilon_\gamma, \mathcal{T}) = \gamma_c \frac{E_r^2 + E_0^2}{(E_r^2 - E_0^2)^2 + (\gamma_c \epsilon_\gamma)^2}, \quad \gamma_c \equiv \gamma_c(\epsilon_\gamma, \mathcal{T}) = \frac{2\hbar}{\tau_c(\epsilon_\gamma, \mathcal{T})}, \quad (4)$$

where E_0 is the energy of the one-particle one-hole excitations which are considered as degenerated ones; τ_c is the collision relaxation time ([22] - [24]); $\tilde{\alpha} = (1 - E_r^2/E_0^2)^2 E_0^2/2$.

The quantity Γ at the energy $\epsilon_\gamma = E_r$ can be considered as the GDR width in nucleus at the temperature \mathcal{T} , $\Gamma^{(r)}(\mathcal{T}) = \Gamma(\epsilon_\gamma = E_r, \mathcal{T})$. The relationship (4) for this width has the resonance form which is similar to that one obtained in Ref.[25].

The quantities σ_r and $\Gamma_r \equiv \Gamma^{(r)}(\mathcal{T} = 0)$ in (3) are the peak value of the photoabsorption cross-section and the GDR width in cold nuclei.

In order to take into consideration the experimental values of the photoabsorption characteristics at zero temperature, the magnitude of the $\tilde{\alpha}$ in (4) is modified. It is obtained from fitting the $\Gamma(\epsilon_\gamma = E_r, \mathcal{T} = 0)$ to the GDR width in cold nuclei and has the form:

$$\tilde{\alpha} = \Gamma_r / \bar{\Gamma}(E_r, \mathcal{T} = 0). \quad (5)$$

As mentioned above, all models with the spectral function of the modified Lorentzian form (3) are called as a *MLO approach*. In what follows the MLO model with the width $\Gamma(\epsilon_\gamma, \mathcal{T})$ according to Eqs. (4), (5) is denoted as the MLO1 model.

The dipole spectral function of the general form (3) (but with different expression for the width) was also obtained within framework of the extended hydrodynamic Steinwedel- Jensen (ESJ) model with friction force between the proton and neutron fluids ([16]-[19]). These previous TPA-versions of the modified Lorentzian approach are named below as the MLO2 and MLO3 models.

The processes of the emission and absorption of the γ -rays are generally connected with different radiative strengths. For cold nuclei, the photoexcitation (upward) strength function $\vec{f}_{E\lambda}(\epsilon_\gamma)$ can be only defined. It determines the photoabsorption cross-section $\sigma_{E\lambda}$ of cold nuclei by the relation (for dipole case):

$$\sigma_{E\lambda=1}(\epsilon_\gamma) = 3\epsilon_\gamma (\pi\hbar c)^2 \vec{f}_{E\lambda=1}(\epsilon_\gamma). \quad (6)$$

For MLO approach, the strength function \vec{f}_{E1} coincides with the spectral function $\mathcal{F}(\epsilon_\gamma, \mathcal{T})$ given by Eq.(3) with zero temperature $\mathcal{T} = 0$ and $\mathcal{L} \equiv 1$:

$$\vec{f}_{E1}(\epsilon_\gamma) \equiv \mathcal{F}(\epsilon_\gamma, \mathcal{T} = 0) = 8.674 \cdot 10^{-8} \sigma_r \Gamma_r \frac{\epsilon_\gamma \Gamma(\epsilon_\gamma, \mathcal{T} = 0)}{(\epsilon_\gamma^2 - E_r^2)^2 + (\Gamma(\epsilon_\gamma, \mathcal{T} = 0) \epsilon_\gamma)^2}, \quad MeV^{-3}. \quad (7)$$

3 Comparison of the RSF calculations within different approaches with experimental data

The calculations of the E1 radiative strength functions are performed within the framework of the five analytical models. Three of them are the MLO models with the spectral function \mathcal{F} given by Eq. (3). The values of the GDR parameters E_r , Γ_r and σ_r are taken either from ground-state photoabsorption experimental data or from the systematics. The energy E_0 of the particle-hole state is taken as equal the harmonic oscillator energy $\hbar\omega_0 = 41/A^{1/3}$ MeV. All deformed nuclei are considered as the axially symmetric spheroids and the E1 strengths is taken as the sum of two spectral functions with the GDR parameters $E_{r,1}$,

$\Gamma_{r,1}$, $\sigma_{r,1}$ and $E_{r,2}$, $\Gamma_{r,2}$, $\sigma_{r,2}$ corresponding to the collective motion in the directions along two principal axes of spheroid.

Two expressions for relaxation times are used:

i) relaxation time according to the Fermi-liquid approach ([22] - [24])

$$\frac{\hbar}{\tau_c(\epsilon_\gamma, \mathcal{T})} \equiv \frac{1}{\alpha} [(\epsilon_\gamma/2\pi)^2 + \mathcal{T}^2], \quad \alpha = \frac{9\hbar^2/16m}{\sigma(np)} = \frac{9\hbar^2/16m}{F\sigma^{free}(np)}, \quad (8)$$

where the magnitude of the in-medium cross section $\sigma(np)$ of the neutron-proton scattering near Fermi surface is taken proportional to the value of the free space cross section $\sigma^{(free)}(np) = 5 \text{ fm}^2$ with a factor F .

ii) relaxation time within doorway state mechanism in heated nuclei[24]:

$$\frac{\hbar}{\tau_c(\epsilon_\gamma, \mathcal{T})} = \frac{1}{\alpha_e} (\epsilon_\gamma + U), \quad \frac{1}{\alpha_e} = \frac{E_r}{4\pi^2} \frac{1}{\alpha}. \quad (9)$$

This expression for relaxation time is used in the MLO1 model given by Eqs. (3), (4), (5).

The MLO2 and MLO3 models are given by Eq.(3) but with damping width $\Gamma \equiv \Gamma_I$ according to the extended Steinwedel-Jensen model with friction [18, 19]. The width Γ_I is taken in approximation of independent sources of dissipation [23, 26] as a sum of the collisional damping width and a term which simulate the fragmentation component of the width,

$$\Gamma_I(\epsilon_\gamma, \mathcal{T}) = \frac{\hbar}{\tau_c(\epsilon_\gamma, \mathcal{T})} + k_s \Gamma_w, \quad \Gamma_w = \frac{3\hbar v_F}{4R_0}. \quad (10)$$

The energy-dependent power approximation is adopted for scaling factor k_s : $k_s \equiv k_s(\epsilon_\gamma) = k_r + (k_s(0) - k_r)|(\epsilon_\gamma - E_r)/E_r|^{n_s}$ if $\epsilon_\gamma < 2E_r$ and $k_s = k_s(0)$ when $\epsilon_\gamma \geq 2E_r$. Here, the quantities $k_s(0) \equiv k_s(\epsilon_\gamma = 0)$, $k_r \equiv k_s(\epsilon_\gamma = E_r)$ determine the contribution of the "wall" component Γ_w to the width at zero energy and GDR-energy, respectively. The value of the k_r is taken from fitting the GDR width Γ_r at zero temperature by the expression (10) at $\epsilon_\gamma = E_r$. The quantities n_s and $k_s(0)$ are considered as free parameters which are obtained from fitting the low-energy behaviour of the gamma-decay strengths.

The MLO model given by expressions (3), (10) with relaxation time according to the doorway state mechanism (9) and the Fermi-liquid approach (8) are denoted as MLO2 and MLO3 models, respectively.

The parameters $F = 1.0$, $k_s(0) = 0.3$, $n_s = 1$ are used in the calculations without any additional fitting.

These versions of MLO-approach are compared with E1 strengths within the SLO and EGLO models [12, 13]. The spectral function of the SLO model, $\mathcal{F} \equiv \mathcal{F}_{SLO}$, has the Lorentzian shape with energy independent width Γ_r

$$\mathcal{F}_{SLO}(\epsilon_\gamma, \mathcal{T}) = 8.674 \cdot 10^{-8} \sigma_r \Gamma_r \frac{\epsilon_\gamma \Gamma_r}{(\epsilon_\gamma^2 - E_r^2)^2 + (\Gamma_r \epsilon_\gamma)^2}. \quad (11)$$

The EGLO spectral function, $\mathcal{F} \equiv \mathcal{F}_{EGLO}$, is given by [13, 12, 11]

$$\mathcal{F}_{EGLO}(\epsilon_\gamma, \mathcal{T}) = 8.674 \cdot 10^{-8} \sigma_r \Gamma_r \left[\frac{\epsilon_\gamma \Gamma_k(\epsilon_\gamma, \mathcal{T})}{(\epsilon_\gamma^2 - E_r^2)^2 + (\epsilon_\gamma \Gamma_k(\epsilon_\gamma, \mathcal{T}))^2} + 0.7 \frac{\Gamma_k(\epsilon_\gamma = 0, \mathcal{T})}{E_r^3} \right], \quad (12)$$

where the energy-dependent width $\Gamma_k(\epsilon_\gamma, \mathcal{T})$ is taken proportionally to the collisional damping width in Fermi-liquid scaled by an empirical function $\mathcal{K}(\epsilon_\gamma)\kappa + (1 - \kappa)[(\epsilon_\gamma - \epsilon_0)/(E_r - \epsilon_0)]$,

$$\Gamma_k(\epsilon_\gamma, \mathcal{T}) = \mathcal{K}(\epsilon_\gamma) \frac{\Gamma_r}{E_r^2} [\epsilon_\gamma^2 + (2\pi\mathcal{T})^2]. \quad (13)$$

The factor κ was obtained by fitting the average resonance capture data and it depends on the model used for level density; $\epsilon_0 = 4.5 \text{ MeV}$. In the case of the Fermi gas model the κ is given by [13]: $\kappa = 1$ if $A < 148$ and $\kappa = 1 + 0.09(A - 148)^2 \exp(-0.18(A - 148))$ when $A \geq 148$.

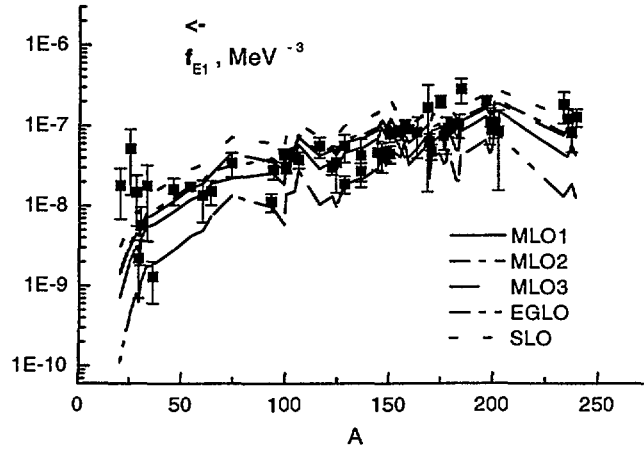


Figure 1: The $E1$ gamma-decay strength function versus mass number; $\epsilon_\gamma = U = \bar{\epsilon}_\gamma$.

The foregoing expression for spectral functions are only appropriated for the $E1$ radiative strengths in spherical nuclei. All deformed nuclei are considered as the axially symmetric spheroids and the $E1$ strengths is taken as the sum of two spectral functions with the GDR parameters $E_{r,1}$, $\Gamma_{r,1}$, $\sigma_{r,1}$ and $E_{r,2}$, $\Gamma_{r,2}$, $\sigma_{r,2}$ corresponding to the collective motion in the directions along two principal axes of spheroid.

The dipole γ - decay strength functions \bar{f}_{E1} are shown on Fig.1 in relation to the mass number. The experimental data taken from *Kopecky.dat* file of the RIPL-handbook[13]. The calculations are performed for nuclei from this data file (50 nuclei corresponding to (n,γ) reaction). The calculations in Fig.1 are carried out for the values of the excitation energies and gamma-ray energies which are agreed with the mean energy $\bar{\epsilon}_\gamma$ of $E1$ transitions from *Kopecky.dat* file. The lines connect the values which are calculated for fixed mass numbers.

The experimental data on gamma-decay with $\epsilon_\gamma \approx B_n$ are described better within the framework of the EGLO model and different versions of the MLO approach as compared with the SLO model. The calculations within MLO approach coincide rather closely with experimental data for heavy nuclei with $A \gtrsim 150$ in comparison with other models.

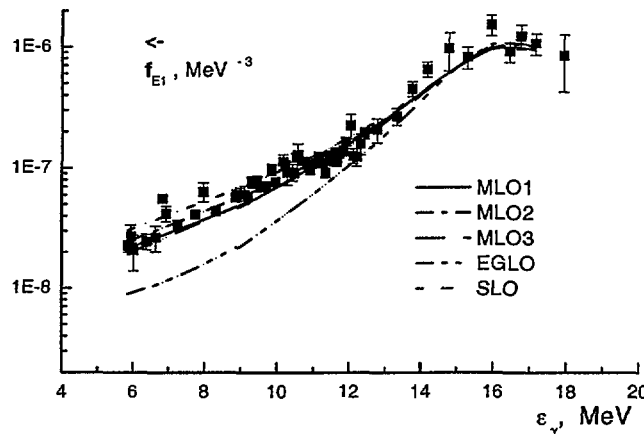


Figure 2: The $E1$ gamma-decay strength function versus energy ϵ_γ for ^{90}Zr .

In Fig.2 the results of the calculations of the gamma-decay strengths \overline{f}_{E1} in ^{90}Zr are shown. The experimental data are taken from Refs.[27]. The MLO and EGLO strengths are calculated at the fixed values of the energies U , ϵ_γ corresponding to the experimental ones. The curves connect the calculated values.

We see from this figure that the MLO and SLO models describe experimental data better than the EGLO for this nucleus and energy range. The calculations by MLO models lie also more close to the experimental data than within SLO method. For example, the values of the least-squares deviations per one degree of freedom from experimental data are equal to 4.22,2.86, 4.41 for the models MLO1, MLO2, MLO3 and 5.22, 29 for SLO and EGLO models, respectively.

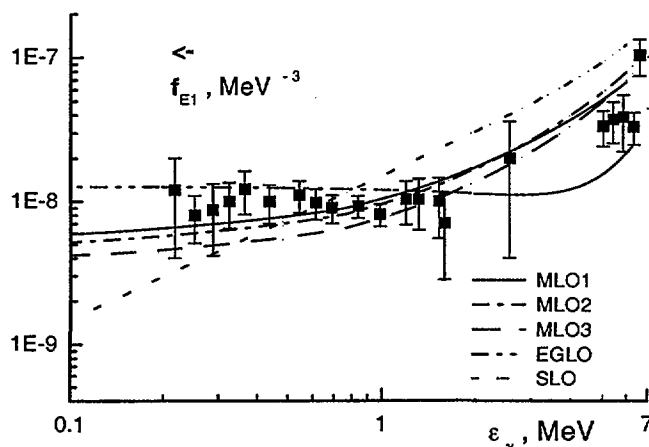


Figure 3: The $E1$ gamma-decay strength function of ^{144}Nd for $U = B_n$.

In Fig.3 the results of the calculations of the strength functions \overline{f}_{E1} in ^{144}Nd with the initial excitations energy E which is equal to the neutron binding energy $B_n \approx 7.8 \text{ MeV}$ are shown. The experimental data are taken from Ref.[7].

The results obtained by EGLO and MLO approaches are rather close at low energies $\epsilon_\gamma \lesssim 3 \text{ MeV}$. In this range the EGLO and MLO models describe experimental data much better than the SLO model and give a non-zero temperature-dependent limit of the strength function for vanishing gamma-ray energy. The calculations by MLO and SLO models at the energies $\epsilon_\gamma \gtrsim 5 \text{ MeV}$ lie more close to experimental data than within EGLO method.

4 Conclusion and results

The numerical studies led to the following conclusions.

The calculations of the γ - decay $E1$ strength functions within EGLO and MLO approaches give almost the same results at low γ -ray energies $\epsilon_\gamma \lesssim 3 \text{ MeV}$. In this range the EGLO and MLO models describe experimental data much better than the SLO model. They give a non-zero temperature-dependent limit of the strength function for vanishing gamma-ray energy as opposed to the SLO model. The calculations by the MLO and SLO models at the energies $\epsilon_\gamma \gtrsim 5 \text{ MeV}$ are more close to experimental data than that ones within the EGLO method.

The values of the $E1$ photoexcitation strength functions calculated by the MLO method and within the SLO model agree rather good in cold nuclei for a wide enough range of gamma-ray energies near the GDR peak energy.

The overall comparison between calculations within the MLO, EGLO and SLO models and experimental data showed that the MLO approaches provides a rather reliable method of the γ - decay strength function description in a relatively wide energy interval, ranging from zeroth gamma-ray energy to values above GDR

peak energy. The MLO methods are not time consuming. They can be applicable for calculations and predictions of the statistical contribution to the dipole strength functions as well as for extraction of the GDR parameters of heated nuclei with small errors with the use of the γ -emission data.

The parameters $F = 1.0$, $k_s(0) = 0.3$, $n_s = 1$ can be recommended for global calculations within the MLO models.

The computer codes for the calculations and plotting of the E1 radiative strength functions versus mass number and gamma- energy within the framework of the different versions of the modified Lorentzian approach and standard SLO and EGLO models are written and they will be attached to the GAMMA segment of the RIPL II.

The codes for dipole RSF are written in Fortran and Object Pascal (within Delphi 5 development system) under MS-DOS and Windows 9X operating systems. They are adapted for UNIX by Dr.M. Herman. The options of a comparison between the calculations and experimental data are included by the calculation of the mean-square deviation and in visual way on display. Numerical data output in the computer readable form is also done. The Fortran codes are the following ones.

i) The *fE1_A.for* is a code for calculation of the E1 gamma-decay strength functions as a function of mass number at fixed excitation energy. The calculations are performed for 50 nuclei from 'Kopecky.dat' file which contains experimental data base of the radiative strength functions. The recommended data for (n, γ) reaction are used only.

ii) The *fE1_E.for* is a code for calculation of the E1 strength functions or cross-sections as a function of gamma-ray energy at fixed excitations (energy or temperature).

iii) The *fE1_UE.for* is a code for calculation of the E1 strength functions or cross-sections at fixed both excitation- and gamma- energies.

Now the implantation of the *fE1_E.for* code to EMPIRE nuclear code system of Dr. M.Herman is continued. It is expected that this work will be done on the end of the December.

The experimental E1 strengths are available on the following nuclei for plotting and comparison with calculations: A) photoabsorption: ^{45}Sc , ^{51}V , ^{90}Zr , ^{106}Pd , $^{106,117,118,120,124,\text{nat}}\text{Sn}$, $^{157,158}\text{Gd}$, ^{174}Yb , ^{197}Au , ^{208}Pb , ^{238}U ; B) gamma-decay: ^{51}V , ^{54}Cr , $^{57,59}\text{Co}$, $^{61,62,63,65}\text{Cu}$, ^{90}Zr , ^{94}Nb , ^{106}Pd , ^{114}Cd , ^{124}Te , $^{137,139}\text{Ba}$, ^{144}Nd , $^{156,157,158}\text{Gd}$, ^{160}Tb , ^{174}Yb , ^{197}Au , ^{205}Tl , ^{208}Pb , ^{238}U .

The sum of the experimental γ -decay RSF for the E1+M1 transitions in the energy interval up to B_n obtained in Refs.([28]-[30]) by analysis of the two-step γ -cascades after thermal neutron capture in the following nuclei can be also used for comparison and plotting: ^{40}K , ^{80}Br , ^{114}Cd , $^{124,125}\text{Te}$, ^{128}I , $^{137,138,139}\text{Ba}$, ^{140}La , ^{146}Nd , ^{150}Sm , $^{156,157}\text{Gd}$, ^{160}Tb , ^{164}Dy , ^{166}Ho , ^{168}Er , ^{170}Tm , ^{174}Yb , $^{176,177}\text{Lu}$, ^{181}Hf , ^{182}Ta , ^{183}W , $^{188,190,191,193}\text{Os}$, ^{192}Ir , ^{196}Pt , ^{198}Au , ^{200}Hg .

The code GRSF (written on the Object Pascal) contains all mentioned above variants of the E1 strength calculations. A code "GRSF Monitoring" will be added to the GRSF to find automatically (if it is needed) the set of the optimal parameters(F , $k_s(0)$, n_s) for given nuclei by fitting theoretical calculations to experimental data by least-squares deviation method.

In heavy-ion reactions, nuclei are often produced at quite high angular momentum and excitation energy. It is well known that the equilibrium shapes of rotating nuclei are deformed. In a spheroidal approximation for rotating nuclei

The dipole RSF of the rotating nuclei in a spheroidal approximation is the sum of two spectral functions with the GDR parameters ($E_{r,1}$, $\Gamma_{r,1}$, $\sigma_{r,1}$ and $E_{r,2}$, $\Gamma_{r,2}$, $\sigma_{r,2}$) corresponding to the collective motion in the directions along two principal axes of the spheroid. These input quantities can be calculated by the use of their global parametrization on the deformation parameters[13]. Therefore the values of the deformation are needed in order to calculate RSF in this case.

We used liquid-drop nuclear model in the spheroidal approximation and found the following simple expression for deformation parameter of rotating nucleus as a function of angular momentum and mass number A in the case of the arbitrary rotations[31, 32]:

$$\beta = \beta(I, A) = E_S(I) (a_1 + a_2 E_S(I)) / (1 + a_3 E_S(I))^2, \quad (14)$$

where

$$a_i = b_i + c_i (A + d_i)^2. \quad (15)$$

Here, the $E_S(I) = E_{rot}^0 I(I+1) = 34.5A^{-5/3} I(I+1)$ (MeV) is the rotation energy of the equivalent spherical nucleus with spin I .

Slow rotating spheroidal nuclei have oblate shape which is changed sharply to prolate one at angular momentum greater than a critical value I_{cr} .

The coefficients b_i, c_i, d_i in Eq.(14) have the following values in the case of oblate shapes (small rotation)

$$\begin{aligned} b_1 &= -7,46 \cdot 10^{-3}; & c_1 &= -1,94 \cdot 10^{-7}; & d_1 &= -107,1; \\ b_2 &= -4,2 \cdot 10^{-5}; & c_2 &= -4,25 \cdot 10^{-9}; & d_2 &= -93,9; \\ b_3 &= 5,7 \cdot 10^{-3}; & c_3 &= 2,44 \cdot 10^{-7}; & d_3 &= -73,51 \end{aligned} \quad (16)$$

The values b_i, c_i, d_i in Eq.(14) are the following for prolate shapes (fast rotation):

$$\begin{aligned} b_1 &= -6,36 \cdot 10^{-3}; & c_1 &= -6,33 \cdot 10^{-7}; & d_1 &= -48,3; \\ b_2 &= 1,02 \cdot 10^{-3}; & c_2 &= 1,42 \cdot 10^{-7}; & d_2 &= -95,9; \\ b_3 &= 0,02; & c_3 &= 8,59 \cdot 10^{-7}; & d_3 &= -74,1 \end{aligned} \quad (17)$$

The dependence of the critical value I_{cr} of the spin on mass number A and number of protons Z was obtained in the form:

$$I_{cr} = I_{cr}(A, Z) = q_1 + q_2 Z^2, \quad (18)$$

where

$$q_i = \tilde{q}_{i,1} + \tilde{q}_{i,2} \cdot A + \tilde{q}_{i,3} \cdot A^2, \quad (19)$$

with

$$\begin{aligned} \tilde{q}_{1,1} &= 55,1; & \tilde{q}_{1,2} &= -0,063; & \tilde{q}_{1,3} &= 5,12 \cdot 10^{-3}; \\ \tilde{q}_{2,1} &= -0,013; & \tilde{q}_{2,2} &= 2,84 \cdot 10^{-6}; & \tilde{q}_{2,3} &= -2,57 \cdot 10^{-7}. \end{aligned} \quad (20)$$

5 Acknowledgment

Valuable discussions with Profs. A.V. Ignatyuk, P. Oblozinsky, M.G. Urin and Drs. M.Herman, J. Kopecky are greatly acknowledged. I am also very thankful to Dr.A.M.Sukhovej for experimental data of the RSF in the E1+M1 transitions. This work is supported in part by the IAEA(Vienna) under contract 302-F4-UKR-11567.

References

- [1] G.A. Bartholomew, E.D. Earle, A.J. Fergusson, J.W. Knowles, A.M. Lone, *Adv. Nucl. Phys.* 7, 229 (1973).
- [2] M.A. Lone, In: Neutron induced reactions. Proc. 4th. Intern. Symp., Smolenice, Czechoslovakia, June, 1985. Eds. J. Kristiak, E. Betak, D.Reidel. Publ. Comp. Dordrecht, Holland, p.238, (1986).
- [3] D.M. Brink, Ph. D. Thesis, Oxford University, 955, p.101.
- [4] P.Axel, *Phys. Rev.* 126 (1962) 671.
- [5] B.L. Berman, S.C. Fultz, *Rev. Mod. Phys.* 47 (1975) 713.
- [6] S.S.Dietrich, B.L.Berman, *Atom. Data and Nucl. Data Tabl.* 38 (1988) 199.
- [7] Yu.P. Popov, In: Neutron induced reactions. Proc. Europhys. Top. Conf., June 21-25, 1982 Smolenice. *Physics and Applications*. Vol.10. Ed. P. Oblozinsky. Bratislava, p.121 (1982).
- [8] C.M.McCullagh, M.Stelts, R.E. Chrien, *Phys.Rev.C*23 (1981)1394.
- [9] J. Kopecky, M.Uhl. *Phys. Rev.* C41 (1990) 1941.
- [10] C. Coceva, *Nuovo Cimento* 107A (1994) 85.
- [11] S.G. Kadenskij, V.P. Markushev, V.I. Furman, *Yad. Fiz.* 37, 277 (1983) [*Sov.J. Nucl. Phys.* 37, 165 (1983)].
- [12] J. Kopecky, M.Uhl, R.E. Chrien, *Phys. Rev.* C47, 312 (1993).

- [13] J. Kopecky, In: RIPL I. IAEA- TECDOC- 1034, August 1998, Ch.6. The directory GAMMA on the Web site - [http: // www -nds.iaea.or.at /ripl/](http://www-nds.iaea.or.at/ripl/).
- [14] P. Ring, L.M. Robledo, J.L. Egido, M. Faber, Nucl. Phys. A419 (1984) 261.
- [15] G.F. Bertsch, R.A. Broglia, Oscillations in Finite Quantum Systems, Cambridge University Press, N.Y., 1994.
- [16] V.A.Plujko (Plyuiko), Yad.Fiz. 52, 1004 (1990) [Sov.J.Nucl.Phys. 52, 639 (1990)].
- [17] V.A.Plujko, Nucl.Phys. A649, 209c (1999).
- [18] V.A.Plujko, Acta Phys. Pol. B31, 435 (2000).
- [19] V.A. Plujko, Proc. 9th Inter. Conf. Nucl. Reaction Mechanisms, Varenna, June 5- 9, 2000. Ed. E. Gadioli. Universita degli Studi di Milano, Suppl. N.115, p.113 (2000).
- [20] V.A. Plujko, S.N. Ezhov, M.O. Kavatsyuk, A.A. Grebenyuk, R.V. Yermolenko. Proc. Int. Conf. Nuclear Data for Science and Technology, Oct. 7-12, 2001, Tsukuba, Ibaraki, Japan. No. 5-P-18 Journal Nucl. Sci. Technol.(in press).
- [21] G. F. Burgio and M. Di Toro, Nucl. Phys., A476, 189 (1988).
- [22] V.M.Kolomietz, V.A. Plujko, S.Shlomo, Phys. Rev. C 52, 2480 (1995).
- [23] V.A.Plujko. Acta Phys. Pol. B30, 1383(1999).
- [24] V.A. Plujko,O.M. Gorbachenko, M.O. Kavatsyuk, Acta Phys. Slovaca. 51, 231 (2001).
- [25] N. Vinh Mau, Nucl. Phys. A548, 381 (1992).
- [26] V.M. Kolomietz, V.A. Plujko, S. Shlomo, Phys. Rev. C54, 3014(1996).
- [27] Z.Szeflinski, G.Szeflinska, Z.Wilhelmi et al., Phys. Lett. B126, 159 (1983).
- [28] E.V.Vasilieva, A.M.Sukhovej, V.A.Khitrov, Preprint P3-99-203, JINR, Dubna, 1999.
- [29] E.V.Vasilieva, A.M.Sukhovej, V.A.Khitrov, Fyzika elementarnich chastitz i atomnogo yadra. 31, 350 (2000).
- [30] E.V.Vasilieva, A.M.Sukhovej, V.A.Khitrov, Yadernaya Fyzika. 64, 3 (2001).
- [31] O.M. Gorbachenko, V.A. Plujko, Visnik Kyivskogo Universitetu, seria fis.- mat.nauk. N1, 434 (2001).
- [32] V.A. Plujko, O.M. Gorbachenko. Abstracts of the 51th Conf. on Nucl. Spectr. and Nucl. Structure, 3-8 September 2001, Sarov,Russia, VNIIEPH, P.130(304). Izvestija Rossiyskoy Akademiyi Nauk. Seriya Fizicheskaya (in press).

Test of RIPL-2 cross section calculations

M. Herman

International Atomic Energy Agency, Vienna, Austria

29th November 2001

The new levels and optical segments and microscopic HF-BCS level densities (part of the density segment) were tested in practical calculations of cross sections for neutron induced reactions on 22 targets (40-Ca, 47-Ti, 52-Cr, 55-Mn, 58-Ni, 63-Cu, 71-Ga, 80-Se, 92-Mo, 93-Nb, 100-Mo, 109-Ag, 114-Cd, 124-Sn, 127-I, 133-Cs, 140-Ce, 153-Eu, 169-Tm, 186-W, 197-Au, 208-Pb). For each target all reactions involving up to 3 neutron, 1 proton and 1 α -particle emissions (subject to actual reaction thresholds) were considered in the incident energy range from 1 keV up to 20 MeV (in some cases up to 27 MeV). In addition, total, elastic, and neutron capture cross sections were calculated.

The 2-17beta version of the statistical model code EMPIRE-II has been used with all default parameters except of those differentiating the 3 series of runs. In all cases TUL MSD and Heidelberg MSC models were used for preequilibrium emission of neutrons, and exciton model (DEGAS) for preequilibrium emission of protons and γ 's. These were complemented with Hauser-Feshbach calculations including widths fluctuations (HRTW model) at incident energies below 5 MeV. The results were converted into the ENDF-6 format and compared with experimental data available from the EXFOR library.

The aim of this exercise was to test formal correctness and performance of the new file with discrete levels provided by Belgya, Koning's global optical model potentials and microscopic level densities provided by Goriely. Accordingly, the following three series of calculations were performed:

- | | |
|----------|---|
| standard | default parameters in EMPIRE-2-17beta (i.e., Wilmore-Hodgson omp for neutrons and Becchetti-Greenlees for protons, EMPIRE-specific level densities with internal systematics, and internal library of discrete levels with N_{max} set arbitrarily to 10) |
| Ko-Be | Koning's optical model potential for neutrons and protons, Belgya's file of discrete levels with recommended N_{max} (limited to 40 by the ENDF-6 format), and EMPIRE specific level densities |
| Ko-Be-Go | as above but using HF-BCS microscopic level densities provided by Goriely instead of EMPIRE-specific ones |

Typical plots comparing results obtained in the three runs are shown in Figs.1-22. General conclusions resulting from this exercise are following:

- No problems were encountered while processing the new RIPL-2 files. This indicates that there are no fatal formatting errors that would prevent files from being used in cross section calculations.
- Comparison with the experimental data shows reasonable overall agreement for all three series of calculations. No clear 'winner' could be declared since for each data set there are reactions for which this set is the best. However, general preference goes to the Ko-Be set, which demonstrates improvement brought about by RIPL-2.

- HF-BCS microscopic level densities were found to perform comparable to the phenomenological level densities and in some cases appear to be clearly the best (e.g., $^{58}\text{Ni}(n,p)$ reaction cross sections and double-differential cross sections for neutron production on ^{93}Nb at 14 MeV). On the other hand, microscopic level densities tend to overestimate capture cross sections in certain number of cases.
- Significant discrepancies among the results of the three sets of calculations were observed in several cases. Taking into account that none of the sets can be considered as absolutely superior we have to accept that a set of parameters which would be 'universally the best' can not be recommended.

The results of the present comparison, although short of completeness, stress importance of the model parameters and prove practical usefulness of the RIPL-2 library for applications and basic research.

28-Nov-2001 16:19

22-TI-47(N,P),,SIG

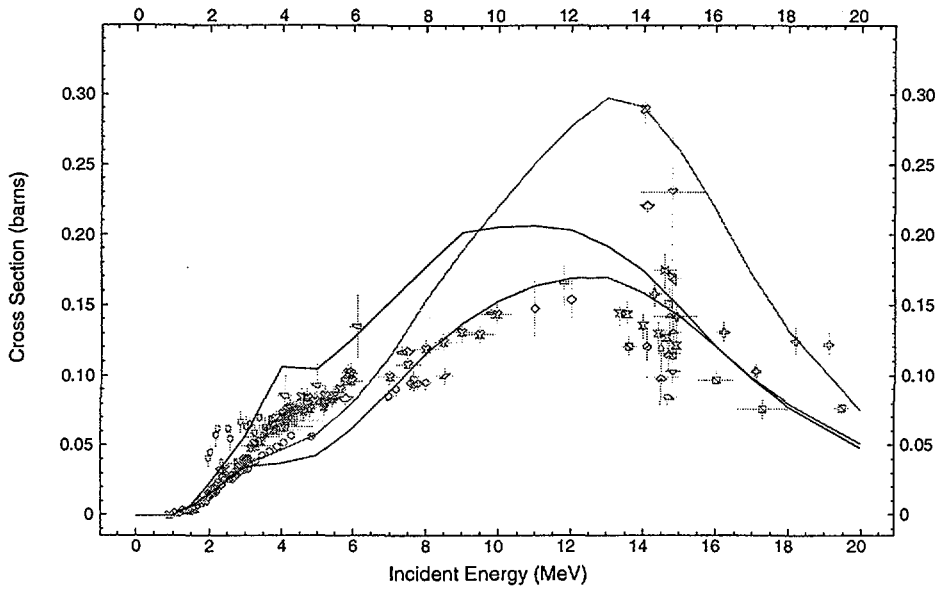


Figure 1: Comprison of experimental data with results calculated using three sets of parameters (see text) for the $^{47}\text{Ti}(n,p)$ reaction.

28-Nov-2001 15:08

24-CR-52(N,2N),,SIG

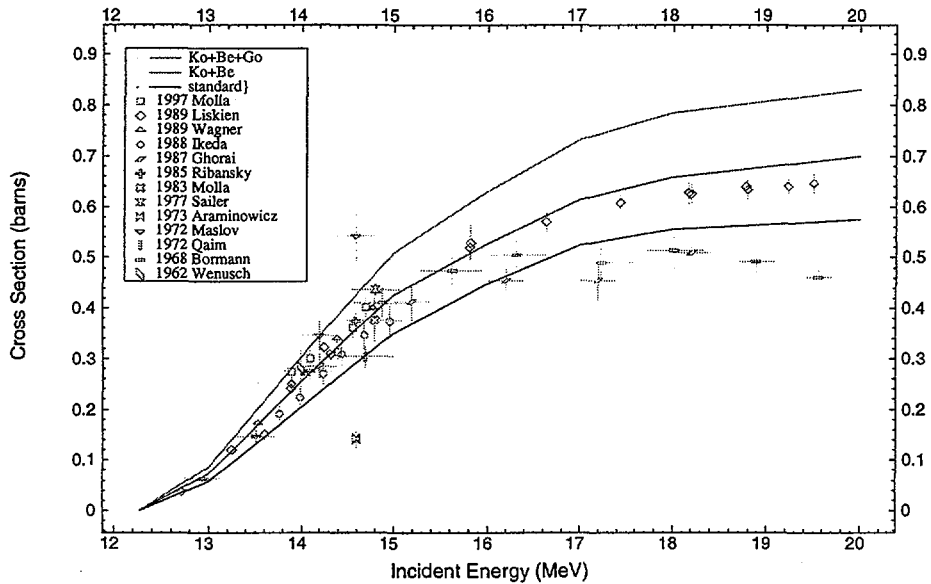


Figure 2: Comprison of experimental data with results calculated using three sets of parameters (see text) for the $^{52}\text{Cr}(n,2n)$ reaction.

28-Nov-2001 15:49

24-CR-52(N,P),,SIG

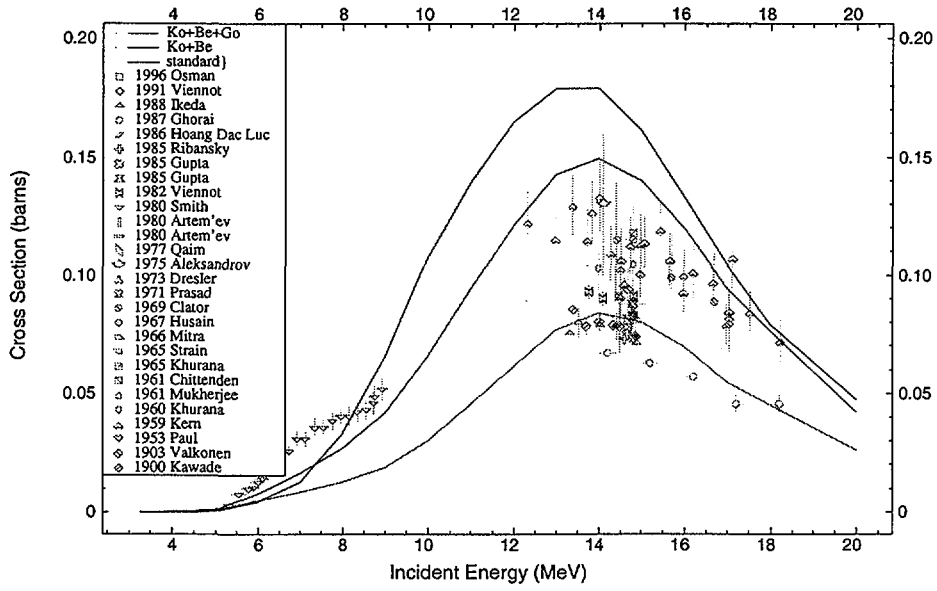


Figure 3: Comprison of experimental data with results calculated using three sets of parameters (see text) for the $^{52}\text{Cr}(n,p)$ reaction.

28-Nov-2001 15:12

25-MN-55(N,2N),,SIG

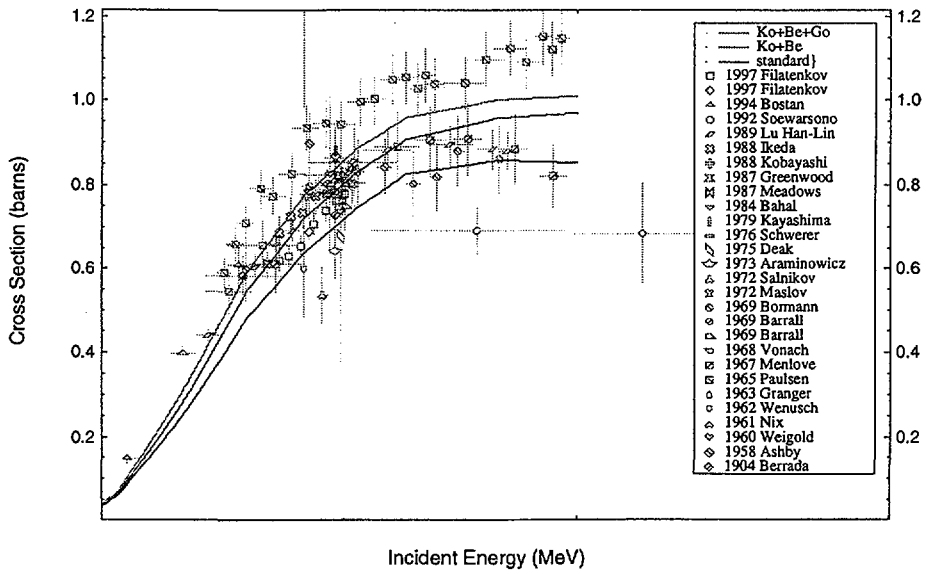


Figure 4: Comprison of experimental data with results calculated using three sets of parameters (see text) for the $^{55}\text{Mn}(n,2n)$ reaction.

28-Nov-2001 15:51

25-MN-55(N,P),,SIG

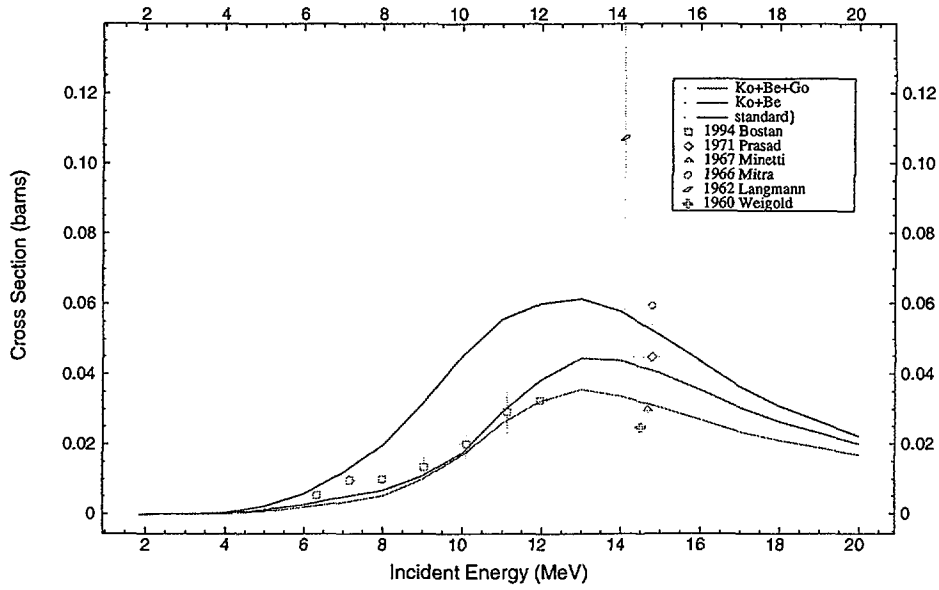


Figure 5: Comprison of experimental data with results calculated using three sets of parameters (see text) for the $^{55}\text{Mn}(n,p)$ reaction.

28-Nov-2001 15:59

25-MN-55(N,A),,SIG

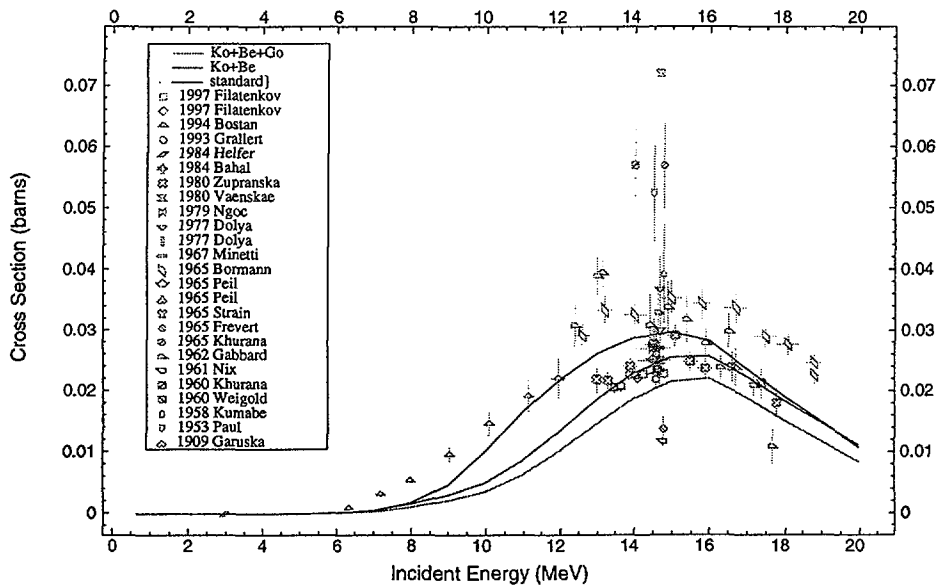


Figure 6: Comprison of experimental data with results calculated using three sets of parameters (see text) for the $^{55}\text{Mn}(n,\alpha)$ reaction.

28-Nov-2001 15:30

25-MN-55(N,G),,SIG

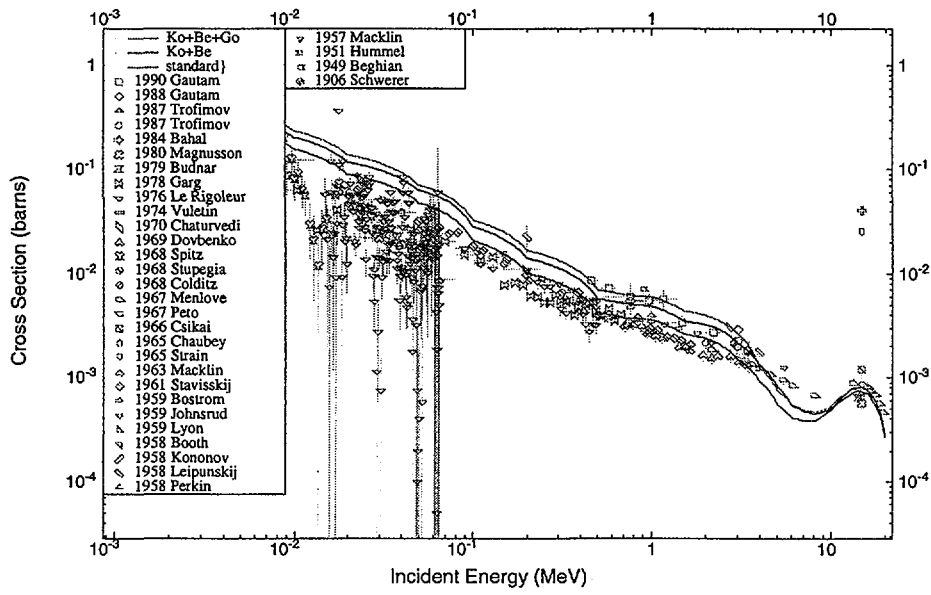


Figure 7: Comprison of experimental data with results calculated using three sets of parameters (see text) for the $^{55}\text{Mn}(n,\gamma)$ reaction.

28-Nov-2001 16:18

28-NI-58(N,2N),,SIG

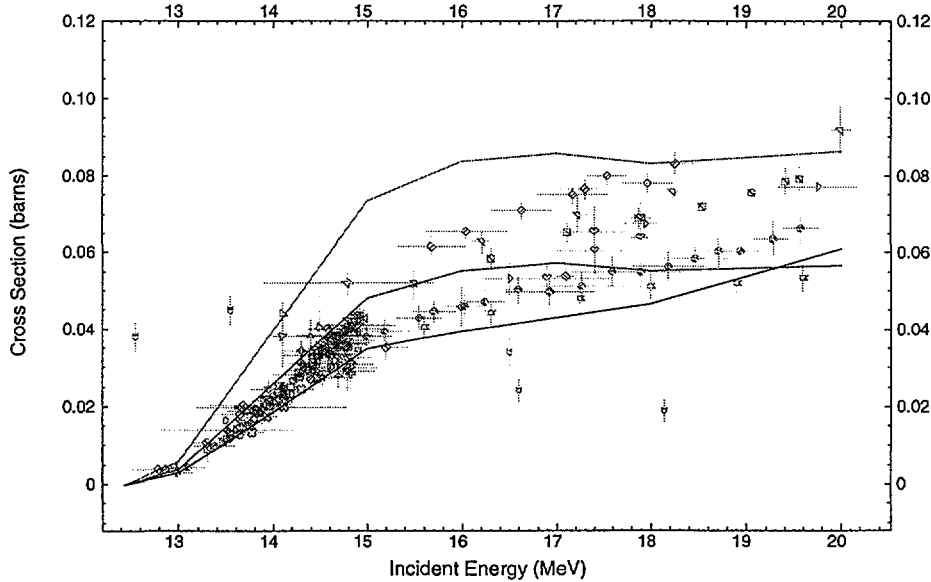


Figure 8: Comprison of experimental data with results calculated using three sets of parameters (see text) for the $^{58}\text{Ni}(n,2n)$ reaction.

28-Nov-2001 15:53

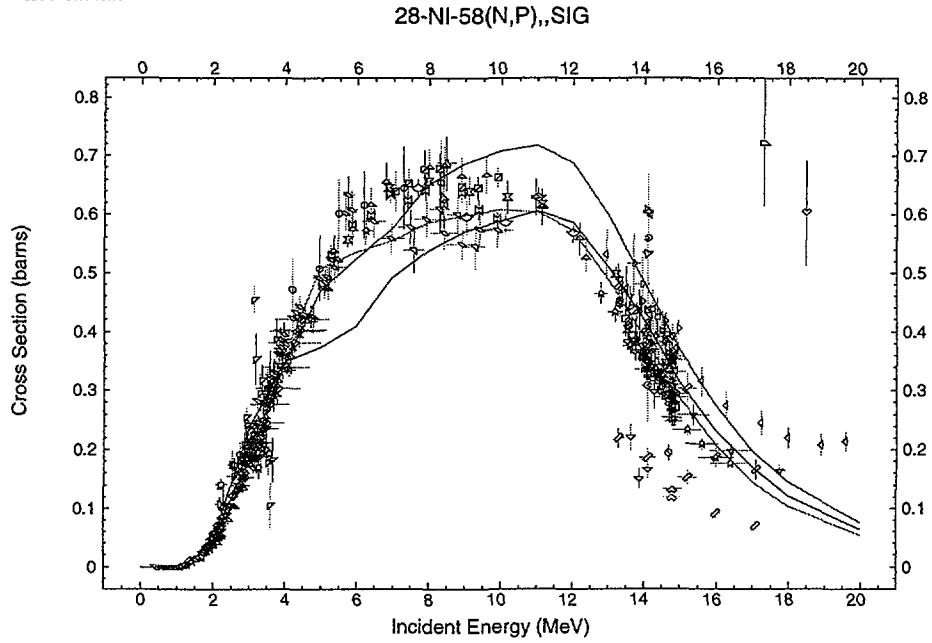


Figure 9: Comprison of experimental data with results calculated using three sets of parameters (see text) for the $^{58}\text{Ni}(n,p)$ reaction.

28-Nov-2001 15:19

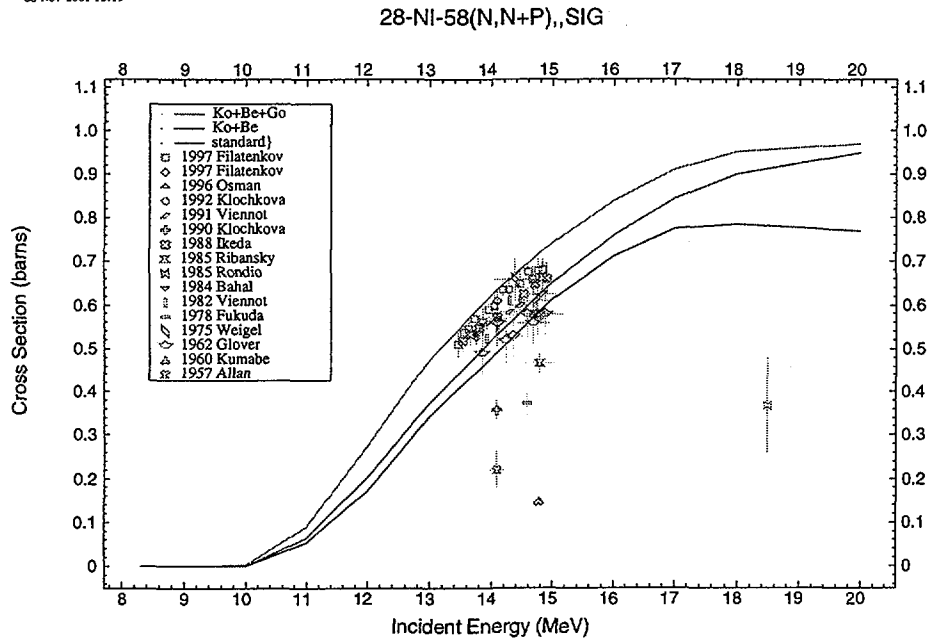


Figure 10: Comprison of experimental data with results calculated using three sets of parameters (see text) for the $^{58}\text{Ni}(n,np)$ reaction.

28-Nov-2001 16:11

29-CU-63(N,2N),,SIG

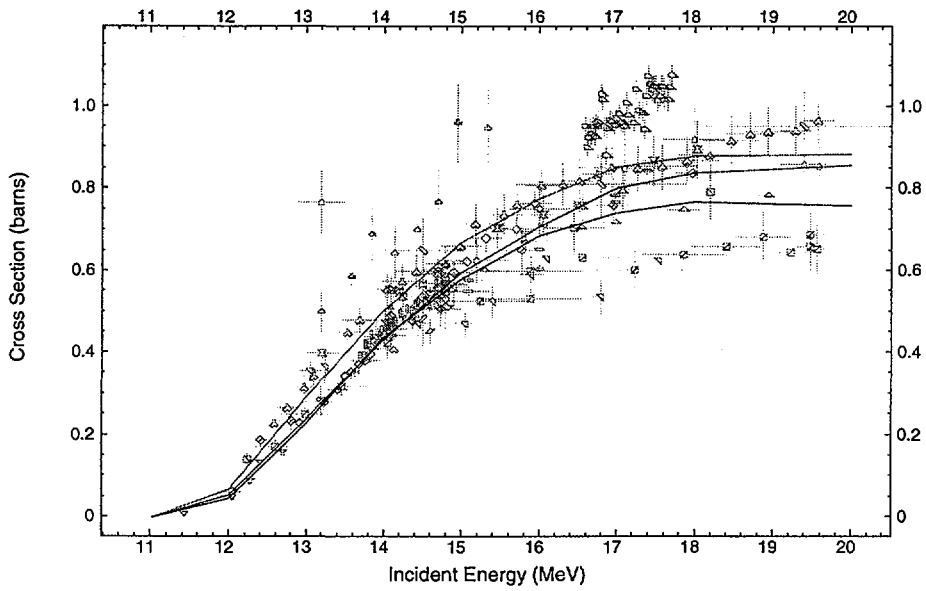


Figure 11: Comprison of experimental data with results calculated using three sets of parameters (see text) for the $^{63}\text{Cu}(n,2n)$ reaction.

28-Nov-2001 15:29

31-GA-71(N,G),,SIG

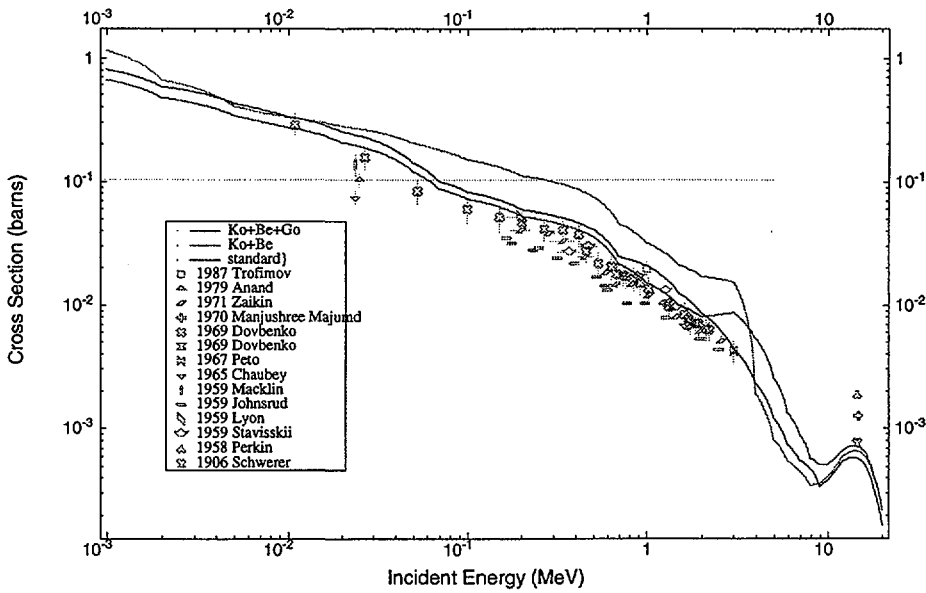


Figure 12: Comprison of experimental data with results calculated using three sets of parameters (see text) for the $^{71}\text{Ga}(n,\gamma)$ reaction.

28-Nov-2001 15:41

34-SE-80(N,G),,SIG

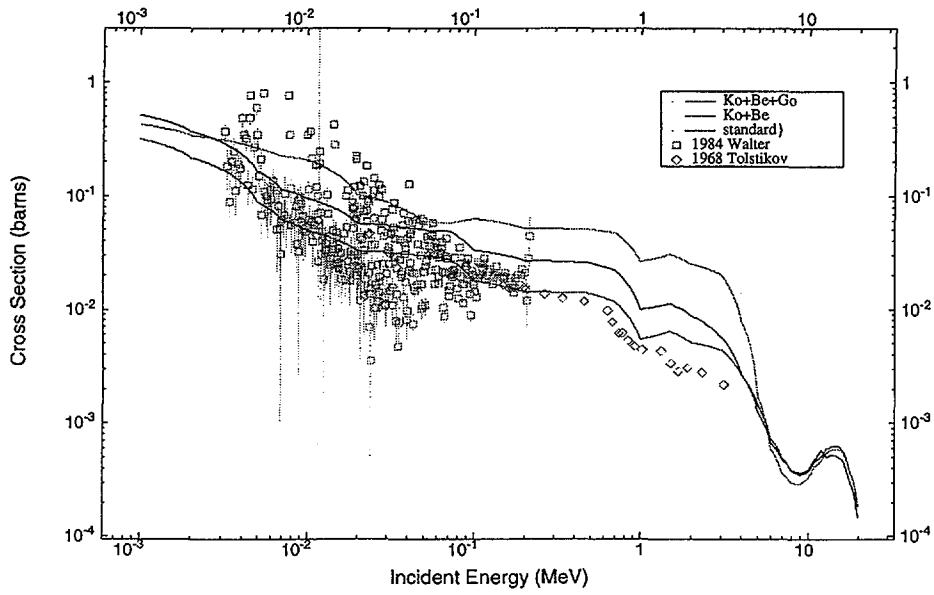


Figure 13: Comprison of experimental data with results calculated using three sets of parameters (see text) for the $^{80}\text{Se}(n,\gamma)$ reaction.

28-Nov-2001 16:16

41-NB-93(N,INL),,SIG

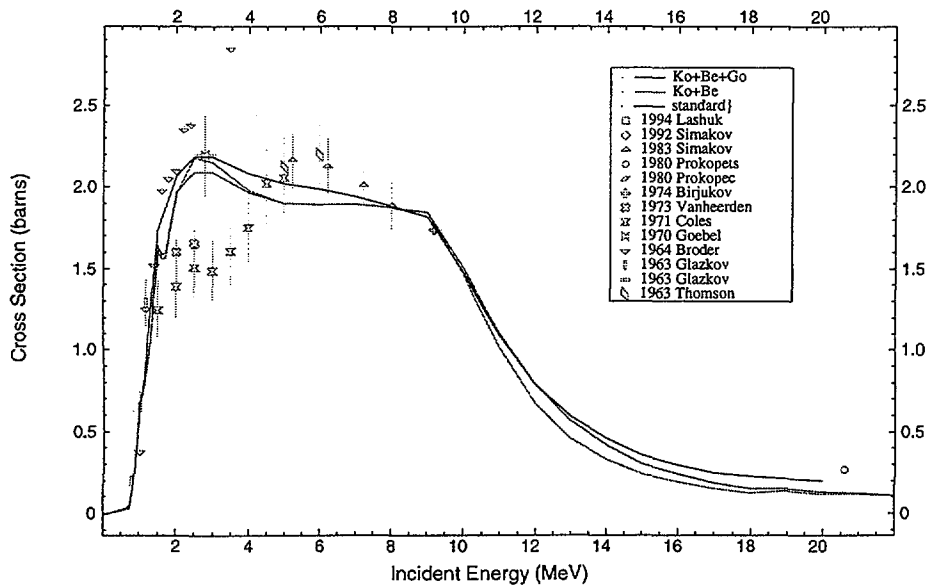


Figure 14: Comprison of experimental data with results calculated using three sets of parameters (see text) for the $^{93}\text{Nb}(n,\text{inl})$ reaction.

28-Nov-2001 15:14

41-NB-93(N,2N),,SIG

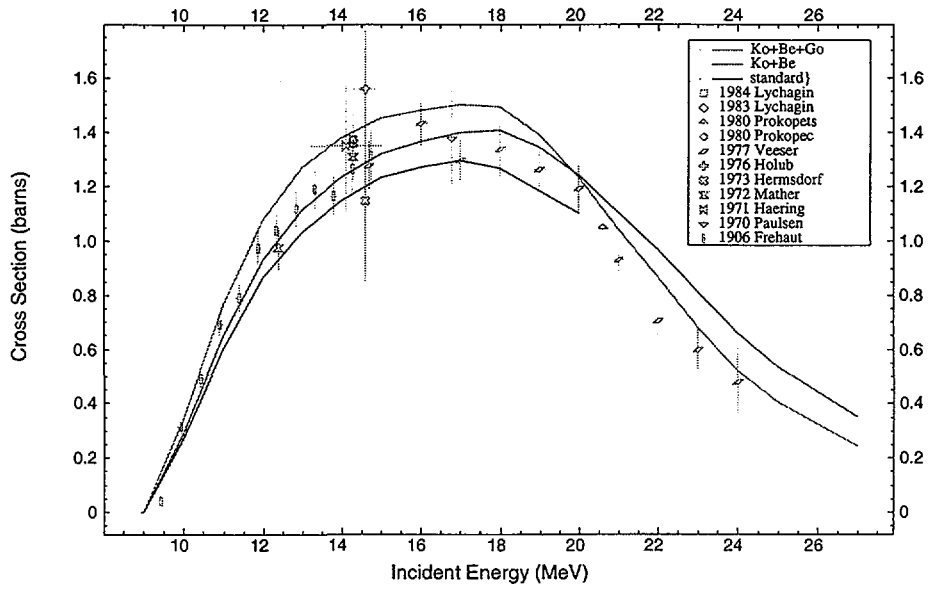


Figure 15: Comprison of experimental data with results calculated using three sets of parameters (see text) for the $^{93}\text{Nb}(n,2n)$ reaction.

28-Nov-2001 15:32

41-NB-93(N,G),,SIG

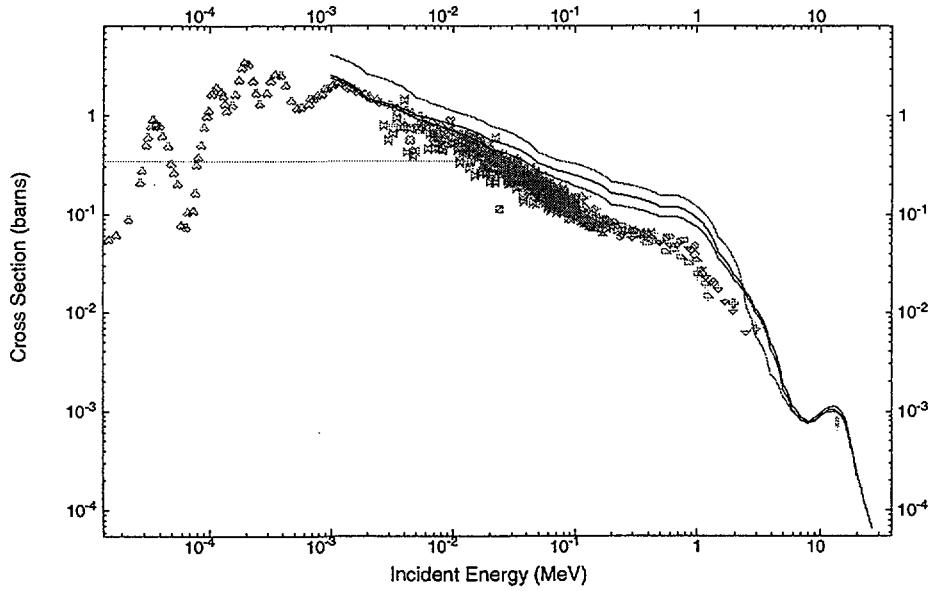


Figure 16: Comprison of experimental data with results calculated using three sets of parameters (see text) for the $^{93}\text{Nb}(n,\gamma)$ reaction.

28-Nov-2001 15:31

42-MO-100(N,G),,SIG

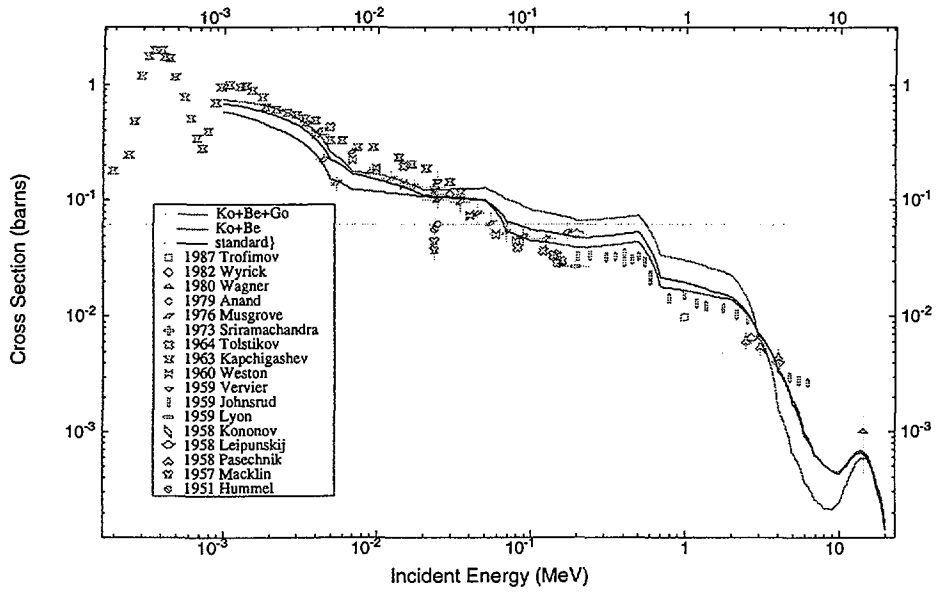


Figure 17: Comprison of experimental data with results calculated using three sets of parameters (see text) for the $^{100}\text{Mo}(n,\gamma)$ reaction.

28-Nov-2001 15:14

42-MO-92(N,2N),,SIG

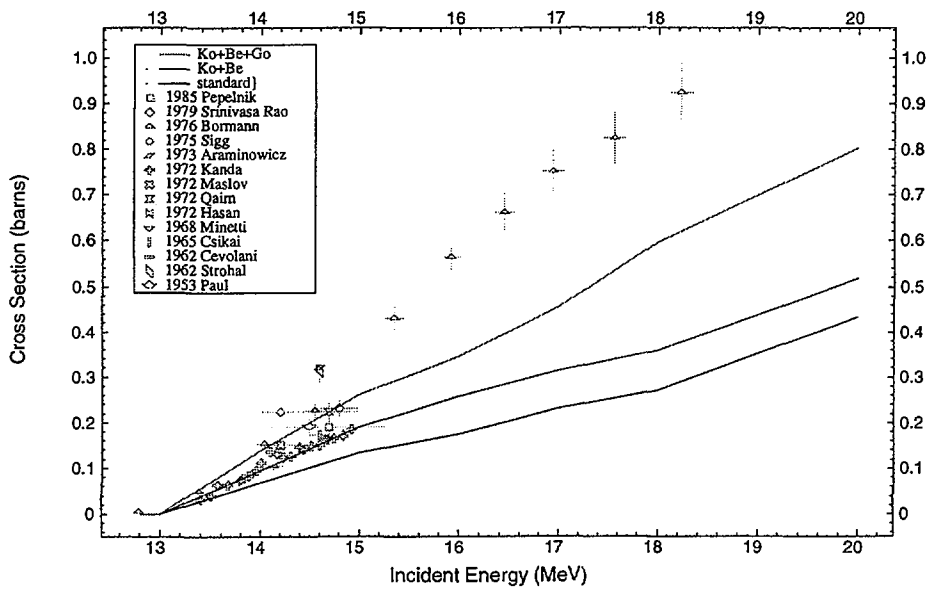


Figure 18: Comprison of experimental data with results calculated using three sets of parameters (see text) for the $^{92}\text{Mo}(n,2n)$ reaction.

28-Nov-2001 16:13

53-I-127(N,G),,SIG

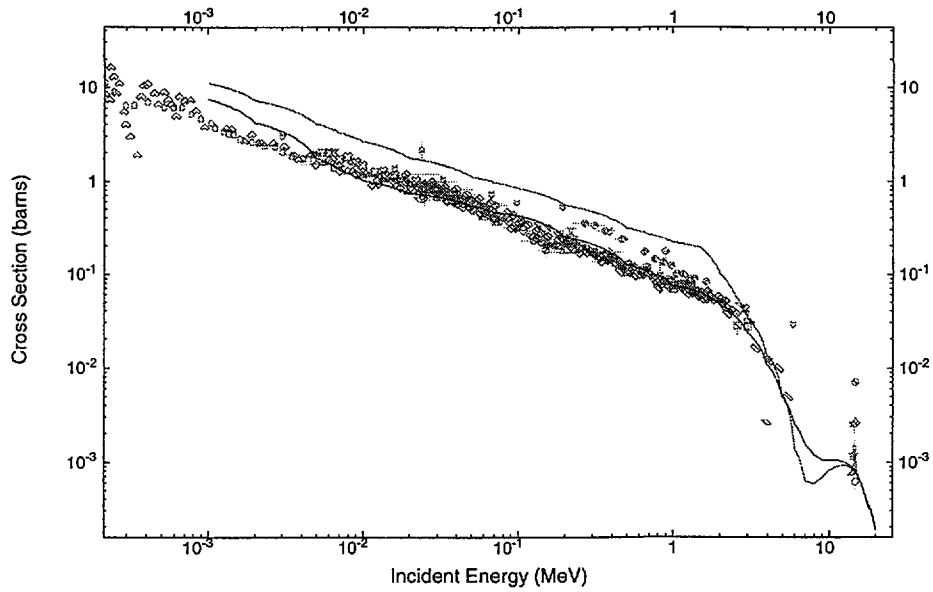


Figure 19: Comprison of experimental data with results calculated using three sets of parameters (see text) for the $^{127}\text{I}(n,\gamma)$ reaction.

28-Nov-2001 15:43

69-TM-169(N,G),,SIG

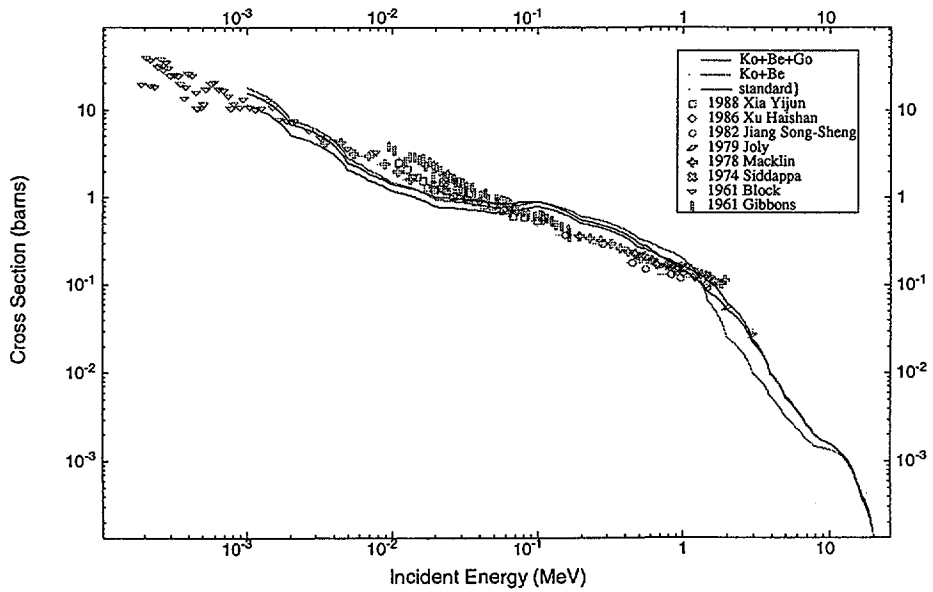


Figure 20: Comprison of experimental data with results calculated using three sets of parameters (see text) for the $^{169}\text{Tm}(n,\gamma)$ reaction.

28-Nov-2001 16:21

74-W-186(N,G),,SIG

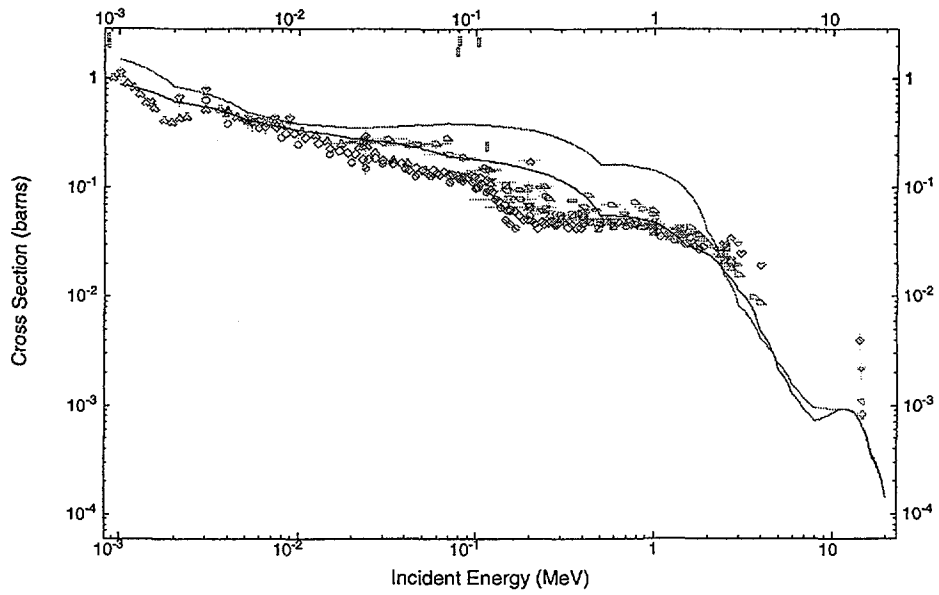


Figure 21: Comprison of experimental data with results calculated using three sets of parameters (see text) for the $^{186}\text{W}(n,\gamma)$ reaction.

28-Nov-2001 15:16

82-PB-208(N,2N),,SIG

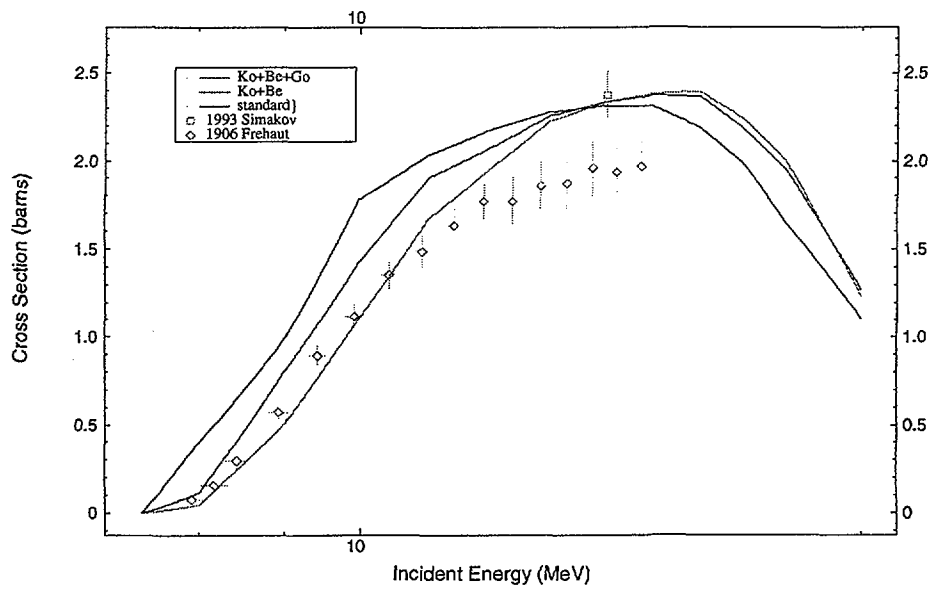


Figure 22: Comprison of experimental data with results calculated using three sets of parameters (see text) for the $^{208}\text{Pb}(n,2n)$ reaction.

The UNF code and its interface PREUNF

Zhang Jingshang Ge Zhigang Sun Zhengjun

China Nuclear Data Center, China Institute of Atomic Energy

P.O.Box 275-41, Beijing 102413, P.R.China

Tel: +86-10-69357275, Fax: +86-10-69377008, E-mail: gezg@iris.ciae.ac.cn

The UNF code (2001 version) has been completed, which consists of the spherical OM, the unified H-F and Exciton mode and used to calculate neutron introduced reaction data for structure materials with incident energies from 1 keV up to 20 MeV. UNF can calculate the following physical quantities;

- Cross sections of total, elastic and non-elastic scattering, and all reaction channels.
- Angular distributions of scattering both in CM and LAB.
- The energy spectra of the particle emitted in all channels.
- Double-differential CS of the all particle (n,p,He4,d,t and He3) emissions and the recoil nuclei.
- Partial and total kerma factor.
- Gamma production data.
- Total double-differential CS of all outgoing particles from all channels.
- CS of isomeric state, if the level is a isomeric state of the residual nucleus.

UNF can also handle the calculations for a single element and natural nucleus. The output can be provided as ENDF format. Some self-checking functions are also designed.

UNF is used as the main code in the activities of the Chinese Evaluated Nuclear Data Library (CENDL-3).

An interface code PREUNF has been developed at CNDC. The PREUNF can be used to create automatically the all input files (unf.dat, dir.dat and oth.dat) of code UNF. All characters of the target, projectile and information, parameters of the nuclear reaction model, which used in UNF code, are taken from the RIPL database, except for a few constants and control swatches of the code, which must be inputted by users.

With the PREUNF and the RIPL database the users can very easily to generate the input files and to run the UNF code to do the nuclear data calculation and evaluations.

The Basic Testing of RIPL with UNF code

Ge Zhigang Zhang Jingshang Sun Zhengjun

China Nuclear Data Center, China Institute of Atomic Energy

P.O.Box 275-41, Beijing 102413, P.R.China

Tel: +86-10-69357275, Fax: +86-10-69377008, E-mail: gezg@iris.ciae.ac.cn

Introduction

For the general testing and validation of the RIPL database, a nuclear model code UNF is used to perform the testing with RIPL database. The testing is done in an incident energy region of 0.1-20 MeV for 103 nuclei and mass region from 69 to 160.

Testing and Results

All information and the parameters about the projectile, target, residual nuclei and nuclear model are taken from the RIPL database. We did the model calculations with the original information from RIPL firstly. As ones know that the optical potential parameters is most important for the total cross sections calculations, and the optical parameters collected by RIPL obtained by the fitting the experimental total cross sections and elastic angular distributions. So the calculated total cross sections with the parameters are very good in agreement with the experimental data (the errors are less than 3%). As some examples, Fig.1 to Fig. 9 presented the UNF calculated results for other main reaction channels, for instance, (n, gamma), (n,2n) and (n,3n), et al. One can see that the calculated results (labeled by UNF-r in the Figs.) could repeated the behavior of the experimental data in physical shape, except for the absolute value for these reaction channels. When some necessary and certain adjustments for some parameters of the RIPL according to the related experimental information are introduced, the calculated results (labeled by UNF in the Figs.) could be very good in agreement with the experimental data.

Conclusions

Through the comparisons of the two calculations, a conclusion in this energy and mass region for the RIPL database are obtained. For the common nuclear data model calculations and evaluations the RIPL database

- RIPL database covered the most of the information and parameters for nuclear study, nuclear data model calculations and its applications.
- The information of the nuclei of RIPL are update and accurate.

- The related nuclear mode parameters collected by RIPL are acceptable and reasonable in physical consideration.
- Certain adjustments for some parameters are necessary in the practical applications.
- The RIPL database should be expanded and updated.

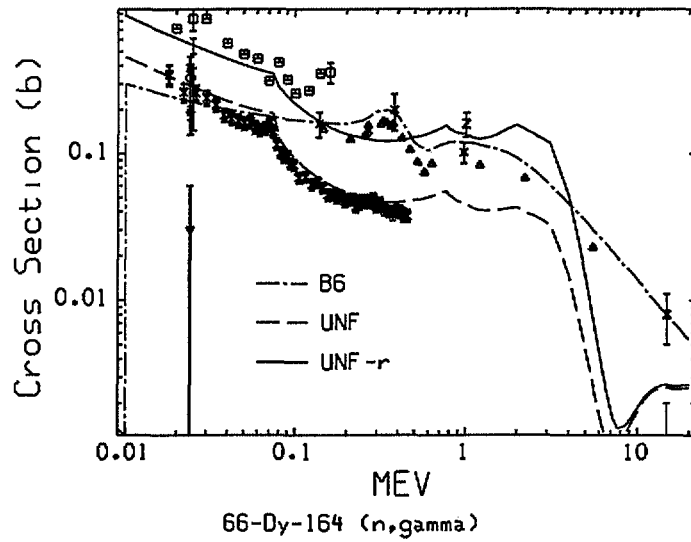


Fig. 1

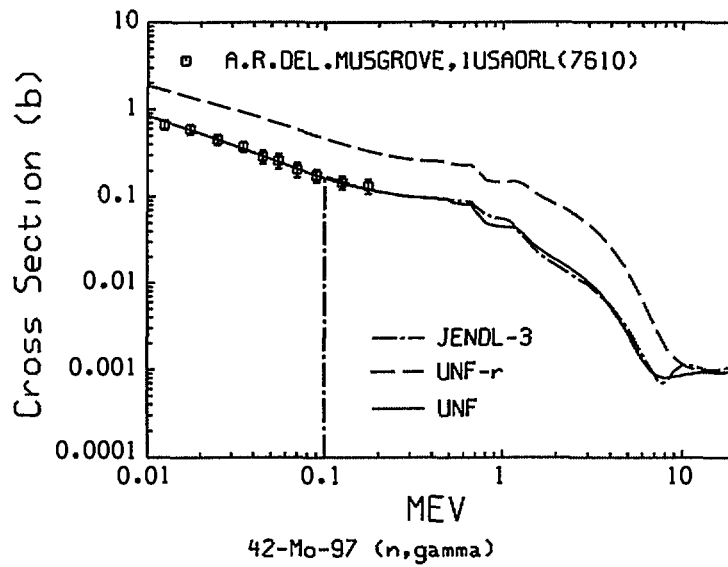


Fig. 2

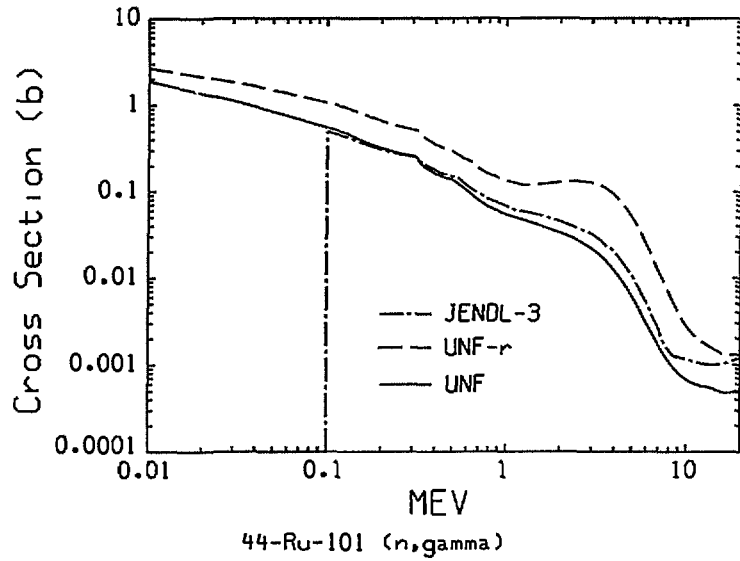


Fig. 3

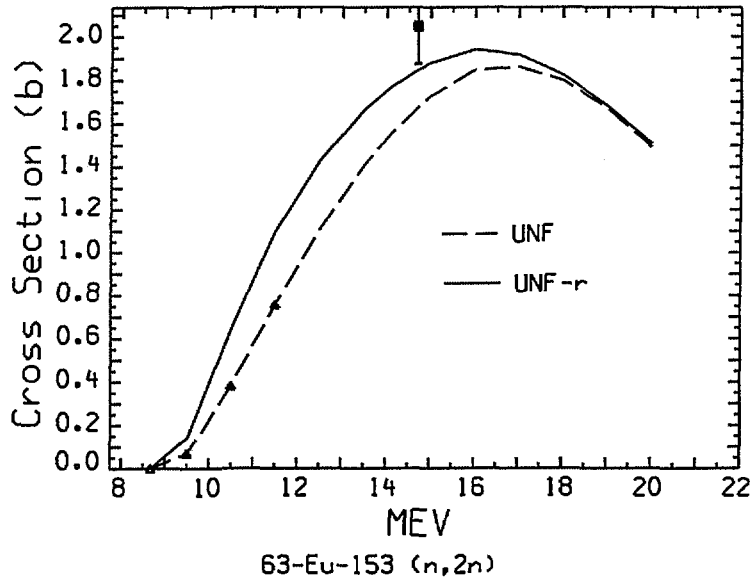


Fig. 4

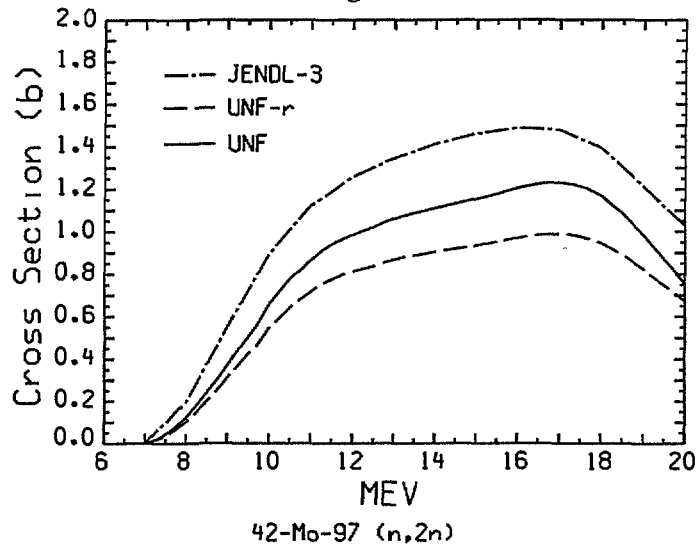


Fig. 5

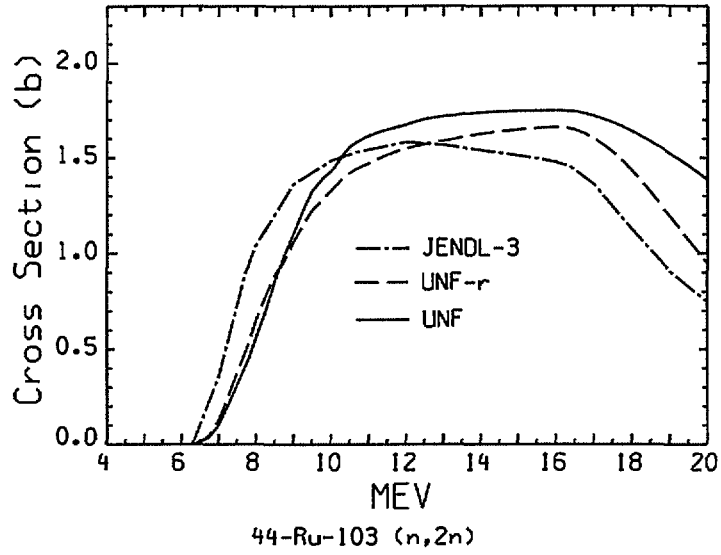


Fig. 6

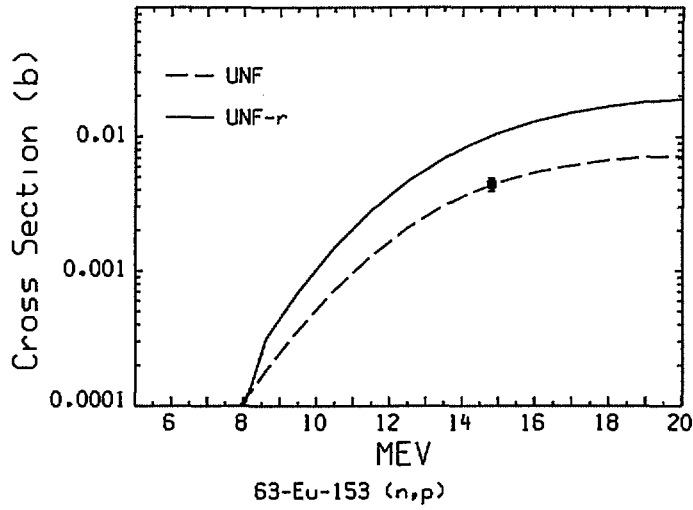


Fig. 7

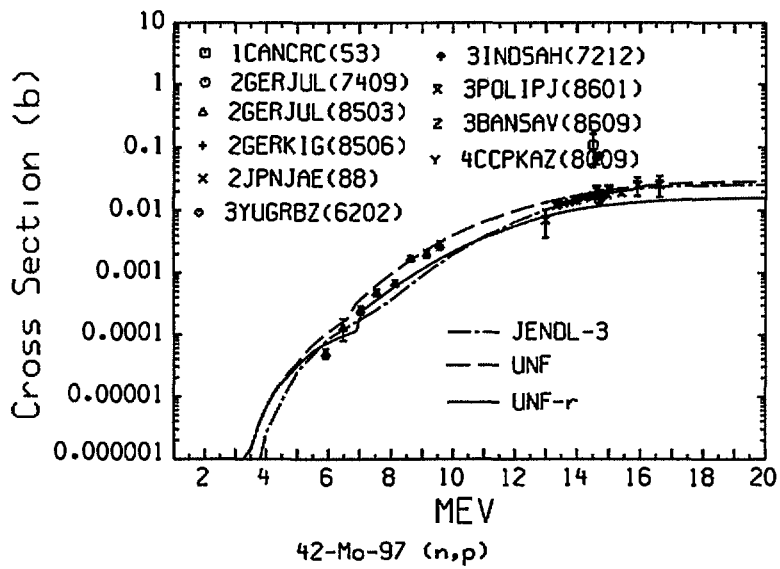


Fig. 8

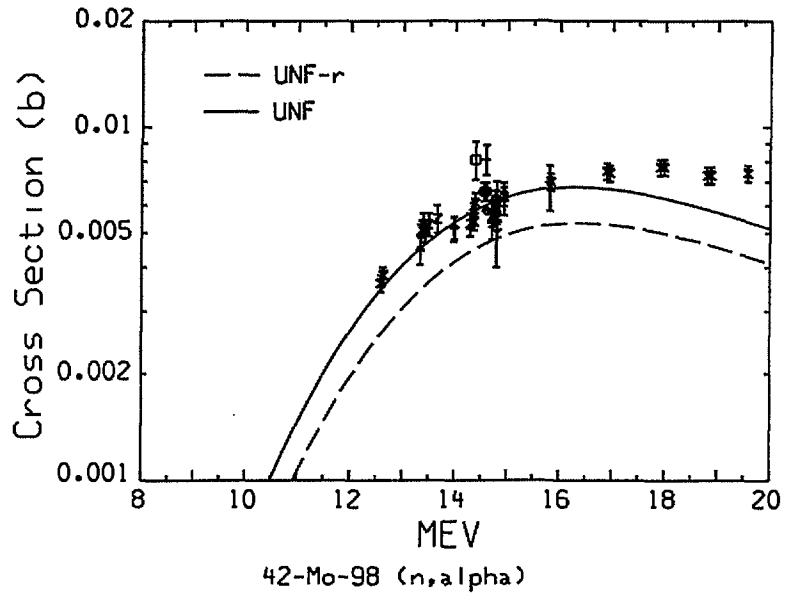


Fig. 9

Comparison of phenomenological and microscopical level densities in nuclear reaction calculations

A. J. Koning

*Nuclear Research and Consultancy Group NRG,
P.O. Box 25, 1755 ZG Petten, The Netherlands
(January 25, 2002)*

I. INTRODUCTION

Our nuclear model code TALYS, version 0.49, has been tested against several experimental nuclear reaction data sets. As model input, many of the databases present in RIPL-II have been used. We show excitation functions for various neutron-induced reactions on ^{52}Cr , ^{58}Ni , ^{93}Nb , ^{127}I and ^{208}Pb . A key issue of this test is a comparison of the use of microscopical nuclear level densities, as provided by S. Goriely for RIPL-II, and level densities obtained in a phenomenological Gilbert-Cameron/Ignatyuk approach. We emphasize that all the calculations shown here have been calculated using default parametrizations and models only, i.e. there was no parameter fitting involved. Hence, the results should not be considered as optimal fits.

II. THE TALYS CODE

TALYS is a nuclear reaction program created at NRG Petten, the Netherlands and CEA Bruyères-le-Châtel, France. The idea to make TALYS was born in 1998, when we decided to implement our combined knowledge of nuclear reactions into one single software package. The basic objective behind the construction of TALYS is the simulation of nuclear reactions that involve neutrons, photons, protons, deuterons, tritons, ^3He - and alpha-particles, in the 1 keV - 200 MeV energy range and for target nuclides of mass 12 and heavier. To achieve this, we have implemented a suite of nuclear reaction models into a single code system. This enables us to evaluate nuclear reactions from the unresolved resonance region up to intermediate energies.

As specific features of TALYS we mention

- In general, a non-approximative implementation of many of the latest nuclear models for direct, compound, pre-equilibrium and fission reactions.
- A continuous, smooth description of reaction mechanisms over a wide energy range (0.001- 200 MeV) and mass range ($12 < A < 260$).
- Completely integrated optical model and coupled-channels calculations through the ECIS code.
- Incorporation of new optical model parameterizations for many nuclei.

- Total and partial cross sections, energy spectra, angular distributions and double-differential spectra.
- Excitation functions for residual nuclide production, including isomeric cross sections.
- Automatic reference to nuclear structure parameters as masses, discrete levels, resonances, level density parameters, deformation parameters, fission barrier and gamma-ray parameters, generally from the RIPL library.
- Various width fluctuation models for binary compound reactions, and multiple compound emission until all reaction channels are closed.
- Various phenomenological and microscopical level density models.
- Classical (exciton model) and quantum-mechanical (multi-step direct/compound) models for pre-equilibrium reactions.
- An exact modelling of exclusive channel cross sections (e.g. (n,2np)) and spectra.
- Use of systematics if an adequate theory for a particular reaction mechanism is not yet available or implemented, or simply as a predictive alternative for the nuclear models in TALYS.

The central message is that we always provide a complete set of answers for a nuclear reaction, for all open channels and the associated integrated, single- and double-differential cross sections, as well as activation/residual-production and fission cross sections. It depends on the current status of nuclear reaction theory and our ability to model it whether these answers are generated by more or less sophisticated physical methods or by simple systematics. With TALYS, a complete set of cross sections can already be obtained with minimal effort, through a four-line input file of the type:

```
projectile n
element    Fe
mass       56
energy     14.
```

which, if you are only interested in robustness, reasonable answers or mass production of nuclear data, will give you all you need. If you want to be more specific, you simply add some of the more than 100 keywords that can be specified in TALYS.

For the calculations shown in this paper an input of the type above has been used, e.g.

```
projectile n
element    I
mass       127
energy     energies
ldmodel 2
```

where the file "energies", present in the working directory, contains a list of incident energies, and `ldmodel 2` specifies that Goriely's level density tables are used instead of the default phenomenological level densities.

TALYS is not yet generally available.

III. NUCLEAR MODELS AND PARAMETERS

We give a very short list of some of the models that are used in TALYS.

A. Optical model

For neutrons or protons, when a nucleus-specific optical model is available in the list of Koning and Delaroche, we adopt it. If not, TALYS automatically uses our global optical models, as presented elsewhere in the RIPL-report. For deuterons up to alpha's, we use Watanabe's folding approach to get the complex particle optical potentials out of the potentials we use for neutrons and protons. Hence, we have not yet connected the full RIPL OMP-library to TALYS, but instead use our own optical model parameterizations for all transmission coefficients and reaction cross sections.

B. Level densities

The default level density model of TALYS is the Gilbert-Cameron/Ignatyuk model with an energy-dependent level density parameter for the Fermi Gas part, to take into account the damping of shell effects. The mass corrections are taken as the difference between RIPL's mass table and the spherical mass formula of Myers and Swiatecki. The asymptotic and damping parameters from Mengoni and Nakajima (RIPL-I) are taken to drive the energy dependence of the level density parameter. A Wigner-type spin distribution is used with spin cutoff parameters as predicted by systematics. For the constant temperature part, the maximum discrete level is taken from Goriely's table. Next, an automatic search routine fits the temperature part smoothly to the Fermi Gas part, so that the full set of Gilbert-Cameron parameters (T, E_0, E_{match}) is obtained. In the figures, this model is labeled "Ignatyuk".

Another option, used in this work, is to read in Goriely's Hartree-Fock based tables and use them directly in TALYS.

C. Compound reactions

At low incident energies, Moldauers' width fluctuation model is used. At higher energies, and for multiple emission, we use the Hauser-Feshbach model. Spin-dependent transmission coefficients are used and particle and gamma decay is followed until all channels are closed.

D. Gamma-ray strength functions

The Kopecky-Uhl generalized Lorentzian is used, with GDR parameters taken from RIPL-I. The gamma-ray transmission coefficients are normalized using the theoretical level density and the experimental Γ_γ width.

E. Direct reactions

For the first few excited states, automatic direct nuclear reaction calculations are performed with ECIS. For the (near-) spherical cases of this paper, DWBA cross sections are included in the results. Collective effects in the continuum are taken into account by including a phenomenological giant resonance model in our calculations. Contributions of the GQR, LEOR and HEOR are added to the pre-equilibrium cross sections.

F. Pre-equilibrium reactions

The default model of TALYS is the two-component exciton model, using equidistant-spacing particle-hole state densities with finite well effects. Multiple pre-equilibrium emission is followed up to arbitrary order, made possible by an extensive book-keeping of excited particle-hole configurations. For complex particle emission, Kalbach's phenomenological models for pickup, stripping and knockout reactions are used.

IV. RESULTS

We present the comparison between the two level density methods in Figs. 1-20. The level density option is the *only* difference between the two calculations. All experimental data has been taken from EXFOR, without any further study.

V. CONCLUSIONS

For the set of results shown here, we wish to mention two conspicuous items that are related to shortcomings of TALYS-0.49:

- The (n, γ) pre-equilibrium strength seems to be too low around 14 MeV (even though the Akkermans-Gruppelaar photon pre-equilibrium model has been implemented).
- There are large uncertainties in the (n, α) cross section, but this is known to be a general problem.

Concerning level densities, it is hard to draw conclusions, apart from the fact that the use of microscopic level densities has been well verified (i.e. no strange discontinuities or other anomalous effects). One interesting aspect concerns the inelastic scattering off ^{93}Nb . The total inelastic scattering cross section seems to be somewhat higher for Goriely's level density, whereas this leads to a lower cross section for the production of the isomer. Apparently, the spin distributions differ sufficiently to lead to significant differences in the cross section.

TALYS-0.49: $^{52}\text{Cr}(n,2n)$

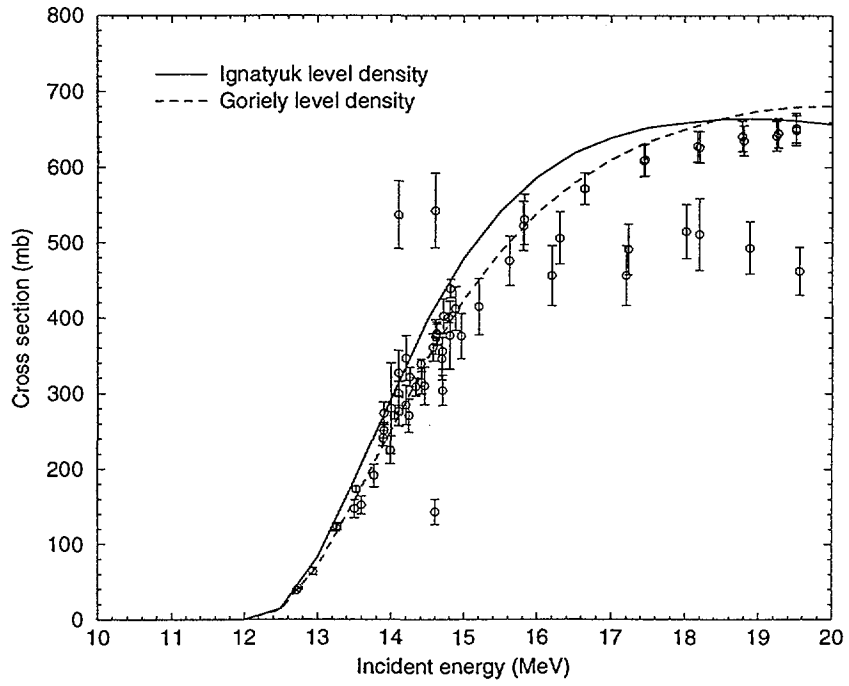


FIG. 1. Comparison between Goriely and phenomenological level density for $^{52}\text{Cr}(n,2n)$.

TALYS-0.49: $^{52}\text{Cr}(n,p)$

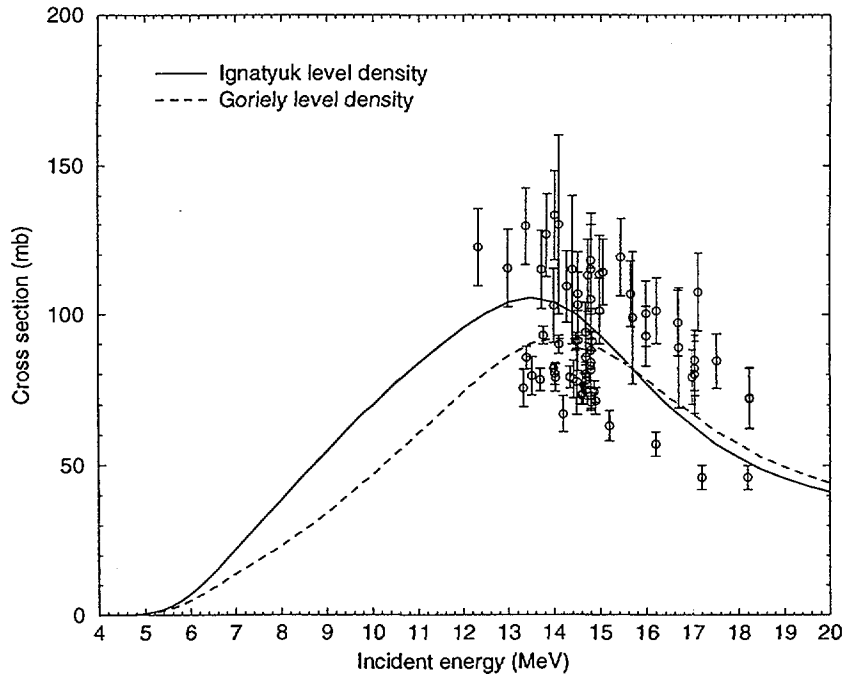


FIG. 2. Comparison between Goriely and phenomenological level density for $^{52}\text{Cr}(n,p)$.

TALYS-0.49: $^{58}\text{Ni}(n,2n)$

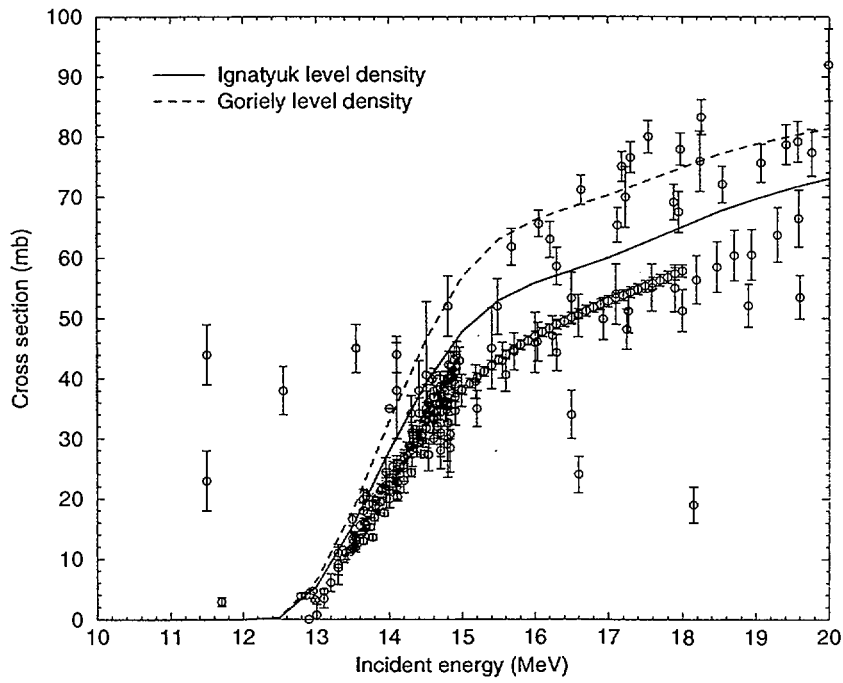


FIG. 3. Comparison between Goriely and phenomenological level density for $^{58}\text{Ni}(n,2n)$.

TALYS-0.49: $^{58}\text{Ni}(n,n+p)$

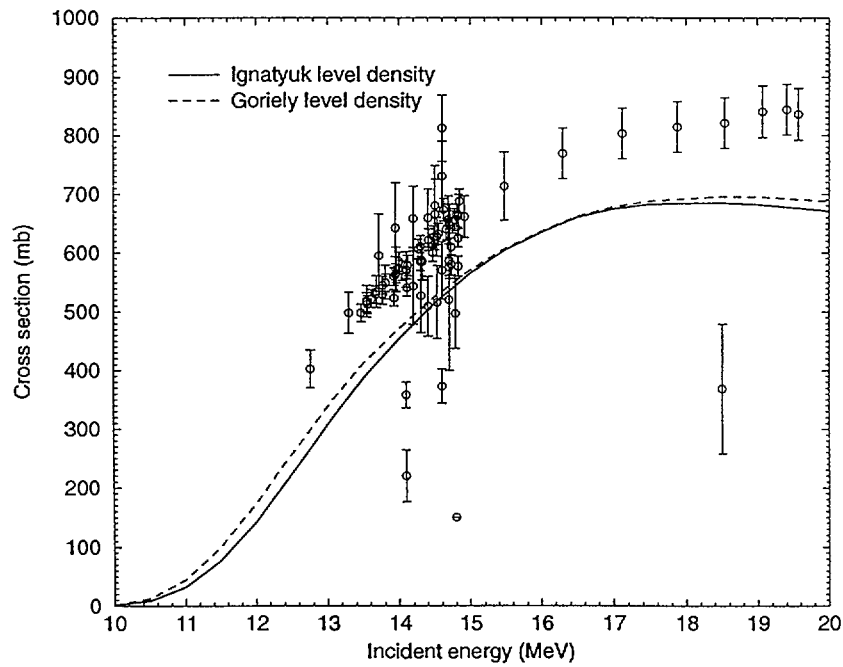


FIG. 4. Comparison between Goriely and phenomenological level density for $^{58}\text{Ni}(n,n+p)$.

TALYS-0.49: $^{58}\text{Ni}(n,\alpha)$

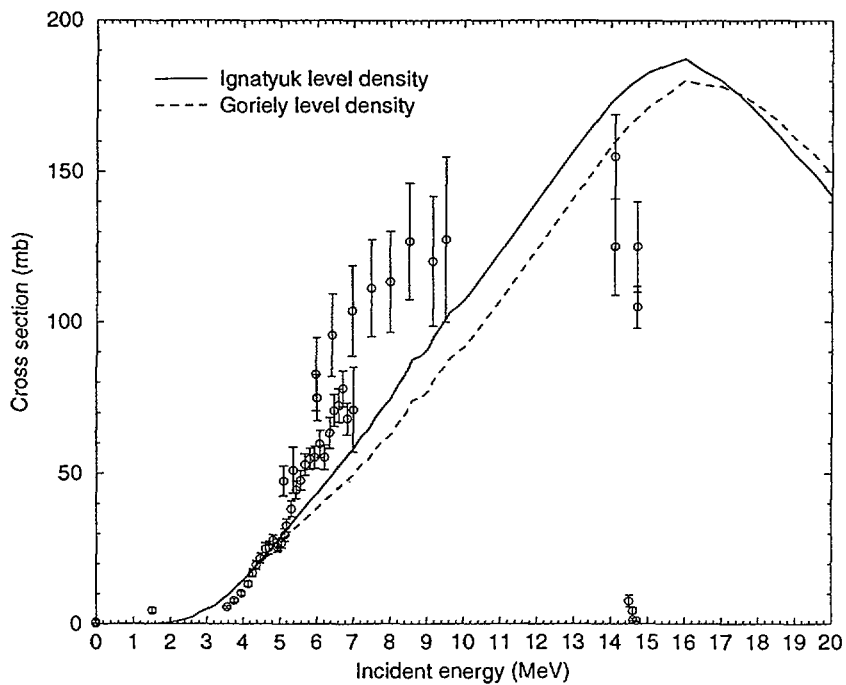


FIG. 5. Comparison between Goriely and phenomenological level density for $^{58}\text{Ni}(n,\alpha)$.

TALYS-0.49: $^{93}\text{Nb}(n,\gamma)$

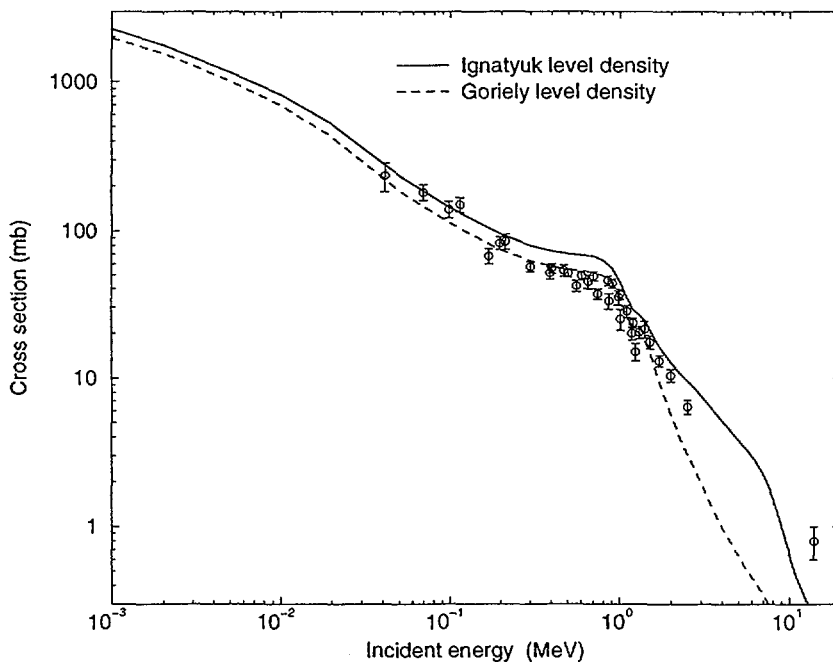


FIG. 6. Comparison between Goriely and phenomenological level density for $^{93}\text{Nb}(n,\gamma)$.

TALYS-0.49: $^{93}\text{Nb}(n,n')$

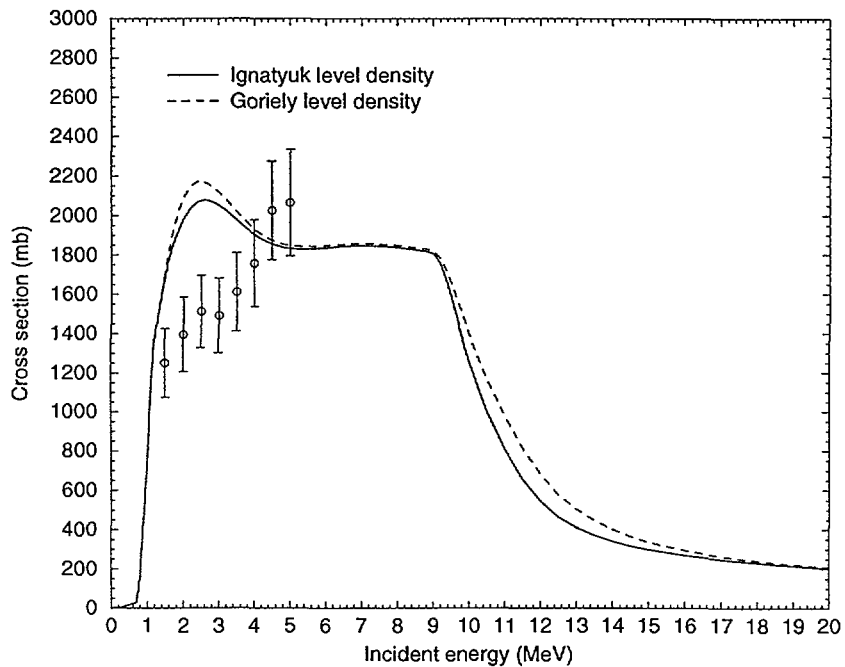


FIG. 7. Comparison between Goriely and phenomenological level density for $^{93}\text{Nb}(n,n')$.

TALYS-0.49: $^{93}\text{Nb}(n,n')^{93m}\text{Nb}$

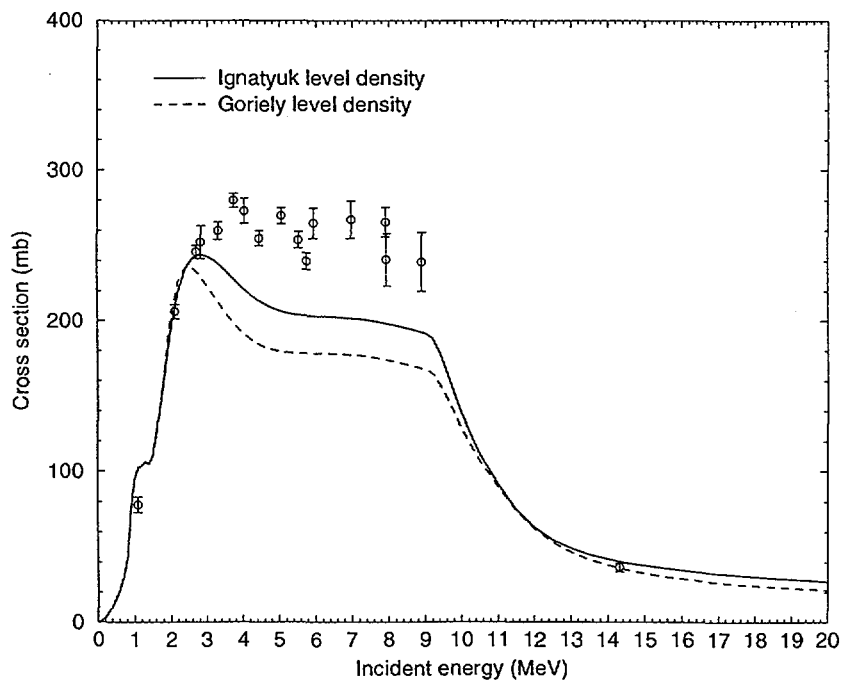


FIG. 8. Comparison between Goriely and phenomenological level density for $^{93}\text{Nb}(n,n')^{93m}\text{Nb}$.

TALYS-0.49: $^{93}\text{Nb}(n,2n)$

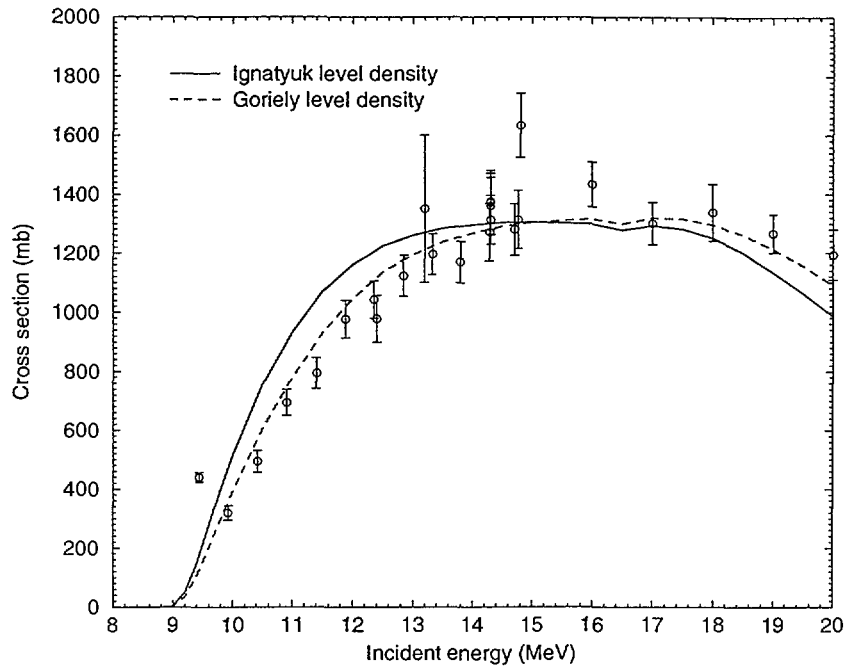


FIG. 9. Comparison between Goriely and phenomenological level density for $^{93}\text{Nb}(n,2n)$.

TALYS-0.49: $^{93}\text{Nb}(n,2n)^{92m}\text{Nb}$

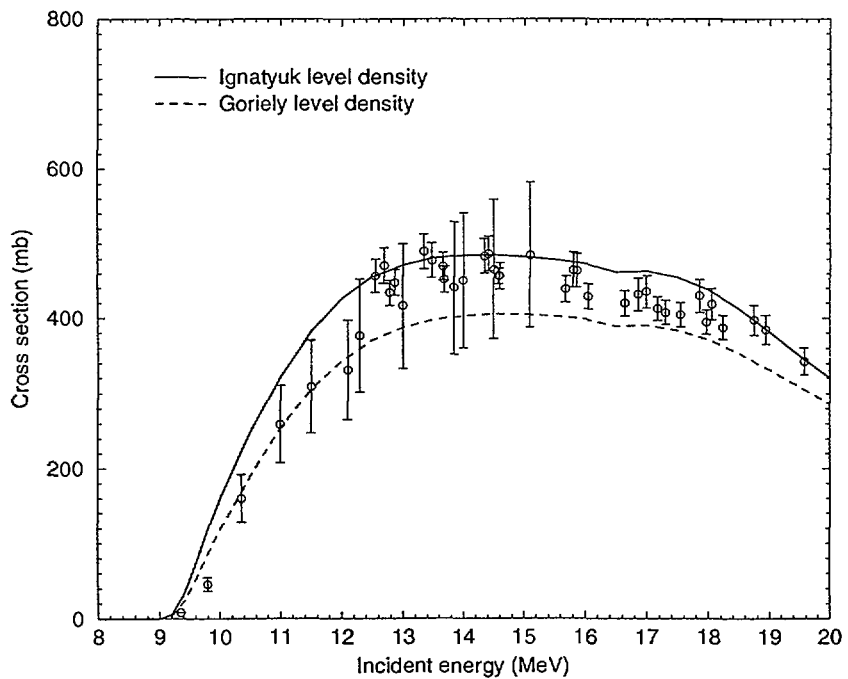


FIG. 10. Comparison between Goriely and phenomenological level density for $^{93}\text{Nb}(n,2n)^{92m}\text{Nb}$.

TALYS-0.49: $^{127}\text{I}(n,2n)$

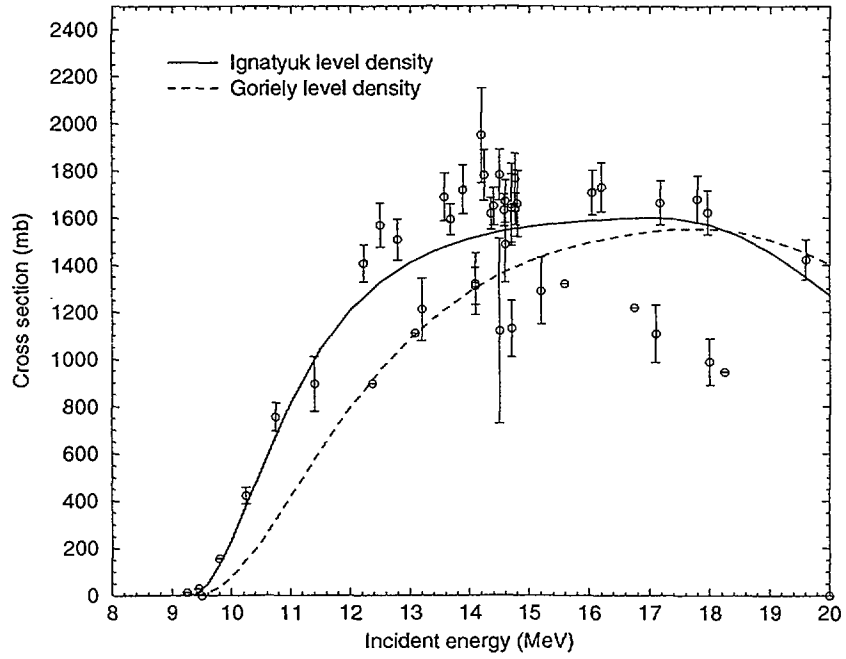


FIG. 11. Comparison between Goriely and phenomenological level density for $^{127}\text{I}(n,2n)$.

TALYS-0.49: $^{127}\text{I}(n,\alpha)$

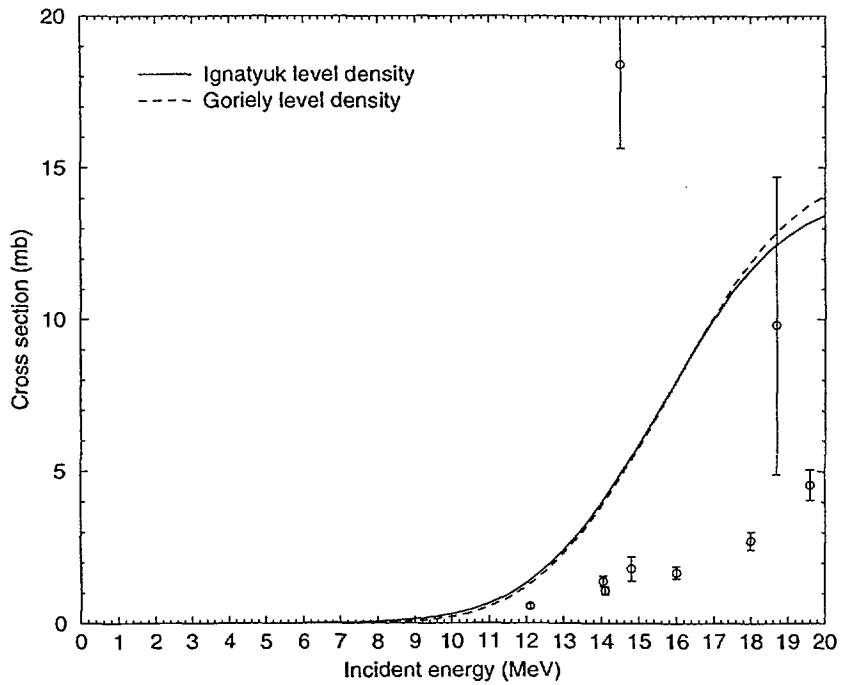


FIG. 12. Comparison between Goriely and phenomenological level density for $^{127}\text{I}(n,\alpha)$.

TALYS-0.49: $^{208}\text{Pb}(n,n')$

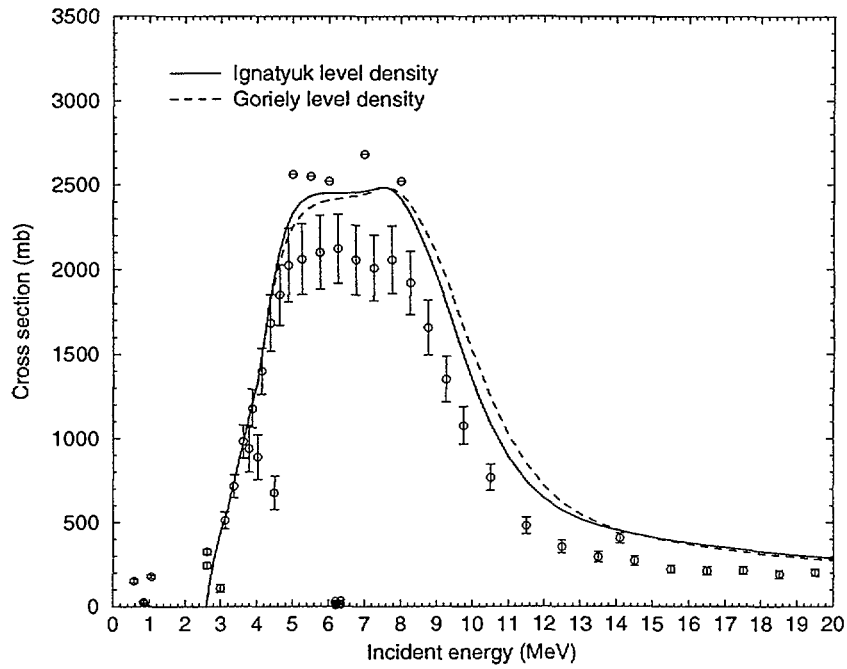


FIG. 13. Comparison between Goriely and phenomenological level density for $^{208}\text{Pb}(n,n')$.

TALYS-0.49: $^{208}\text{Pb}(n,2n)$

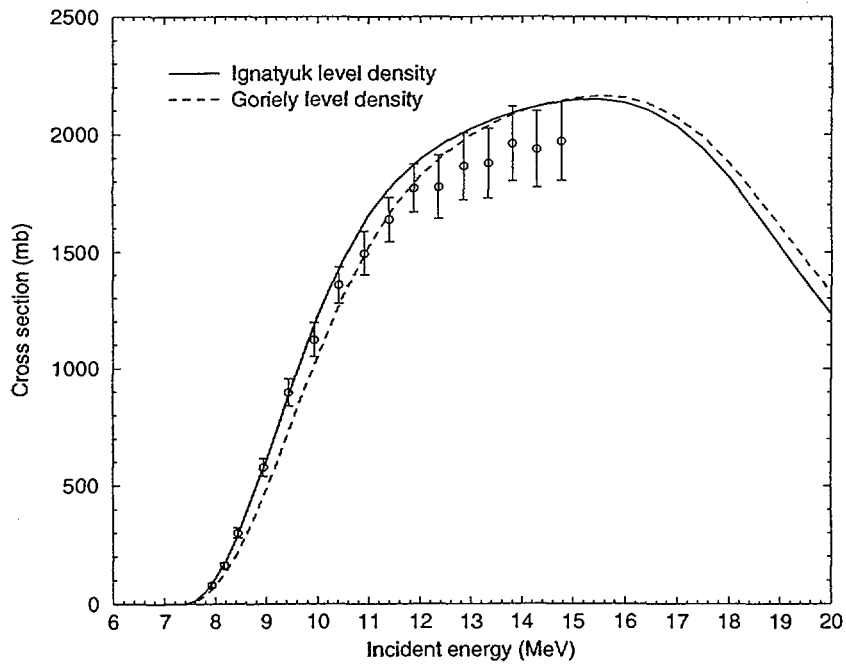


FIG. 14. Comparison between Goriely and phenomenological level density for $^{208}\text{Pb}(n,2n)$.

TALYS-0.49: $^{132}\text{Sn}(n,\gamma)$

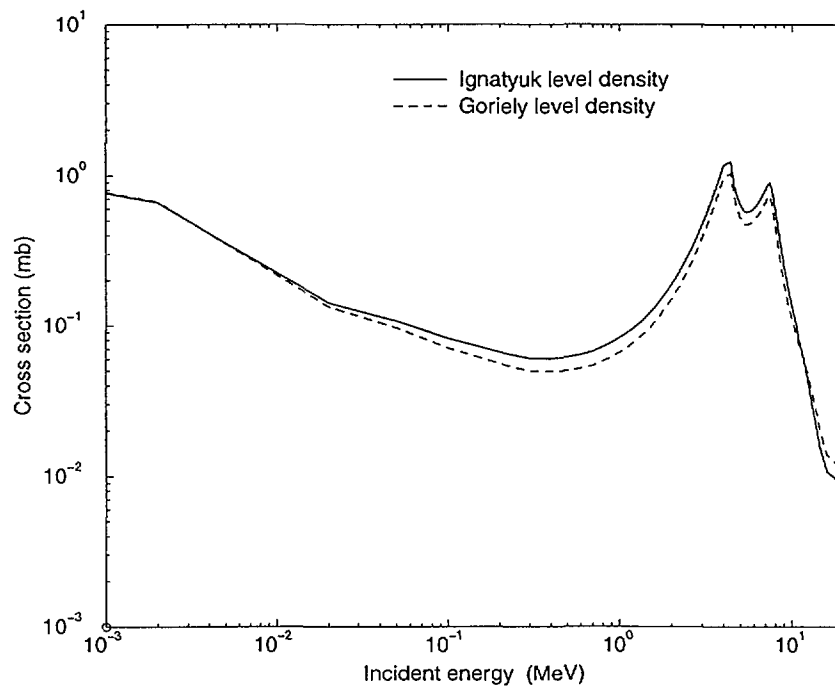


FIG. 15. Comparison between Goriely and phenomenological level density for $^{132}\text{Sn}(n,\gamma)$.

TALYS-0.49: $^{132}\text{Sn}(n,2n)$

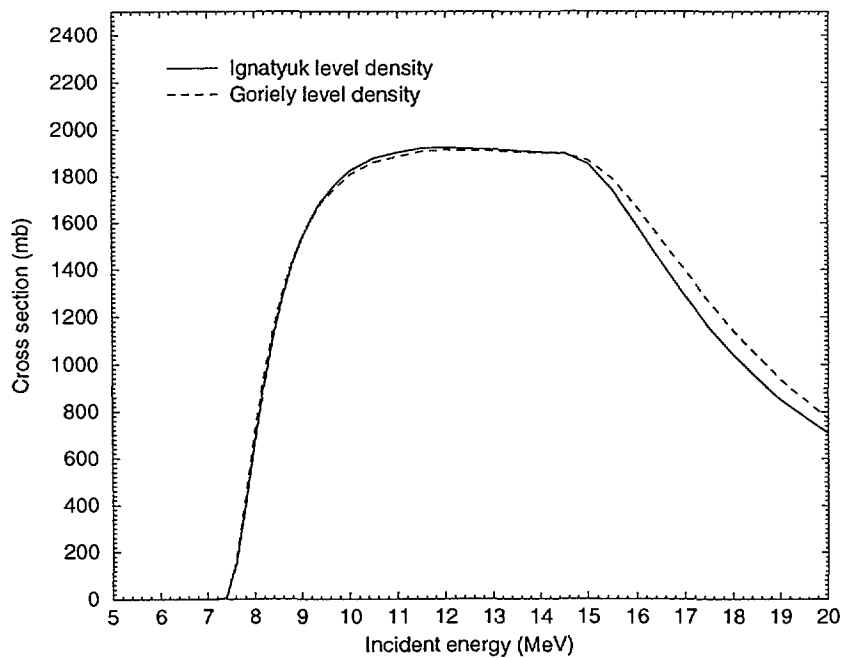


FIG. 16. Comparison between Goriely and phenomenological level density for $^{132}\text{Sn}(n,2n)$.

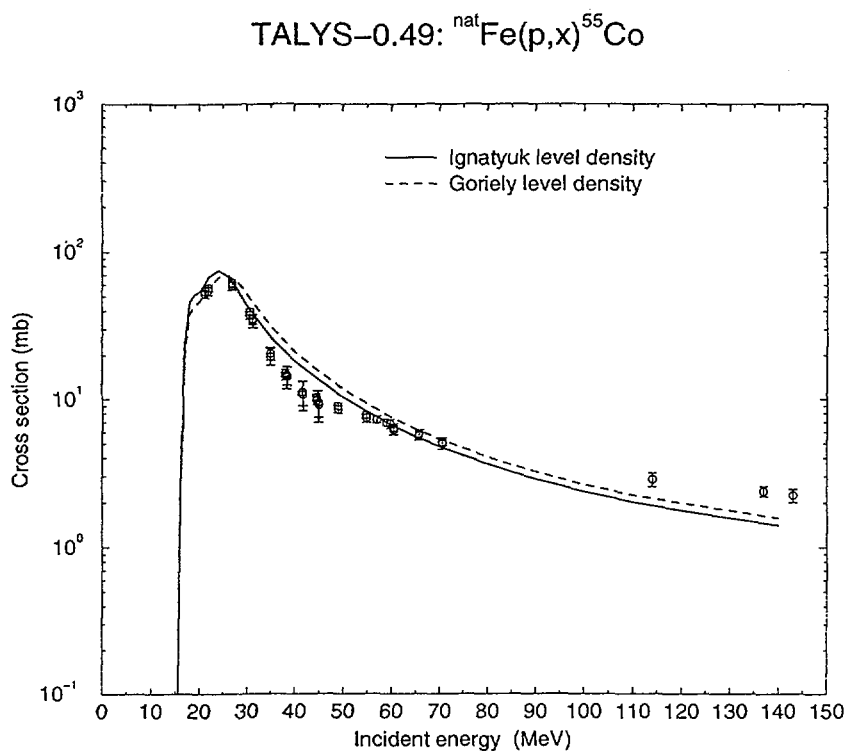


FIG. 17. Comparison between Goriely and phenomenological level density for ${}^{\text{nat}}\text{Fe}(p,x){}^{55}\text{Co}$.

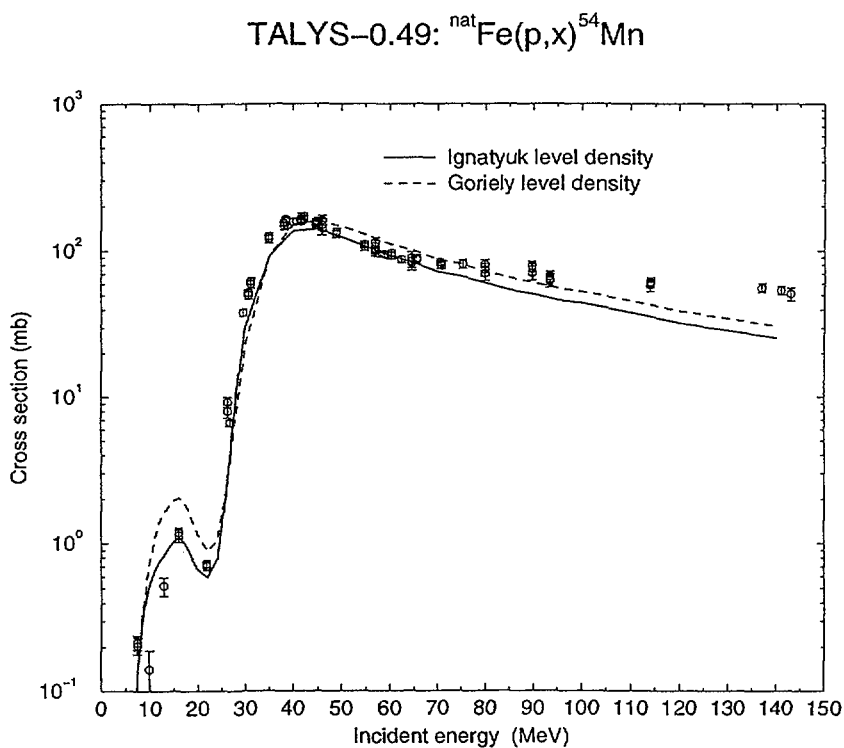


FIG. 18. Comparison between Goriely and phenomenological level density for ${}^{\text{nat}}\text{Fe}(p,x){}^{54}\text{Mn}$.

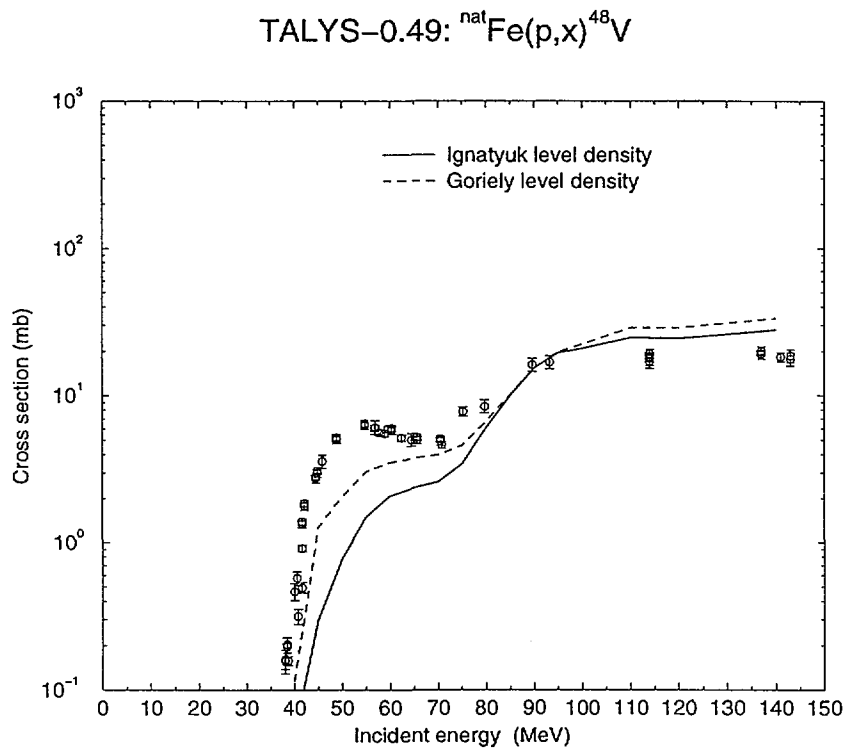


FIG. 19. Comparison between Goriely and phenomenological level density for ${}^{\text{nat}}\text{Fe}(p,x){}^{48}\text{V}$.

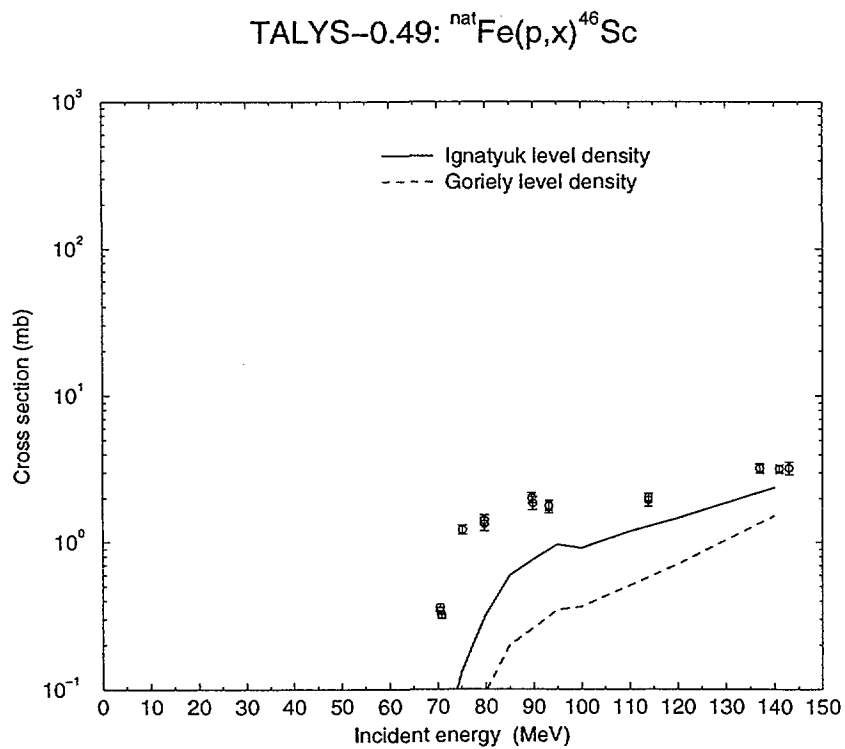


FIG. 20. Comparison between Goriely and phenomenological level density for ${}^{\text{nat}}\text{Fe}(p,x){}^{46}\text{Sc}$.

Nuclear Data Section
International Atomic Energy Agency
P.O. Box 100
A-1400 Vienna
Austria

e-mail: services@iaeand.iaea.org
fax: (43-1) 26007
cable: INATOM VIENNA
telex: 1-12645
telephone: (43-1) 2600-21710

Online: TELNET or FTP: iaeand.iaea.org
username: IAEANDS for interactive Nuclear Data Information System
usernames: ANONYMOUS for FTP file transfer;
FENDL2 for FTP file transfer of FENDL-2.0;
RIPL for FTP file transfer of RIPL.
NDSOVL for FTP access to files sent to NDIS "open" area.

Web: <http://www-nds.iaea.org>
